UMTA-MA-06-0100-82-2
DOT-TSC-UMTA-82-54, 2

DEVELOPMENT OF A DESIGN TECHNOLOGY FOR GROUND SUPPORT FOR TUNNELS IN SOIL

Volume II: Three-Dimensional Finite Element Analysis of Advanced and Conventional Shield Tunneling

Gyimah Kasali
G. Wayne Clough

Stanford University
Department of Civil Engineering
Stanford CA 94305

February 1983
Final Report

U.S. Department of Transportation
Urban Mass Transportation Administration

Office of Technical Assistance
Office of Systems Engineering
Washington DC 20590

NOTICE

This document is disseminated under the sponsorship of the Department of Transportation in the interest of information exchange. The United States Government assumes no liability for its contents or use thereof.

NOTICE

The United States Government does not endorse products or manufacturers. Trade or manufacturers' names appear herein solely because they are considered essential to the object of this report.

Technical Report Documentation Page

1. Report No.	2. Government Accession No.	3. Recipient's Catalog No.
UMTA-MA-06-0100-82-2		

4. Title and Subtitle
Development of a Design Technology for Ground Support for Tunnels in Soil - Vol. II - Three Dimensional Finite Element Analysis of Advanced and Conventional Shield Tunneling

5. Report Date
February 1983

6. Performing Organization Code
TSC/DTS-75

7. Author(s)
Gyimah Kasali and G. Wayne Clough

8. Performing Organization Report No.
DOT-TSC-UMTA-82-54, 2

9. Performing Organization Name and Address
Stanford University*
Department of Civil Engineering
Stanford, California 94305

10. Work Unit No. (TRAIS)
UM248/R2650

11. Contract or Grant No.
DOT-TSC-1726

12. Sponsoring Agency Name and Address
U. S. Department of Transportation
Urban Mass Transportation Administration
Office of Technical Assistance
Office of Systems Engineering
Washington, D. C. 20590

13. Type of Report and Period Covered
Final Report
Aug. 1979 - Jan. 1982

14. Sponsoring Agency Code
URT-10

15. Supplementary Notes
*Under Contract to: U.S. Department of Transportation
Research and Special Programs Administration
Transportation Systems Center
Cambridge, Massachusetts 02142

16. Abstract

Over the last decade, innovative improvements have been made in soil tunneling shield machines which allow application of continuous support to the face of the tunnel. However, because of the newness of the technology it is not clear exactly what degree of ground control can be achieved using the new machines over conventional ones. This report presents a true three dimensional finite element model which can be used to compare different soil tunneling procedures, and the ground movements which accompany tunnel construction. Parameter studies are described which demonstrate the benefits gained by continuous face support. Generally settlements are reduced when the advanced shield is operated so as to initially leave the soil aside slightly, at the face. Also, the continuous face control avoids any catastrophic collapse problems. However, ultimately settlements occur because of closure into the tail void as with the conventional shield. Future field studies are needed to refine our knowledge of any support which might be obtained by support of the tail void with some of the newer shield concepts. Also additional work is needed on optimization of ground control through the initial leaving process at the shield face.

17. Key Words	18. Distribution Statement
Tunnels, Advanced Shields, Movements, Soft Ground, Finite Element	DOCUMENT IS AVAILABLE TO THE PUBLIC THROUGH THE NATIONAL TECHNICAL INFORMATION SERVICE, SPRINGFIELD, VIRGINIA 22161

19. Security Classif. (of this report)	20. Security Classif. (of this page)	21. No. of Pages	22. Price
Unclassified	Unclassified	232	

PREFACE

This report is the second in a series dealing with ground control for tunnels constructed by shield techniques in soil. The report which precedes this one dealt with the development of finite element procedures which can be used to investigate time-dependent load changes and ground movements due to consolidation in the soil surrounding the tunnel. The report which follows this one presents the results of a field monitoring program performed to document the behavior of the first earth balance shield project undertaken in the United States. This volume addresses the question of analytically modeling the support mechanisms provided by advanced shield machines such as the earth balance shield and the slurry shield, and comparing their response to that of a conventional shield.

The research described herein was sponsored by the U.S. Department of Transportation, Urban Mass Transportation Administration (UMTA) and the Transportation Systems Center (TSC) of Cambridge, Massachusetts. Mr. Philip A. Mattson of TSC served as contract monitor and provided assistance throughout the project. Mr. Gilbert L. Butler of UMTA helped in development of the original ideas for the project. Dr. Paul R. Johnston and Professor Edward Kavazanjian of Stanford University assisted in the concepts for the analytical work. To all these individuals the authors express their appreciation.

METRIC CONVERSION FACTORS

Approximate Conversions to Metric Measures

Symbol	When You Know	Multiply by	To Find	Symbol
	LENGTH			
in	inches	*2.5	centimeters	cm
ft	feet	30	centimeters	cm
yd	yards	0.9	meters	m
mi	miles	1.6	kilometers	km
	AREA			
in^2	square inches	6.5	square centimeters	cm^2
ft^2	square feet	0.09	square meters	m^2
yd^2	square yards	0.8	square meters	m^2
mi^2	square miles	2.6	square kilometers	km^2
	acres	0.4	hectares	ha
	MASS (weight)			
oz	ounces	28	grams	g
lb	pounds	0.45	kilograms	kg
	short tons (2000 lb)	0.9	tonnes	t
	VOLUME			
tsp	teespoons	5	milliliters	ml
Tbsp	tablespoons	15	milliliters	ml
fl oz	fluid ounces	30	milliliters	ml
c	cups	0.24	liters	l
pt	pints	0.47	liters	l
qt	quarts	0.95	liters	l
gal	gallons	3.8	liters	l
ft^3	cubic feet	0.03	cubic meters	m^3
yd^3	cubic yards	0.76	cubic meters	m^3
	TEMPERATURE (exact)			
°F	Fahrenheit temperature	5/9 (after subtracting 32)	Celsius temperature	°C

*1 in = 2.54 (exactly). For other exact conversions and more detailed tables, see NBS Misc. Publ. 286, Units of Weights and Measures, Price $2.25, SD Catalog No. C13.10:286.

Approximate Conversions from Matric Measures

Symbol	When You Know	Multiply by	To Find	Symbol
	LENGTH			
mm	millimeters	0.04	inches	in
cm	centimeters	0.4	inches	in
m	meters	3.3	feet	ft
m	meters	1.1	yards	yd
km	kilometers	0.6	miles	mi
	AREA			
cm^2	square centimeters	0.16	squere inches	in^2
m^2	squere meters	1.2	square yards	yd^2
km^2	square kilometers	0.4	square miles	mi^2
ha	hectares (10,000 m^2)	2.5	ecres	
	MASS (weight)			
g	grams	0.035	ounces	oz
kg	kilograms	2.2	pounds	lb
t	tonnes (1000 kg)	1.1	short tons	
	VOLUME			
ml	milliliters	0.03	fluid ounces	fl oz
l	liters	2.1	pints	pt
l	liters	1.06	quarts	qt
l	liters	0.26	gallons	gal
m^3	cubic meters	35	cubic feet	ft^3
m^3	cubic meters	1.3	cubic yards	yd^3
	TEMPERATURE (exact)			
°C	Celsius temperature	9/5 (then add 32)	Fahrenheit temperature	°F

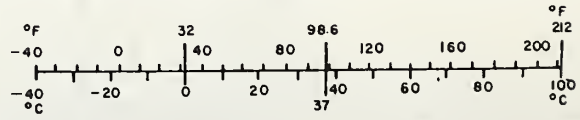

TABLE OF CONTENTS

LIST OF ILLUSTRATIONS

LIST OF TABLES

EXECUTIVE SUMMARY

A major objective in tunneling in urban areas is the prevention or reduction of ground movements which can cause damage to overlying structures and utilities. One important variable which influences this process is the choice of a construction procedure. In soils, it is common practice to use a shield to help support the ground and create a working space where the temporary liner can be erected. The basic conventional shield consists essentially of a circular steel element with an open face when the soil is excavated. Near the rear of the shield the liner is erected and the shield propels itself forward by pushing off of the most recently erected liner ring. This simple scheme encounters difficulty in pervious soils below the water table and in soft cohesive soils. In such cases, water can flow into the shield through the pervious soil, carrying soil with it, or the cohesive soils may tend to yield to a substantial degree into the shield. Conventional procedures to deal with these problems involve use of breast-boarding techniques or compressed air in the tunnel, both of which reduce tunneling efficiency and drive costs up.

Over the past decade, new types of shield machines have been developed to improve on the existing technology. In this report these are referred to as advanced shields. They use closed-face rotary cutterheads to excavate the soil, and allows the application of a pressure at the face to support the soil and prevent runs into the

machine. This technique can be semi-automated for improved efficiency, and avoids the need for any compressed air. The most commonly used of the advanced shields to date have been the slurry and the earth pressure balance shields. Over two hundred of these machines have been utilized overseas, but only one in the United States, as of the time of this writing (June, 1982).

In spite of the relatively wide application of the advanced shield technology however, little hard data are available as to assess exactly how well these machines control ground movements. This report is directed towards this issue. A true three-dimensional finite element procedure is developed so that the stresses and displacements induced in and around the tunneling machine as well as at the ground surface can be defined.

The modeling technique allows for a realistic accounting of the supporting mechanisms offered by the shield-liner system and the sequential nature of the construction. The soil is assumed to behave as clay with a linear elastic response and a modulus that increases linearally with depth. Modulus values are taken to be consistent with the stress levels induced by tunneling and thus, in an indirect way, to account for any yielding which might occur. The predicted behavior is found to yield a response which is consistent with field behavior.

Using the finite element program, comparisons are made illustrating the effects of conventional, slurry and earth pressure balance shields. The advanced shields are found to produce heaving effects at the face, whereas, the face moves in towards the shield for the conventional

machine. In all cases the soil moves inward when the tail of the shield passes as a result of soil movements into the tail void. For all the shield types, there are net ground settlements after shield passage, but those for the advanced shields are less by a small amount than the case of the conventional shield. It is apparent that the positive face support mechanisms in the case of the advanced shield led to reduced settlements. At the same time the tail void effect is the same for all shields, and this serves to equalize the net ground movements. Further study is warranted into the issue of optimizing the positive effects of the initial outward movements induced by the advanced shield for different types of ground conditions. At the same time it is clear that control movements into the tail void will remain a key issue for all types of shields in the future.

Chapter I

INTRODUCTION

1.1 URBAN TUNNELING

Tunnels constructed in urban areas are usually located at shallow depths for functional and economic reasons. One of the major problems associated with tunneling at such shallow depths is the settlement that occurs at the ground surface. These movements can lead to damage to overlying utilities and buildings.

In soils, a tunnel is constructed using a shield, which in its basic form, is a circular element of steel where the workers can excavate the tunnel and erect a liner to prevent a collapse of the ground as the shield advances. The shield is propelled by jacking against the in-place liner segments. Ground movements occur during shield tunneling if the soil displaces towards the face of the shield and inwards against the liner as the shield moves forward. Face movements can become large if the soil is soft or if ground water attempts to flow into the tunnel, and supplementary support measures such as breast boarding, compressed air or a closed-face rotary cutting head are not used. Inward movements after shield passage are increased if the alignment of the shield is not tightly controlled.

The displacement and stress pattern around the shield is three dimensional. The key to understanding the reasons for soil behavior and

settlement associated with shield tunneling lies in being able to define these patterns.

1.2 NEED FOR ANALYTICAL STUDY

In the past, the major technique for the study of the problem of surface settlement during shield tunneling has been field measurements. Carefully conducted field instrumentation projects have been successful in delineating sources of movements and suggesting procedures to limit them. However, field projects of this type are limited since they are costly and the results are often project dependent. Without a sound analytical base, the fundamental mechanisms of soil tunneling are not fully understood. For example, the stress distribution around the opening is not known since it cannot be measured.

The lack of analytical tools has become even more obvious with recent rapid advances in soil tunneling technology. Important improvements have been made with the introduction by European and Japanese manufacturers of the Slurry, Earth Pressure Balance and Mud shields. These machines utilize closed-face rotary cutter heads to excavate the soil and provide almost continuous support of the heading, preventing movements into the shield along the longitudinal axis of the tunnel. Limited field data suggest that ground movements are relatively small when such shields are used. At present, there is very little understanding of the mechanisms involved in their operation, although they are being increasingly used in tunnel projects. The first application of these procedures in the United States has recently been completed in San Francisco for the N-2 contract of a sewer outfall which

passes under the famous Fisherman's Wharf area. The tunnel designer is now faced with an entirely new array of procedures, but with hardly any means of evaluating them.

1.3 RESEARCH GOALS

The problems posed by the new shield techniques necessitates the development of a means to predict the response of the ground in and around the shield machine. Distribution of stresses and displacements near the tunnel face must be analyzed by a three dimensional procedure. It is the objective of this thesis to develop and utilize a full three-dimensional finite element code which will allow the study and comparison of alternative soil tunneling techniques. With such a procedure, the performance of different shields under identical conditions can be examined. The results can be of value in themselves to engineers desiring to understand the nature of conventional and advanced shield tunneling. These results should also serve to enhance the effectiveness of future field measurements. The latter objective is especially important in view of the on-going effort at Stanford University where the performance of the Earth Pressure Balance Shield in the San Francisco project mentioned earlier is being monitored.

The features required of the finite element code are:

1. Treat tunnel in realistic manner

2. Be efficient

3. Allow for proper variation of gravity stresses in the ground and the properties of the ground.

4. Be of suitable form so that it can be extended in future work to include other variables.

In the following chapter, a review of different shield techniques and the various research work related to shield tunneling is presented. In Chapters 3 and 4, the finite element techniques developed to study the different shield techniques are presented. Chapter 5 covers the parametric analyses carried out in an effort to evolve rational modeling procedures for the different shield types. Finally, comparisons between these shield types are presented in Chapter 6, and information is developed to understand ground control processes applicable to the advanced shields.

Chapter II

SHIELD TUNNELING TECHNIQUES AND RELATED RESEARCH WORK

2.1 SHIELD TUNNELING TECHNIQUES

An accurate analytical study of shield techniques cannot be carried out without a proper understanding of the principles behind them. This chapter covers the points relevant to the modeling procedures used in this research. A summary is provided of the operation of the advanced shields; a more detailed discussion of these techniques is provided by Clough (1980).

2.1.1 Conventional Shield

2.1.1.1 Equipment and Its Operation

The basic principle of the conventional shield is to support the ground surrounding the opening temporarily during the time interval between excavation and liner erection. A typical conventional shield is cylindrically shaped and made of heavy steel plates. The cutting edge and hood are at the leading end of the body of the shield and the tail skin is at the rear. (See Figure 2.1). Retractable hydraulic shove jacks are mounted in a circumferential ring located inside the skin plate at the back end of the body of the shield.

The shield is advanced by thrusting against the in-place lining; corrections or changes are made in tunnel alignment by activating an

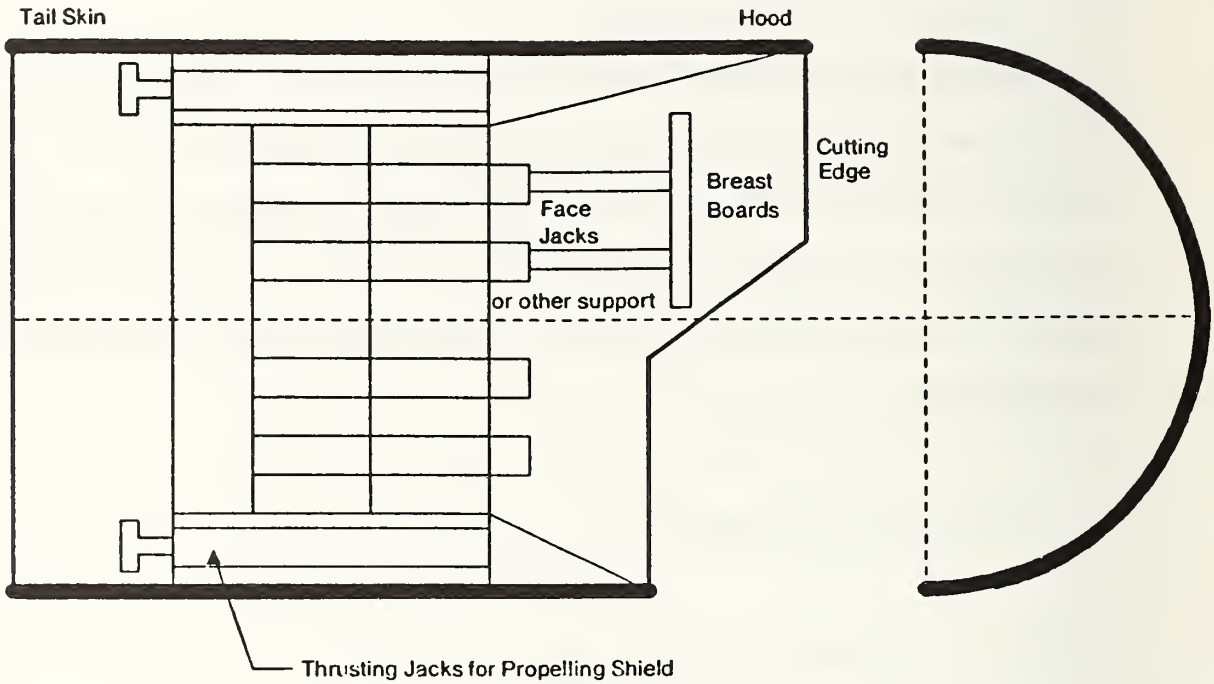

Figure 2.1: Cross-Section of Conventional Shield

individual jack or separate banks of jacks. For rigidity, a number of open-type diaphragms are used to brace the body of the shield. The diaphragms are composed of either ring beams or welded plate sections with horizontal and vertical structural members. These members divide the shield into working platforms or pockets from which the miners work.

The face of the excavation above the spring line may be supported by breast boards or mechanical breasting plates in order to prevent loose soils from collapsing through the face. For subaqueous tunneling in pervious soils, the conventional shield needs compressed air to prevent water from flowing into the tunnel. In such cases, the compressed air helps to maintain the stability of the face. Unfortunately, this also means that the tunnel workers must be in a compressed air atmosphere. This is a major drawback for the conventional shield.

2.1.1.2 Liner Erection

Extending back from the rear open diaphragm of the shield is the tail skin, the length of which is usually about 1-1/2 times the width of a single ring of lining. (See Figure 2.1). After shoving against the in-place lining, and with the tail skin overlapping half of the previously erected ring, the jacks are retracted and the lining segments are positioned by a segment erector pivoting about the axis of the shield. Flanged segments are then bolted to adjacent ring and to each other.

2.1.1.3 Tail Void

The diameter of the shield is about 2 in. to 4 in. (5 cm to 10 cm) larger than the outside diameter of the primary lining. Because of this difference, an annular void is created between the outside of the lining and the surrounding soil as the shield moves forward. This void is called the tail skin void or simply the tail void. It is a key element in the amount of settlement at the ground surface. To prevent ground loss, the void is usually filled with pea gravel blown through grout holes, assuming that it stays open after the shove. (See Figure 2.2). Grout can also be pumped through the same holes. Experience has shown however, that unless the soil has a considerable stand-up time, it will collapse onto the liner before the grout or pea gravel can fill the tail void.

2.1.1.4 Summary

The conventional shield has been developed to provide as immediate a support for the ground as possible during and after tunneling. However, it remains difficult to control movements into the face of the tunnel without the use of compressed air in the tunnel. Unfortunately, the costs associated with the use of compressed air have escalated rapidly over the past few years. This has accelerated the search for alternatives to the conventional shield as discussed in subsequent paragraphs.

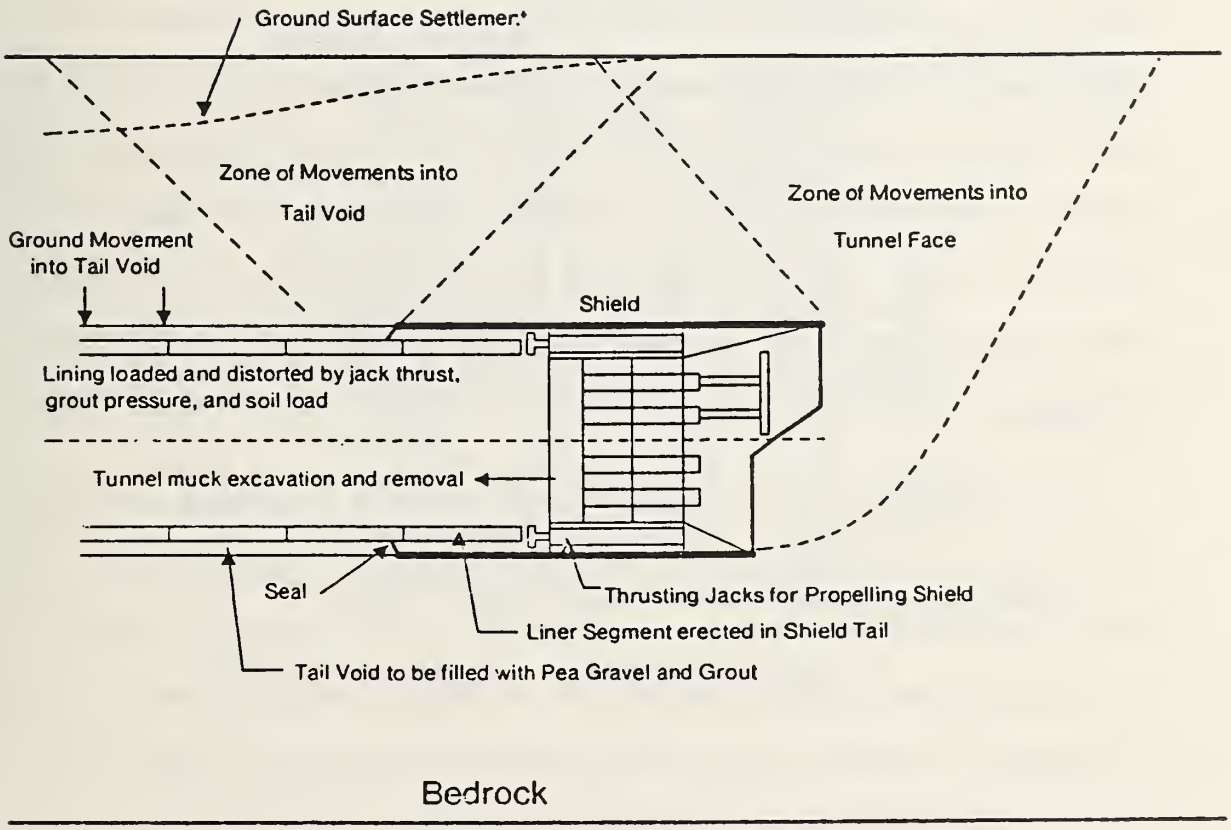

Figure 2.2: Ground Movements During Shield Tunneling
(Adapted from Schmidt, 1976)

2.1.2 Slurry Shield

2.1.2.1 Equipment and Its Operation

The basic principle of the slurry shield is that the face of the tunnel will be supported, and water flow into the tunnel stopped, by means of a pressurized soil-water slurry. It was developed to avoid the use of compressed air inside the shield and the tunnel as needed for the case of a conventional shield. The slurry shield has been used to excavate a tunnel under as much as 45 meters of water head. References containing information on the slurry shield include Abel et al., (1979), Bartlett et al., (1973), Leeney (1978) and Takahasi and Yamazaki (1976).

Basically, the equipment consists of a shield body and a rotating cutter head. During the operation of the machine, the space between the cutter head and the bulkhead is occupied by slurry and soil cuttings. The cuttings come through openings in the cutter head while the slurry is brought in through pipes passing from the surface down through the tunnel. The shield is advanced using hydraulic jacks pushing against the in-place lining as in the conventional shield. A cross-section of a typical slurry shield is shown in Figure 2.3.

The slurry pressure inside the bulkhead is usually kept slightly above that needed to maintain face stability and prevent flow of ground water. Because of the pressure gradient, slurry tends to penetrate lightly into the soil and form a thin impervious cake of fine slurry particles on the face of the soil. This thin cake gives the face some of its stability.

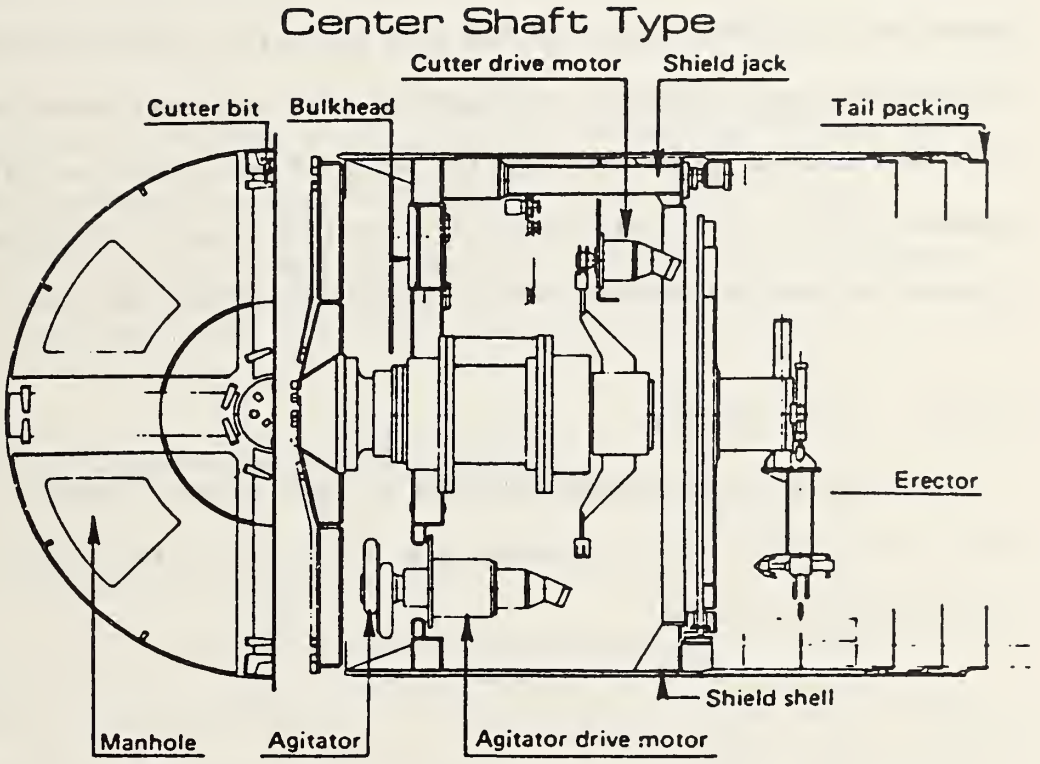

Figure 2.3: Cross-Section of Mitsubishi Central Slurry Shield (After Mitsubishi)

According to Clough (1980), the slurry pressure needed to ensure face stability is calculated on the basis of theory and experience. The water pressure to be balanced is obtained knowing the position of the water table while the soil pressure is obtained using an earth load analysis technique proposed by Terzaghi (1943) and Murayama (1966). In impervious soils, the larger of the soil and water pressures is used. For pervious soils, however, the combined soil and water pressures are to be balanced for stability. On the basis of experience, an extra pressure usually 1 to 3 psi (10 to 20 kN/m^2) is added to the calculated pressure in order to produce the slurry cake described earlier.

2.1.2.2 Liner Erection

Liner segments are assembled using a power erector located in the tail of the shield. The procedure used is similar to that described for the conventional shield.

2.1.2.3 Tail Seals

Located between the tail of the shield and liner segments are the tail seals. These seals are not used in the conventional shield, but are very important in the slurry shield process because they prevent the flow of ground water, slurry or grout into the work area. They are usually made of laminated rubber and steel sheets or fine wire mesh.

2.1.2.4 Tail Void

The tail void is created in a way similar to that described for the conventional shield. However, the tail void created by the slurry

shield is likely to be as large as, or larger than that created by the conventional shield because of the presence of tail seals in the former. Clough (1980) reports that in the deflected position behind the liner, the seals occupy a space of about 2 in (50 mm). This annular space around the liner plus the thickness of the skin of the shield constitute the tail void.

The slurry at the face of the tunnel may or may not migrate around the shield to support the tail void, depending on the soil type. Support of the tail void comes from grouting done as early as possible after the shield advances.

2.1.3 Earth Pressure Balance (EPB) Shield

2.1.3.1 Equipment and Its Operation

The basic principle of the Earth Pressure Balance or EPB shield is that by keeping excavated soil in contact with the tunnel face at all times and under enough pressure to prevent soil movement, the face is stabilized. Two important components of the shield equipment are the spoil chamber located between the cutter head and the bulkhead, and the screw conveyor at the rear end of the shield. A cross-section of the EPB shield is shown in Figure 2.4.

A key feature of the EPB shield is the screw auger and the rate at which it removes excavated soil from the bulkhead area. If this rate is the same as the rate at which new spoil is brought into the shield, the bulkhead area is filled with soil at all times and the flow of soil from the face into the shield is prevented.

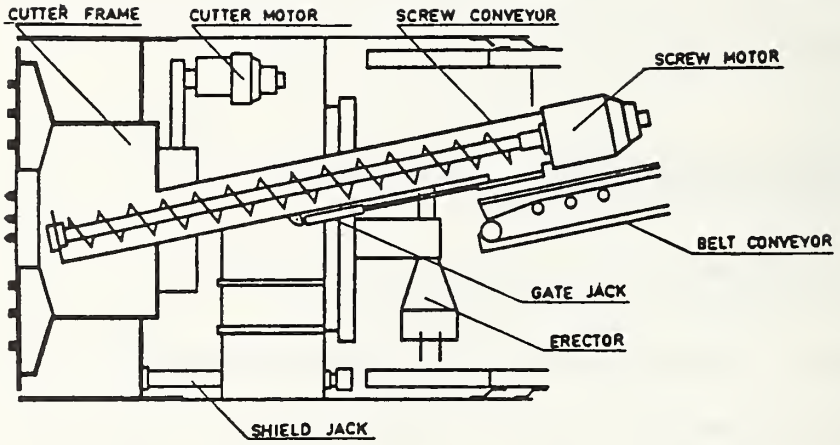

Figure 2.4: Cross-Section of Earth Pressure Balance Shield

The shield is advanced by means of hydraulic jacks reacting against the in-place lining. Pressure may be kept on the tunnel face by carrying the shield advance as a steady forward movement. In theory, this constant pressure balances the external earth pressure. In actual practice, the thrusting force from the hydraulic jacks can have the effect of pushing the soil ahead of the face. This pushing effect can cause heaving of the soil, especially where earth cover is thin. Field measurements made by Kitamura et al., (1981) and by Stanford University (Clough et al., 1982) confirm that heaving can occur in tunneling with the EPB shield. A diagram of time dependent change in ground surface settlement plotted from the field measurements of Kitamura et al., (1981) in a diluvial clay layer is shown in Figure 2.5.

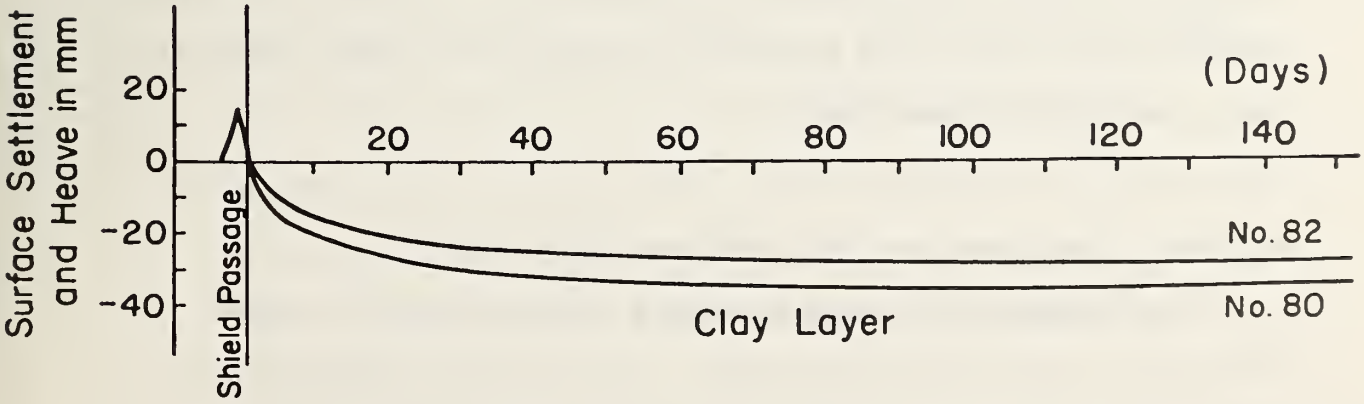

Figure 2.5: Time-Dependent Change in Settlement

The diagram shows that the ground surface is pushed up slightly before the shield passes, and subsequently begins to settle. This behavior is significant to the analysis of the EPB shield as will be discussed in Chapter 6. Instrumentation of an EPB shield project by Stanford researchers Clough, et al., (1982) has also shown the initial heave process very clearly.

The EPB shield is used primarily in silts, clays and sands above the ground water table. In sands below the water table, special action must be taken to prevent ground water flow into the tunnel. These may include chemical stabilization of the sands if they are of limited extent. An alternative approach to the problem is to use a version of the EPB shield called the Water Pressure Balance Shield in which water pressure can be applied to the face of the tunnel through the screw auger system. The water pressure balances the ground water pressure and prevents the flow of ground water into the tunnel. This type of shield has been used on only a few projects as opposed to the rather extensive use of the slurry or EPB shield.

2.1.3.2 Liner Erection, Tail Seals and Tail Void

Liner segments are assembled using a similar procedure to that described for the conventional shield. Like the slurry shield, tail seals are needed between the tail of the EPB shield and the liner segments to prevent ground water or grout flow into the work area. The tail seal problem -- the fact that the seal must occupy about 2 in. (50 mm) between the tail of the shield and the liner, exists in the case of the EPB shield also. Thus, prompt grouting of the tail void is important for movement control.

2.1.4 Mud Pressurized or Mud Shield

2.1.4.1 Equipment and its Operation

The Mud shield uses the concepts employed in the Slurry and EPB shields. It uses an open spoke cutter--a departure from the closed face cutter head used in the Slurry and EPB shields. The bulkhead located behind the cutter head is penetrated at the bottom by a screw auger which removes soil cuttings into the shield. The procedure used to handle soil is similar to that for the EPB shield: the screw auger removes the muck and drops it into a conveyor belt for transport.

Face stability is achieved as follows:

1. As soil is broken by the cutter, special slurry is mixed with the soil in the area between the cutter head and the bulkhead. The slurry and soil mixture behaves not as a fluid, but as a very plastic mass. The slurry admixture renders the soil impermeable, thus preventing the flow of water through the screw auger.

2. Enough pressure to prevent tunnel face instability is applied to the plastic mass. The mixture is removed by the screw auger at a rate so that the amount removed is equal to the advance volume of the shield.

2.1.4.2 Liner Erection, Tail Seals and Tail Void

Liner segments are erected as described for the other shields. Like the slurry and EPB shields, tail seals are required. Thus, the creation of a large tail void results. Grouting of the tail is therefore critical.

2.1.5 Shield Usage

The conventional shield has been used extensively under a variety of soil conditions. It remains the most widely used technique, particularly in the United States where contractors have been slow to adopt the advanced shield tunneling techniques.

The slurry shield has been the most widely used of the advanced shields primarily because it was developed first. It has been used under a variety of soil conditions: mixed alluvial soil, gravelly sands and even fills with wooden obstructions (Clough, 1980). It is also suitable for subaqueous tunneling. Kurosawa (1979) reports its use under 135 ft. (41 m) of water head. A major drawback to wider use of the slurry shield is its high cost. Thus, unless soil and ground water conditions necessitates its use, alternative advanced shields which are cheaper to build and operate are employed instead.

At its present rate of use, the EPB shield may soon replace the slurry shield as the most widely used advanced shield. It is cheaper than the slurry shield and avoids the complex procedure for slurrying and treating the muck. However, there are soil conditions where it cannot be used at present. With further developments, such as the

addition of water pressure balance scheme to the EPB shield, the range of conditions under which it can be used may be extended.

The mud shield has been used the least of the advanced shield machines. It is the most recently developed and has had little opportunity yet to be tested in the market place. It has a number of advantages however, particularly in that it theoretically can be used in a wide variety of ground conditions and is cheaper than the slurry shield.

2.1.6 Summary

The basic equipment and operation of the conventional shield and three advanced shields have been covered. Perhaps the most important difference between the conventional shield and the advanced shields is the use, in the latter, of pressure applied through a medium to the tunnel face to minimize soil movement into the shield. As a result, advanced shield proponents argue that surface settlements are smaller than with conventional techniques. However, due to the presence of tail seals in the advanced shields a significant tail void is created which can contribute to ground movements. The primary reasons being offered for increased advanced shield usage are, control of ground water without need for compressed air in the tunnel and better control of the ground itself, resulting in smaller movements.

2.2 RELATED RESEARCH WORK

Studies related to the distribution of stresses and displacements around underground openings have consisted mostly of field measurements, laboratory model tests, and to a lesser extent finite element analyses. Work done in these three areas is briefly reviewed.

2.2.1 Field Measurements -- Concepts and Data

Field measurements around and ahead of an advancing tunnel have been widely reported in recent years. (Hansmire and Cording, 1972; Hansmire, 1975; Schmidt, 1974; Cording and Hansmire, 1975; Attewell and Farmer, 1974). In order to discuss their data, an understanding of certain basic concepts is useful.

In many cases in tunneling, ground movements are expressed in terms of lost ground. The lost ground is the volume which displaces into the theoretical tunnel cross-section as a result of soil movements. It is calculated by summing up the displacements around the periphery which result from removing the original supporting stresses. This quantity is expressed as the volume per unit length of the tunnel. Assuming a purely elastic condition, the lost ground volume V_l is given by

$$V_l = \frac{\Delta V}{V_0} = \frac{(1+K)P(1+\nu)}{E} \qquad (2.1)$$

where

K = Total lateral earth pressure coefficient

V_0 = Theoretical tunnel volume

ΔV = Volume reduction

P = Total overburden stress at the springline

ν = Poisson's ratio

E = Modulus

For saturated clay soils, in the inelastic range, if K = 1, the relative lost ground volume is given approximately by

$$V_l = \frac{\Delta V}{V_0} = \frac{2C(1+\nu)}{E_u} \exp\left(\frac{P}{C} - 1\right) \qquad (2.2)$$

where C is the cohesion and E_u is the undrained modulus applicable to clay in the elastic state. Equation 2.2 assumes no volume change in the plastic zone. (Poisson's ratio ν = 0.5). If an interior pressure (e.g., slurry pressure) of magnitude P_i is applied, identical equations apply with $(P-P_i)$ substituted for P.

From data on clays, it is known that the ratio E_u/C does not vary much. For low plastic clays, C/E_u varies between 0.002 and 0.00067 (Clough and Schmidt, 1977). Using the the value of C/Eu, the maximum lost ground without internal pressure is

$$V_l = m \exp\left(\frac{P}{C} - 1\right) \qquad (2.3)$$

for $P/C \geq 1$, and

$$V_l = m \frac{P}{C} \qquad (2.4)$$

for $P/C < 1$,

where m is a factor varying between 0.0006 and 0.002.

Figure 2.6 shows a graphical representation of equations 2.3 and 2.4 by Clough and Schmidt (1977). A number of field data points are also shown on the graph. The field data indicate that for overload factors (OF = P/C with C taken at the tunnel springline) greater than about 2.5, the data points are consistently below the theoretical curves; they are often above the curves for overload factors less than 2.5. The investigators drew the following conclusions from the graph in Figure 2.6:

1. For overload factors smaller than about 2, the theoretical potential ground loss is less than about two percent. The actual ground loss may be greater than the theoretical value because of loosening along fissures in overconsolidated clays. For these values of OF, no shield is required for soil stability.

2. A potential ground loss of about ten percent is attained for overload factors between about 2 and 4. For these values of OF, ground movements through the tunnel face are small, but the use of a shield is advised.

3. For overload factors between 4 and 6, a shield is required to minimize settlement. The shield serves to reduce face displacements, but for values of OF near 6, the face displacements are of such magnitude that face support is advised.

Clough and Schmidt (1977) also reviewed data on face movements during shield tunneling. They observed that about one-quarter to

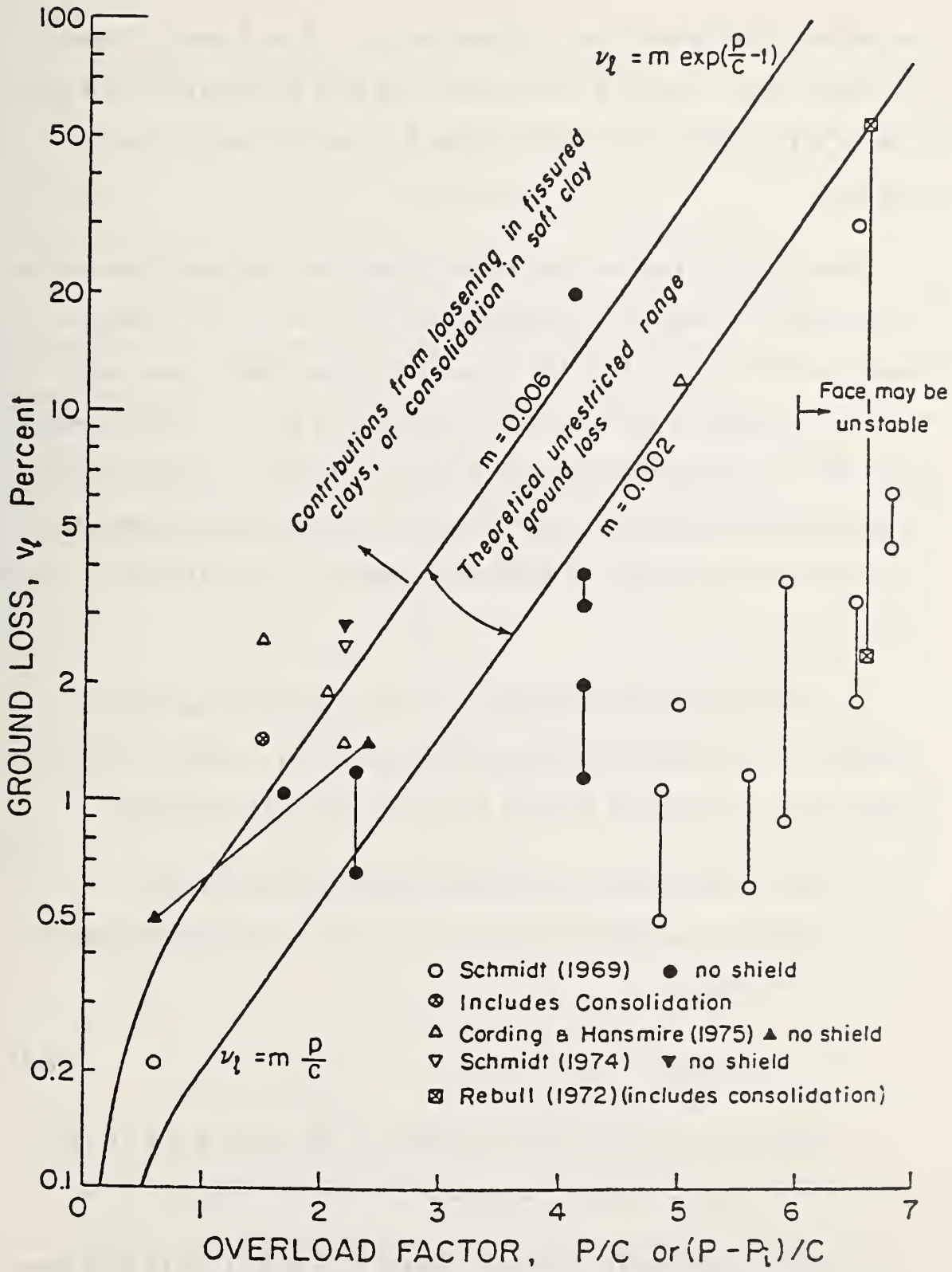

Figure 2.6: Relationship Between Overload Factor and Ground Loss (After Clough And Schmidt, 1977)

one-third of the ground loss in clays with OF = 2 to 5 occurs through the tunnel face. Figure 2.5 shows that the face contribution to ground loss is even higher for OF greater than 5 if no face support is supplied.

Rebull (1972) examined the effect of halting the tunnel advance on displacements by measuring displacements at several points along the tunnel axis and in front of the tunnel face under that circumstance. The soil encountered was soft clay (OF between 6 and 7). Displacements were observed at a distance within 2.5 to 3.5 times the tunnel radius. Terzaghi (1943) and Ward (1969) also noted that ground movements begin at least a distance equal to twice the radius for a variety of OF values.

A detailed summary of data on lost ground from various tunnel projects is provided by Cording and Hansmire (1975). Based on the field measurements, the authors derived two useful empirical formulae:

1. Where lateral and vertical displacements were measured immediately adjacent to the tunnel, volume lost into the tunnel, V_l is given by

$$V_l \simeq S_{mc}\, d \qquad (2.5)$$

where S_{mc} is the maximum settlement at the crown and d is the diameter of the tunnel opening.

2. Where a settlement point was located 0 to 6.6 ft (0 to 2 m) above the crown of the tunnel the data indicate that the volume lost V_l estimated from deep vertical displacement is given by

$$V_l \simeq \delta_v \, 2(r+y) \tag{2.6}$$

where

δ_v is the deep vertical displacement

r is the radius of the tunnel

y is the distance of the settlement point above the crown.

The distance y is assumed to be small with respect to r. V_l is overestimated for y approaching r.

In order to find surface settlement from the volume of lost ground, one must relate the two. To do this, the following facts are relevant:

1. When tunneling in clay, since the initial ground loss occurs without volume change (i.e., undrained conditions) the volume of the settlement trough is approximately equal to the ground loss in the tunnel.

2. The shape of the settlement trough approximates that of the error function (Schmidt, 1969). The equation for the settlement trough is given by

$$S = S_{max} \exp\left(\frac{-x^2}{2i^2}\right) \tag{2.7}$$

where S_{max} is the maximum settlement over the center line of the tunnel, and i is the distance from the center line to the point of inflection of the curve. The shape of the curve given by equation 2.7 is shown with other characteristics in Figure 2.7.

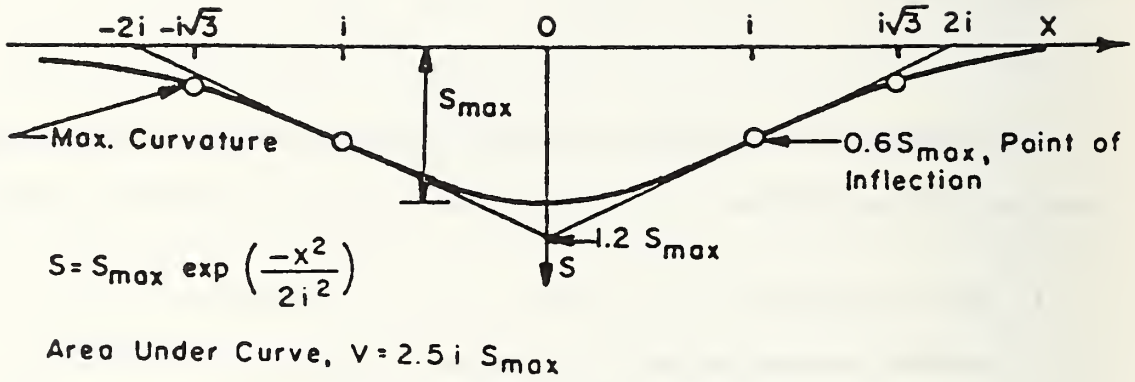

Figure 2.7: The Error Function Used to Describe the Settlement Trough (After Schmidt, 1967)

3. The volume of the settlement trough (per unit length along the center line) is given by

$$V = 2.5\ i\ S_{max} \tag{2.8}$$

4. From empirical evidence, the quantity i can be determined approximately based on purely geometric considerations for tunnels in clay as follows:

$$\frac{i}{a} = \left(\frac{z}{2a}\right)^{4/5} \tag{2.9}$$

where Z is the depth at the tunnel centerline and a is the tunnel radius.

Equation 2.9 is shown with data from the sources indicated in Figure 2.8. Thus, with the data and empirical relations, the shape and size of the settlement trough, for a given ground loss, can be determined.

To establish an acceptable ground loss, a maximum permissible slope of the settlement trough (relative differential settlement) is specified. The value of the maximum permissible slope (i.e., the limiting distortion expected prior to structural distress) is usually 1/300 (Clough and Schmidt, 1977).

The maximum slope of the trough occurs at distance i and is given by

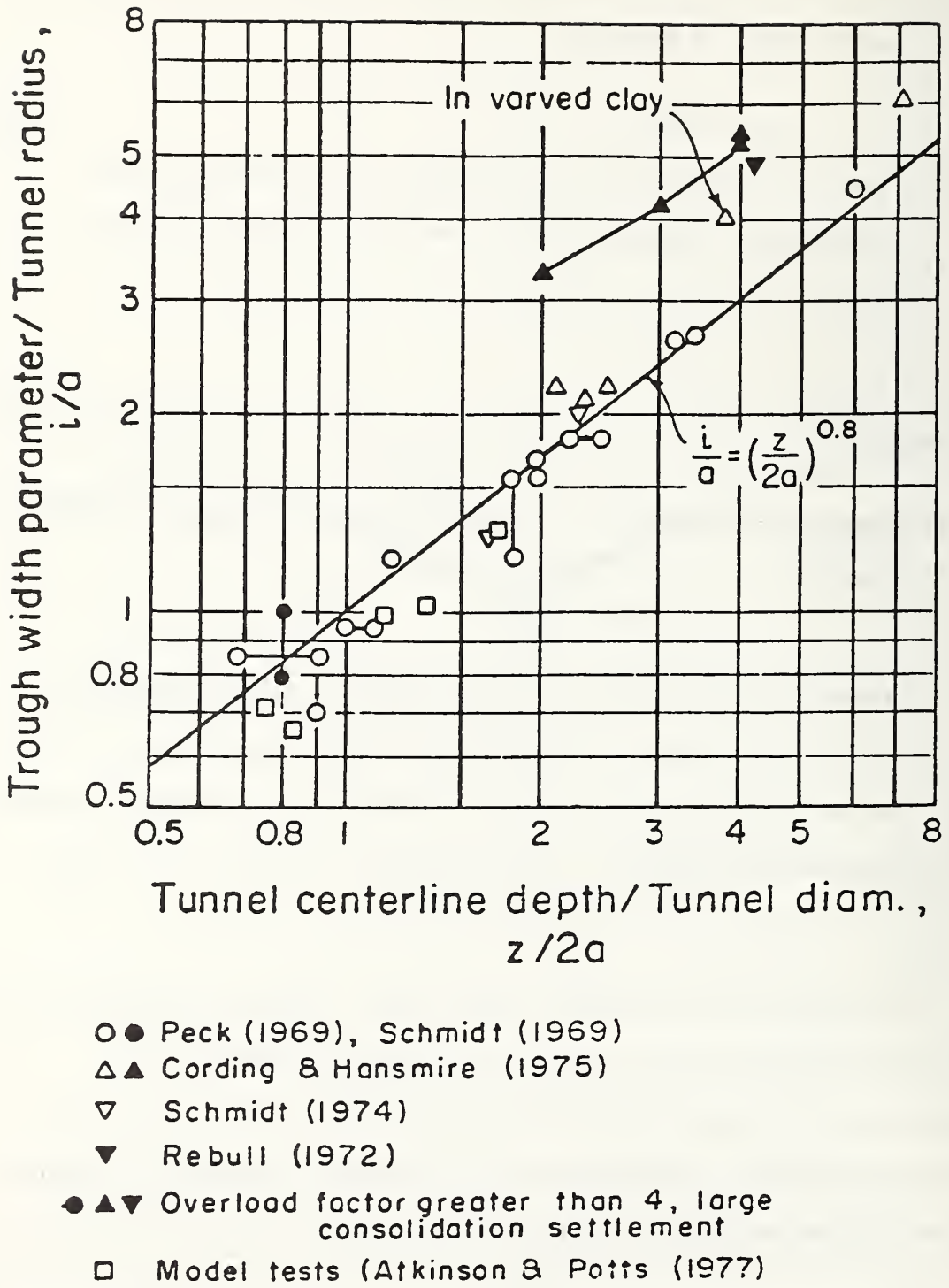

Figure 2.8: Settlement Trough Width Parameter i vs. Tunnel Depth z, Normalized Logarithmic Plot
(After Clough And Schmidt, 1977)

$$\frac{ds}{dx} = \frac{0.61\ S_{max}}{i} \qquad (2.10)$$

To obtain S_{max} for a given ground loss V_l, the equality of volumes is invoked.

$$\frac{\pi a^2 V_l}{100} = 2.5i\ S_{max} \qquad (2.11)$$

$$S_{max} = 0.0126\ V_l \frac{a^2}{i} \qquad (2.12)$$

Using equation 2.9 to obtain i, we have

$$\frac{ds}{dx} = 0.023\ V_l(\%)\left[\frac{a}{z}\right]1.6 \qquad (2.13)$$

This equation will show whether an estimated ground loss V_l will produce unacceptable differential settlements for a given tunnel depth Z and radius a.

2.2.2 Model Tests

Model tests have often been used to study tunnel behavior because the control of variables can be readily carried out. In some cases, stresses and displacements have been measured around the tunnel opening. Galle and Wilhoit (1969) performed several three dimensional photo elastic experiments to study the distribution of stresses around the bottom of a well bore. They found that with the hydrostatic loading, all the stresses around the bottom of the hole were compressive whereas zones of tensile stresses were formed for certain combinations of

unequal principal stresses. Abel and Lee (1973) also conducted several model tests in which they measured stress changes occurring at a point as a cylindrical hole was deepened towards it. The two researchers compared their results to those of Galle and Wilhoit and found that the only difference between the two sets of data was a small compressive stress concentration observed in their results, but absent in the latter's.

Researchers at Cambridge have carried out numerous tests to study ground deformations around tunnels (Atkinson and Potts, 1977a, 1977b; Atkinson et al., 1978). These tests, performed under static conditions and in the centrifuge, were aimed at examining the nature of the deformations occurring about a conventionally mined tunnel prior to and at failure. Loose and dense sands and clay were the materials in which the tunnels were modeled. In the tests, deformations about the tunnel were measured as a load factor (LF) defined as the ratio of the actual stability ratio (N) and the stability ratio at collapse (N_c)

LF was increased from 0 to 1. The stability ratio N is given by

$$N = \frac{\sigma_s - \sigma_t + \rho g\ (C + D/2)}{C_u} \qquad (2.14)$$

where

σ_s is a uniform pressure applied at the ground surface

σ_t is the fluid pressure in the tunnel or tunnel support pressure

ρ is the soil density

C is the height of the tunnel cover

D is the diameter of the tunnel, and

C_u is the undrained shear strength of the soil.

The results indicate that in dense sand, at low stresses, vertical displacements decrease rapidly above the tunnel crown in association with dilation close to the crown. However, in loose sand and clay, little dilation and much less attenuation of displacements with the distance above the tunnel was observed. (Atkinson and Potts, 1977b, Atkinson et al., 1978). Also, for a particular value of the load factor LF, the crown settlements in dense and loose sands and clay were found to be the same.

Atkinson and Potts (1977b) reported that their model test data suggest that there is a simple relation between the ratios V_s/V_t and S_s/S_c, where V_t is the amount of ground lost close around the tunnel; V_s is the amount of ground lost at the surface during tunneling, S_s is the maximum settlement at the ground surface over the tunnel axis, and S_c is the vertical displacement above the tunnel crown. The authors suggested a linear relation between the ratio S_s/S_c and depth:

$$\frac{S_s}{S_c} = 1 - \alpha\left(\frac{C}{D}\right) \eta \geq 0 \qquad (2.15)$$

where α is the average measure of the dilation of the ground. It is less than unity and is relatively large for dense sand at low stresses but relatively small for undrained clay. For sands, α has a value close to 0.40, and for normally or lightly overconsolidated soft clay under undrained conditions, the value is about 0.13. Field data suggest that this relationship is only approximate at best.

2.2.3 Finite Element Studies

Most of the previous analytical work relating to shield tunneling in soft ground have involved plane strain or axisymmetric analysis owing to the cost involved in a true three dimensional analysis. A brief survey of these investigations is presented in this section.

Kawamoto and Okuzono (1977) conducted a case history study of a shield driven tunnel constructed in a diluvium deposit in Nagoya City, Japan. This shield was a conventional machine. The surface settlement measurements were made by survey and the final values ranged from 9.8 in. to 27.6 in. (25 cm to 70 cm). They observed that 95% of the final settlement was finished when the face moved approximately six times the tunnel diameter (about 126 ft. (38.4 m)) beyond the point of measurement. To obtain settlements analytically, they used an empirical equation proposed by Murayama and Matsuoka (1969) to calculate settlement due to local yielding and a finite element analysis for the settlement due to instantaneous elastic deformation. The finite element analysis involved linear and nonlinear material models and plane strain conditions were assumed.

The results showed that a nonlinear finite element analysis using the hyperbolic nonlinear elastic model proposed by Duncan and Chang (1970) gives a reasonable indication of the magnitude and pattern of surface settlements. The authors concluded from a comparison of the field and analytical data that when only final surface settlement due to tunnel opening is required, it can be estimated from the summation of elastic settlement and settlement caused by local yielding. The former

is computed by elastic finite element analysis and the latter by the empirical equation proposed by Murayama and Matsuoka.

Sakurai (1978) performed a time dependent analysis of a tunnel support structure considering the progress of a tunnel face. To take into account the three dimensional effects of the tunnel face without actually performing a three dimensional analysis, he proposed an equivalent initial stress concept. This takes the three dimensional effects approximately into account in terms of two dimensional plane strain analysis. To make this possible, the tunnel is assumed to be located at a large depth beneath a horizontal ground surface. Thus, the tunnel approximates an infinite plate with a hole in it under uniform compressive load. The tunnels considered were circular in shape and driven in homogeneous isotropic linear visco-elastic material having hydrostatic initial stresses. Mathematical formulations were developed to obtain closed-form solutions for the pressure action on tunnel support structures. The theoretical results were then used to interpret data obtained from field measurements.

The author concluded that the equivalent initial stress concept could be used to approximately account for three dimensional effects. The results showed that the maximum pressure acting on the tunnel support structure decreased with the delay in its installation time, provided no failure zone existed around the tunnel. It was found that if the tunnel support structure was installed after the tunnel face was a distance of one tunnel diameter away, the three dimensional effects due to the tunnel face became negligibly small.

Ranken and Ghaboussi (1975) used an axisymmetric finite element analysis to study the distribution of stresses and displacement mobilized around a deep tunnel being advanced through a soil deposit. Unlined, partially lined and completely lined tunnels were considered. Linear elastic and elasto-plastic material behavior were assumed. The aim of this study was to relate the results obtained to the behavior of a liner placed by the extruded liner system described by Parker et al., (1971).

The results showed that the zone of three dimensional stress and strain (displacement) around an unlined tunnel advancing through a soil mass extends out to approximately 2 diameters ahead of the face and back approximately 1-1/2 diameters behind the face. Far ahead of the face, the two dimensional free field stress state remains undisturbed. It was found that at points farther than 1-1/2 diameters behind the face, the stresses correspond closely to the two dimensional plane strain distribution. Results from the elasto-plastic analysis suggest that if the average face displacement axially toward the tunnel is δ, then the ground loss per unit length of tunnel, contributed from the face is given approximately by

$$V_l = \frac{2\delta}{a} \tag{2.16}$$

where a is the tunnel radius.

Ghaboussi and Gioda (1977) also studied the time dependent effects in advancing deep tunnels. The investigators assumed an axisymmetric

condition around the center line of the tunnel and used Kelvin's model to approximate the creep behavior of the medium. The effects of various rates of excavation as well as those of a temporary interruption of the excavation process on stress and deformation distribution were studied.

The results indicated that a decrease of the rate of advance and the presence of an unsupported zone close to the tunnel face (partially lined tunnel) produce a noticeable increase in displacements around the excavation. Liner thrust was found to show a peak close to the tunnel heading and to reach a constant value 2 tunnel diameters behind the face of the tunnel. If the excavation process was temporarily interrupted, a large increase in displacements took place with time in a zone extending 1 to 2 diameters ahead of the leading edge of the liner; no increase in liner deformation was observed, however.

Tan and Clough (1977) performed plane strain, axisymmetric and creep analysis of tunnels surrounded by grouted soil zones. The nonlinear behavior of the grouted material was simulated using the Duncan-Chang model and a modified Singh-Mitchell model was used for the creep behavior of the material. The results from the plane strain and axisymmetric analyses indicate that the higher stiffness of the grouted zone causes a reduction in the amount of deformations induced by tunneling. The creep analysis showed that the creep behavior of grouted soils causes surface settlement to increase with time, and that tunnel liners are needed to restrain this creep movement in order to maintain the settlement reduction effected by the grouted zone.

Johnston (1981) developed a finite element program to study time related consolidation settlements around tunnels in cohesive soils. He also included the large strain behavior around the tail void as it is closed. The Cam-Clay model was used to simulate yielding of the soil. The results indicate that consolidation settlement increases with increasing tail void size; and that the consolidation process substantially increases the bending stresses in the liner.

Orr et al., (1978) and Adachi et al., (1979) carried out finite element analyses, using the Cam-Clay model to simulate the response of the Cambridge model tests. They compared their results to the data from the model tests. Although the finite element results were qualitatively reasonable, they differed quantitatively from those of the model test.

Finally, Hansmire et al., (1981) performed a number of two dimensional finite element analyses in conjunction with field monitoring during the construction of the Red Hook intercepting sewer in Brooklyn, New York. A section of this sewer tunnel passes over two subway tunnels and the investigation was related to this crossing. Elastic soil properties were assumed and shove jack forces were simulated by a prestressed strut which simultaneously pushed forward on the shield and reacted backwards on the lining. The results from these analyses were used in conjunction with field monitoring to decide on construction procedures for the special problem at the crossing.

A number of three dimensional analyses has been carried out by various researchers (Gartung et al., 1981; Azzouz et al., 1979). However, these analyses have been related to specific tunnel problems.

2.2.4 Summary - Related Research Work

A review of literature has revealed that little work using true three dimensional analyses of shield driven tunnels in soils has been carried out. Where three dimensional analysis has been applied, it has been related to specific problems typically large underground chambers. Most work has utilized plane strain and axisymmetric approaches instead. These approaches are applicable for certain limited cases, however, they cannot correctly model the shield tunneling problem at shallow depths since this is a three-dimensional situation.

Field measurements have been useful in indicating the deformation behavior of tunnels, but not in defining the earth pressures in the ground. Also, meaningful comparison of alternative shield types with field data is not possible to date since the ground loading conditions are typically unique to each project. Model tests have provided certain useful basic data on ground behavior around tunnel type openings. However, they have not successfully simulated an advancing tunnel with a shield.

The preceding discussion indicates that there is a need for a three dimensional finite element analysis with which one compares alternative shield types and assess their effects on the all important surface settlements. In this study, the behavior near the tunnel face is simulated through a three dimensional formulation. Modeling procedures are proposed to simulate the actual shield tunnel construction as closely as possible.

Chapter III

DEVELOPMENT OF BASIC FINITE ELEMENT CODE FOR SHIELD TUNNELING

3.1 INTRODUCTION

In this chapter, the steps taken in the basic development of a three dimensional finite element code for geotechnical applications are presented. In the next chapter, the aspects of the code relating specifically to shield tunneling are discussed. A number of texts on finite element analysis cover the basics of the theory of three dimensional analysis, especially with respect to the elements available. (Zienkiewicz, 1977; Brebbia and Connor, 1974). These texts provided valuable information towards the work of this chapter.

It was established in Chapter 2 that the ground surface movement resulting from shield tunneling is primarily a function of the movements around the tunnel face and tail void. If the face is unstable, or if a closed face shield forces the soil outwards, the resulting displacements at the surface are affected by the on-going movements around the moving shield. In this case, a plane strain or two dimensional analysis is not suitable to analyze the problem. Considering advanced, closed-face shields where soil movements at the face of the tunnel may be away from or into the face, a three dimensional type of analysis is needed.

One simplified form of three dimensional analysis which has been used for tunnel study is the axisymmetric type. Ranken and Ghaboussi

(1975) have investigated face stability using this procedure. This approach is useful as an initial study tool, however, the tunnel is assumed to be at such a depth that its behavior is not affected by the ground surface, and the ground stresses cannot reflect a gravity stress distribution. Also, any layering in the soil profile or systematic changes in properties of the soil cannot be considered. Furthermore, only circular tunnels can be studied unless Fourier expansions of forces and displacements are used (Wilson, 1965). Thus, the axisymmetric approach is too limited to be useful for the present study.

The preceding discussion suggests that a full three dimensional analysis is most appropriate for the advanced shield problem. A three dimensional representation takes into account the presence of the ground surface whose deformation is of interest. It considers the variation of initial stresses with depth due to gravity, and allows for the specification of arbitrary material properties with depth as well as eliminating other restrictions associated with axisymmetric representation.

The major reason for the avoidance of a full three dimensional analysis by previous investigators has been the large amount of computer time and funds required for such an analysis. It was therefore a primary objective in the development of the finite element code for this work to maximize efficiency so as to keep costs in a realistic range.

3.2 CHOICE OF FINITE ELEMENT METHOD AS ANALYTICAL TOOL

Prediction of stresses and displacements resulting from a shield tunneling operation requires the analysis of problems characterized by complex geometry and loading and possibly non-homogeneity of materials. The geometry and loading are further complicated by the fact that the initial stresses increase with depth due to gravity effects and by the nearness of shallow tunnels to the ground surface. It is very difficult and sometimes impossible to analyze such problems by methods of classical continuum mechanics. Thus, numerical methods of stress analysis are often considered, and the finite element method is the logical choice because it can be designed to handle the problem mentioned previously.

3.3 CHOICE OF A CODE

One of the major decisions faced in the development of the code was whether any of the existing general finite element codes such as SAPIV, NONSAP, ADINA, and NASTRAN among others could be used for the analytical studies and if so which one. Unfortunately, general as these codes may be, they were written with certain types of problems in mind. Thus, extensive modifications would be required to adopt them for the shield-driven tunnel. They do not have routines to calculate initial stresses or to simulate excavation. Also, some of the codes are structured in such a way as to make them unsuited to the incremental type of analysis required in the analysis of tunnels. Furthermore, others, ADINA being an example, were unavailable without the payment of expensive fees required to join a users group. For these reasons, a new

code was written for the investigation using some of the existing codes as a guide. In this way, the objective of ensuring efficiency could be attained because better numerical procedures developed after some of the existing codes had been written, were incorporated. For example, SAPIV uses a banded storage scheme for the stiffness matrix, but improved storage schemes are presently available. Also, extraneous routines which are present in general purpose codes were avoided. This is especially important in a three dimensional code where computer storage requirement is usually high. It is also easier to attain the objective of making the code of suitable form so it can be extended in future work to include other variables by writing an original version.

3.4 ELEMENT SELECTION

For the finite element representation of the tunnel system (tunnel, liner and shield), three elements were considered: the simple tetrahedral element or the 8 node brick element or the 8 to 21 variable number of nodes element to represent the soil mass, and a thin shell element or the 8 to 21 variable number of nodes element to represent the liner and the shield.

The division of a large space volume such as encountered in tunnel analysis into individual tetrahedra at times present difficulties of visualization and could easily lead to errors in nodal numbering, etc. For this reason, the tetrahedral element was not given much consideration. A more convenient alternative is the subdivision of space into 8 node cornered brick elements. Thus, in this investigation, the initial choice of element to represent the soil mass was the 8 node

isoparametric element with three translational degrees of freedom per node (Figure 3.1). It was then planned to represent the liner with the thin shell element used in SAPIV by Bathe et al., (1974). This shell element is a quadrilaterial of arbitrary geometry formed from four compatible triangles.

Within an isoparametric 8 node brick element, the strains and hence the stresses are constant. Unfortunately, this particular property of the brick element can be a drawback for the type of coarse meshes anticipated for use in this research, since the variation of stresses between integration points within an element can be significant. For this reason, a general three dimensional isoparametric or subparametric element which may have from 8 to 21 nodes (Figure 3.2) was used instead of the 8 node brick element. This element allows for the variation of stresses between integration points within an element. A major advantage of the variable number of nodes element in tunnel analysis is that more nodes could be used in areas of stress concentration such as around the tunnel opening and less nodes elsewhere. This variable number of nodes element can be used for thick shell analysis (Bathe et al., 1974). Thus, in this investigation, the same element was used to represent both the soil and the liner.

Like the 8 node brick element, each node of the variable number of nodes element has three unknown displacements. If the latter element is used as a shell element, and the shell is considered as a two dimensional surface, there are six unknowns per node. This formulation avoids the problem associated with the sixth degree of freedom: the

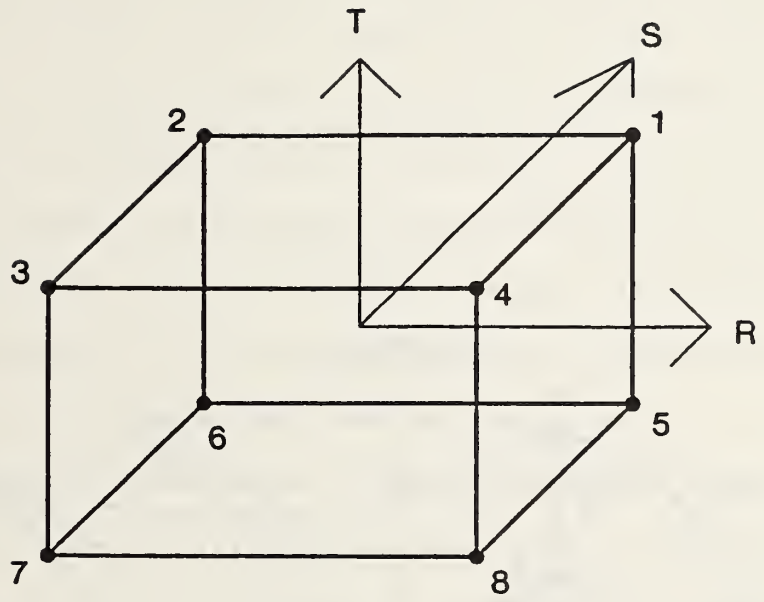

Figure 3.1: 8 Node Brick Element

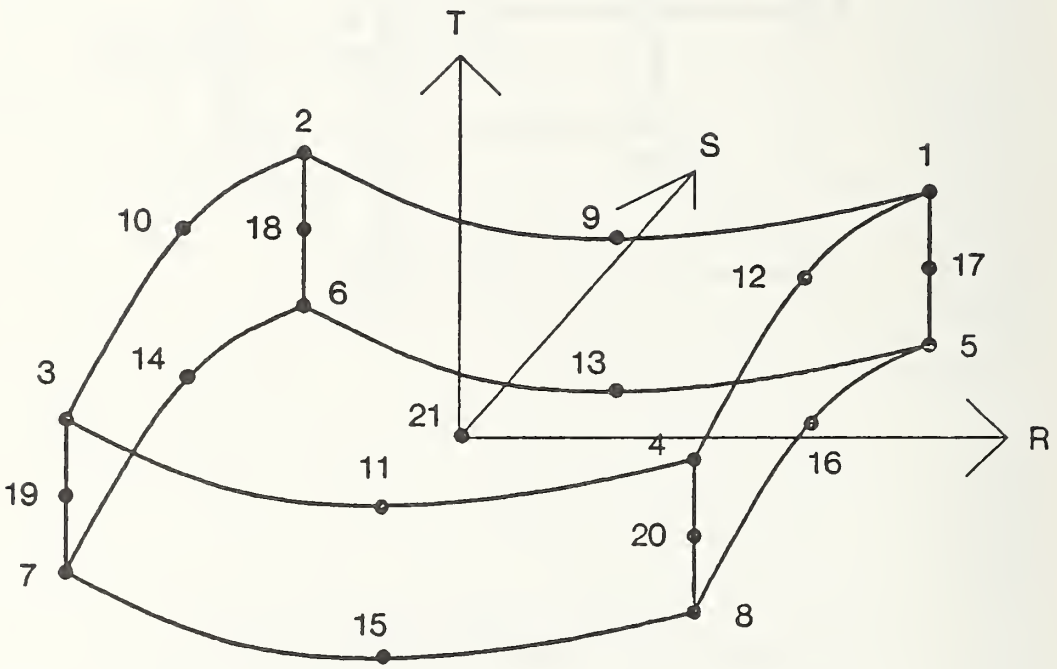

Figure 3.2: 8 to 21 Variable Number of Nodes Element

normal rotation is set to zero when certain finite elements are used in the idealization of shells. For example, in the analysis of flat plates, the stiffness associated with the rotation normal to the shell surface is not defined, therefore the degree of freedom associated with normal rotation is not included in the analysis (a drawback of the thin shell formulation mentioned above). This normal rotation capability of the variable number of nodes element improves accuracy in the use of the element to model the liner in the tunnel analysis. One drawback of the use of the element for shell analysis, however, is that the retention of three degrees of freedom at each node can cause problems. It leads to large stiffness coefficients for relative displacements along the edge corresponding to the shell thickness. When the shell thickness becomes small compared with other dimensions in the element, ill-conditioned equations may result. This fact was taken into account in the preparation of the mesh for the tunnel analyses presented in Chapters 5 and 6.

3.5 STRAIN AND STRESS COMPUTATIONS

The only constitutive model incorporated into the code as of the time of writing is linear elastic isotropic behavior. The reason for this situation is that the finite element code developed in this research is only the first step in an attempt to develop a general code for the analysis of different shield tunneling procedures. Future work will involve the incorporation of a nonlinear constituted model.

For linear elastic isotropic material, the elastic stress-strain relation is given by

$$\{\sigma\} = [D]\{\epsilon\} \qquad (3.1)$$

where $\{\sigma\}$ is the stress vector, $[D]$ is the stress-strain matrix and $\{\epsilon\}$ the strain vector. Equation 3.1 may be written in matrix form as:

$$\begin{vmatrix}\sigma_x\\ \sigma_y\\ \sigma_z\\ \tau_{xy}\\ \tau_{yz}\\ \tau_{zx}\end{vmatrix} = \frac{E}{(1+\nu)(1-2\nu)} \begin{vmatrix} d_1 & \nu & \nu & 0 & 0 & 0\\ & d_1 & \nu & 0 & 0 & 0\\ & & d_1 & 0 & 0 & 0\\ & & & d_2 & 0 & 0\\ & & & & d_2 & 0\\ & & & & & d_2\end{vmatrix} = \begin{vmatrix}\epsilon_x\\ \epsilon_y\\ \epsilon_z\\ \gamma_{xy}\\ \gamma_{yz}\\ \gamma_{zx}\end{vmatrix}$$

where E is Young's modulus

ν is Poisson's ratio

$d_1 = (1-\nu)$ and $d_2 = 1/2(1-2\nu)$

Strains and hence stresses are not constant within the variable number of nodes element and so they may be computed at any sampling point (R, S, T) within the element. In this code, stresses are computed at the Gaussian integration points because they are the best sampling locations (Zienkiewicz, 1977). Also, the stresses at these integration points are required in the excavation simulation scheme adopted in the code and described in Chapter 4. If needed, stresses can be determined at the center of an element.

For any general state of stress at any point, the principal stresses can be obtained by solving the cubic equation

$$\sigma^3 - I_1\sigma^2 + I_2\sigma - I_3 = 0 \qquad (3.2)$$

where σ is a principal stress and I_1, I_2, I_3 are stress invariants given by

$$I_1 = \sigma_x + \sigma_y + \sigma_z \tag{3.3}$$

$$I_2 = \sigma_x\sigma_y + \sigma_x\sigma_z + \sigma_y\sigma_z - \tau_{xy}^2 - \tau_{xz}^2 - \tau_{yz}^2 \tag{3.4}$$

and

$$I_3 = \text{Determinant of} \begin{pmatrix} \sigma_x & \tau_{xy} & \tau_{xz} \\ \tau_{xy} & \sigma_y & \tau_{yz} \\ \tau_{xz} & \tau_{yz} & \sigma_z \end{pmatrix} \tag{3.5}$$

If the direction cosine of the principal stress σ is given by (l, m, n), then by resolving in X, Y, Z directions, the following equations are obtained:

$$l(\sigma - \sigma_x) - m\tau_{xy} - n\tau_{xz} = 0 \tag{3.6}$$

$$-l\tau_{xy} + m(\sigma - \sigma_y) - n\tau_{xy} = 0 \tag{3.7}$$

$$-l\tau_{xz} - m\tau_{yz} + n(\sigma - \sigma_z) = 0 \tag{3.8}$$

In addition, the values of l, m, n must satisfy the law of direction cosines:

$$l^2 + m^2 + n^2 = 1 \tag{3.9}$$

To compute the principal stresses, equation 3.2 was solved in the finite element code using the goniometric method (Appendix A). The direction cosines were obtained by setting σ in turn to each of the three principal stress values, and observing the direction cosine condition, (equation 3.9), for each value of σ.

3.6 LOADING

Like any basic finite element code, this code has the capability to handle applied concentrated nodal loads and displacements. However, to model the advanced shield machines, especially with reference to the

application of pressure to the tunnel face, it was necessary to add a surface pressure loading capability to the code. The surface pressure loading was treated as follows:

Consider the $\zeta = +1$ face shown in Figure 3.3. The displacement and surface force distribution over the face is defined in terms of two dimensional interpolation functions and nodal quantities for that face. If u, P_x contain nodal displacements and force intensities for the $\zeta = +1$ face, then

$$\phi = \phi(\xi, \eta) \tag{3.10}$$

and on face where $\zeta = +1$,

$$v = \phi u \tag{3.11}$$
$$p = \phi p_x \tag{3.12}$$

where ϕ is the interpolation function, v is the displacement vector on the element face where $\zeta = +1$, and P is the force vector on the face where $\zeta = +1$.

The consistent nodal force matrix, P_v is then given by

$$P_v = \left[\int_{\eta}\int_{\xi}(\phi \text{ Transpose})\phi dS\right] p_x \tag{3.13}$$

To evaluate the integral, the differential surface area dS is expressed in terms of $d\xi$ and $d\eta$.

$$dS = d\xi d\eta \left|(\partial r/\partial \xi) \times (\partial r/\partial \eta)\right| = G d\xi d\eta$$

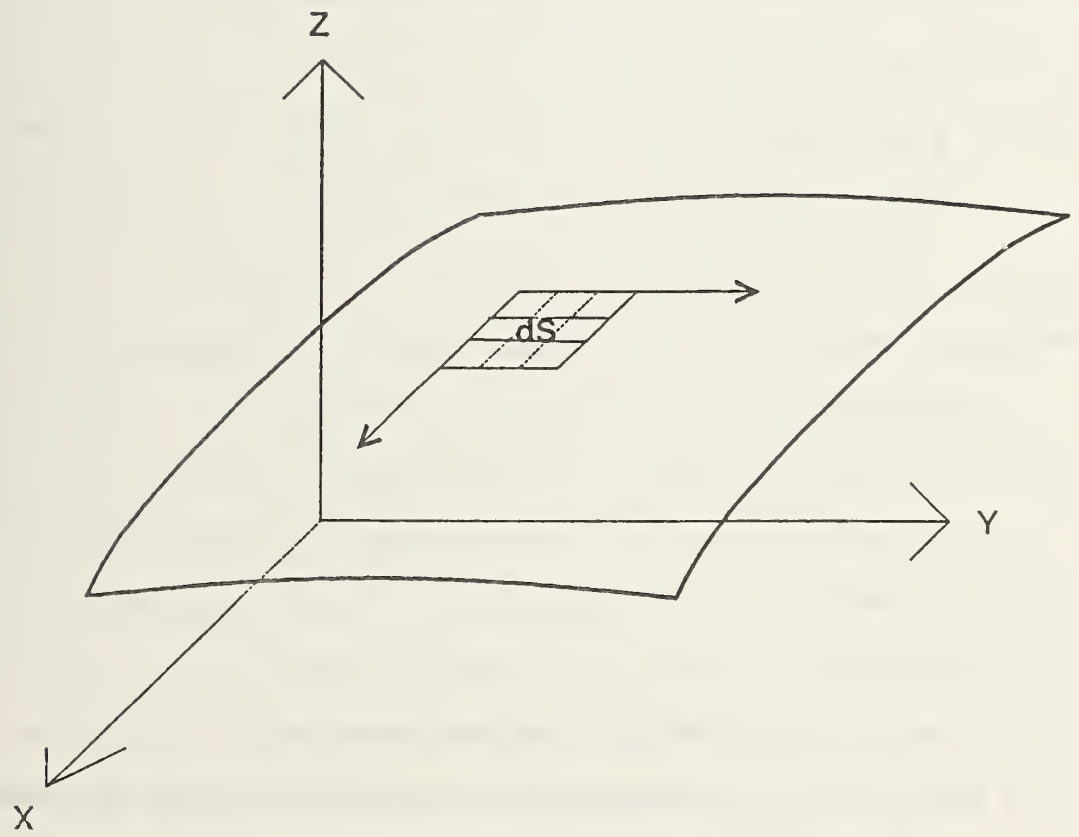

Figure 3.3: Surface Integration

where r is a vector and G is evaluated by expanding the vector cross product at the face where $\zeta=+1$.

The result is given by

$$G = (f_1^2 + f_2^2 + f_3^2)^{1/2} \tag{3.14}$$

where f_1, f_2, f_3 are coefficients expressed as

$$f_1 = P_2P_6 - P_5P_3$$

$$f_2 = P_1P_6 - P_4P_3$$

$$f_3 = P_1P_5 - P_4P_2$$

where $P_1 = \partial x/\partial \xi$

$P_2 = \partial y/\partial \xi$

$P_3 = \partial z/\partial \xi$

$P_4 = \partial x/\partial \eta$

$P_5 = \partial y/\partial \eta$

$P_6 = \partial z/\partial \eta$

and f_1, f_2, f_3 are evaluated at the face where $\zeta=+1$.

These coefficients are also contained in the expansion for the Jacobian.

3.7 STIFFNESS MATRIX STORAGE SCHEME AND EQUATION SOLVER

Since in three dimensional finite element analysis a significant portion of the storage space is devoted to the stiffness matrix, its storage scheme is a very important feature. In the solution of linear equations, the time required for computation is substantially increased when the stiffness matrix is stored on peripheral storage devices and brought in and out of core during the reduction and back substitution processes. For this reason, the stiffness matrix in the finite element code is contained entirely in main core memory.

In the code developed, the characteristic sparsity of a stiffness matrix was considered by stringing each column of the matrix compactly into a vector. This method is variously called the "active column", "skyline" or "profile" storage scheme. The "profile" storage scheme has definite advantages over a banded scheme. One advantage is that the former scheme always requires less storage unless the stiffness matrix is diagonal in which case the storage requirement is the same for both schemes. Also, the storage requirement in the "profile" method is not affected by few very long columns. Furthermore, with the profile method, it is easy to use vector dot product routines to effect triangular decomposition and forward reduction (Felippa, 1975). This last fact is very important in modern machines which are vector oriented. To exploit the symmetry of the matrix, none of the entries below the diagonal was stored.

A number of methods for solving large systems of linear equations have been reported in recent literature. (Wilson et al., 1974; and

Mondkar and Powell, 1974a, 1974b). In this finite element code, the reduction of the stiffness matrix and the back substitution for the displacements are carried out in core using a slightly modified version of an algorithm described by Mondkar and Powell (1974a). This equation solver is based on a Modified-Crout reduction procedure. The modified version of the algorithm incorporated in this code was first implemented by Mana (1978).

3.8 OTHER FEATURES OF THE CODE

3.8.1 Dynamic Storage Allocation

Because of the variable sizes of the arrays needed in different problems, it is very inefficient to fix the dimensioning. Thus, for efficiency, a dynamic storage allocation scheme was utilized in the code. In this scheme, the dimensions of arrays are set in the program at the time of execution. An error flag is triggered if insufficient storage is allocated.

3.8.2 Macro Programming

Because this research is the first step in an effort to develop a comprehensive three dimensional finite element code for advanced shield tunneling analysis, the ease of updating or extending the code was considered an essential feature. In present day practice, there are many complex and efficient systems for finite element analysis capable of dealing with very large numbers of variables and formulations. However, this very complexity means that it is difficult to update them

in order to introduce new developments of technology. For this reason, the macro programming concept proposed by Taylor (1977) was employed in the development of the code.

The macro programming language is associated with a set of compact subprograms each designed to compute one or a few basic steps in a finite element analysis. Examples of commands or mnemonics in macro language are those given to form global stiffness matrix, solve equations, print results, etc. The order in which the subroutines are called is determined by the user.

3.9 VERIFICATION OF CODE FEATURES

Several simple test runs were made using single elements loaded with concentrated and surface pressure loads to verify the features of the code described above.

3.9.1 Single Element With Concentrated Nodal Loads

A single element with 8 nodes was loaded with four concentrated loads, 25 lbs. (0.11 kN) each at the top nodes as shown in Figure 3.4. Movement is constrained in the X and Y directions, thus, only vertical or Z displacements could take place. The displacements may be calculated directly from continuum mechanics and compared to the results predicted by the code. The boundary conditions, and the theoretical and finite element results are shown in Table 3.1. There is excellent agreement between the theoretical and finite element data.

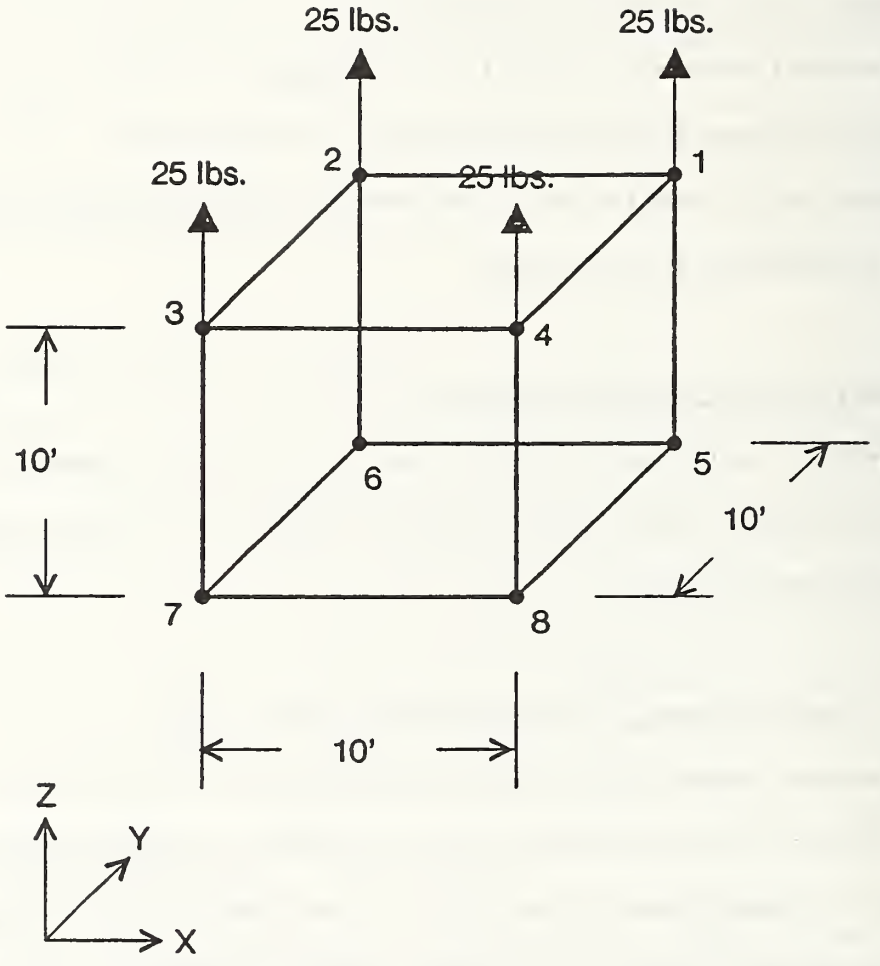

Figure 3.4: Single Element with Concentrated Nodal Loads

TABLE 3.1

Theoretical and Finite Element Results

Node Number	Nodal Restraint* X	Y	Z	Vertical or Z Displacement From Finite Element Analysis (Feet x 10^{-5})	Vertical or Z Displacement From Theory (Feet x 10^{-5})
1	1	1	0	7.42857	7.428
2	1	1	0	7.42857	7.428
3	1	1	0	7.42857	7.428
4	1	1	0	7.42857	7.428
5	1	1	1	0	0
6	1	1	1	0	0
7	1	1	1	0	0
8	1	1	1	0	0

* 1 indicates restraint

0 indicates no restraint

3.9.2 Single Element With Surface Pressure Loading

A single element with 20 nodes was loaded with a surface pressure load of 25 psf (1.2kN/m^2) as shown in Figure 3.5. The nodal restraints were such that displacements could only take place in the vertical or Z direction. The boundary conditions and the theoretical and finite element results are shown in Table 3.2.

The values of vertical displacements at the nodes indicate that there is excellent agreement between the theoretical and finite elements results.

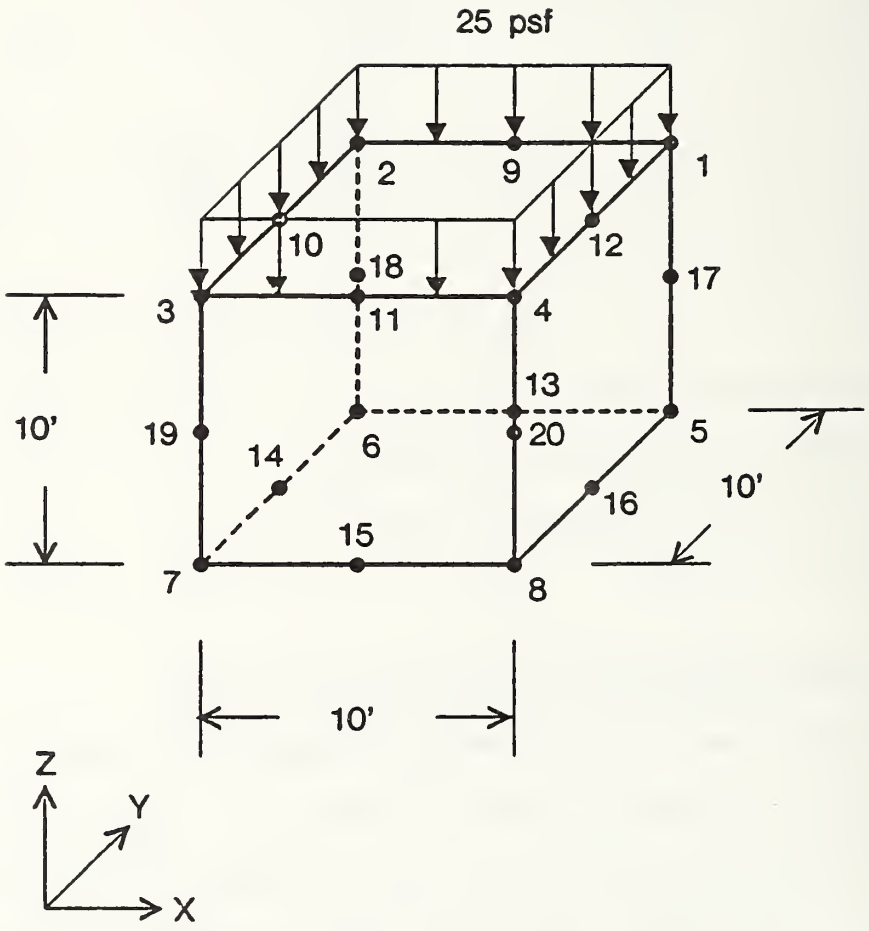

Figure 3.5: Single Element with Surface Loading

TABLE 3.2

Theoretical and Finite Elements Results

Node Number	Nodal Restraint* X	Y	Z	Vertical Displacement From F.E. Analysis (Feet x 10^{-3})	Vertical Displacement From Theory (Feet x 10^{-3})
1	1	1	0	1.85714	1.857
2	1	1	0	1.85714	1.857
3	1	1	0	1.85714	1.857
4	1	1	0	1.85714	1.857
5	1	1	1	0	0
6	1	1	1	0	0
7	1	1	1	0	0
8	1	1	1	0	0
9	1	1	0	1.85714	1.857
10	1	1	0	1.85714	1.857
11	1	1	0	1.85714	1.857
12	1	1	0	1.85714	1.857
13	1	1	1	0	0
14	1	1	1	0	0
15	1	1	1	0	0
16	1	1	1	0	0
17	1	1	0	0.928571	0.9285
18	1	1	0	0.928571	0.9285

* 1 indicates restraint

0 indicates no restraint

3.10 SUMMARY

In this chapter, the basis for the development of a full three dimensional finite element code is established. Instead of using one of the existing general purpose finite element codes, an original one was written. A three dimensional element with 8 to 21 variable number of nodes is chosen for the code. The larger number of nodes are useful in

modeling liner and shield response and soil behavior in areas near stress concentrations. In its present form, the code has a capability for linear elastic analysis only, but future work would include the incorporation of a nonlinear constitutive model. Special emphasis is built into the programming on efficiency in assembling the stiffness matrix and solving the large number of equations normally generated in a three dimensional analysis. Also, allowance is made so that gravity stress distributions and non-homogeneous soil profiles may be considered. Finally, capabilities are added so that surface pressure, concentrated force or specified displacements can be applied. These options are needed to model the tunneling process as described in the next chapter. Verification runs indicate that the analytic procedures incorporated in the code are accurate.

Chapter IV

FINITE ELEMENT MODELING OF SHIELD TUNNELING PROCEDURE

4.1 INTRODUCTION

For accurate modeling of a tunnel constructed by shield techniques, the following aspects of the tunneling procedure and the tunnel-ground system should be simulated:

1. Initial gravity stresses
2. Construction process -- excavation, shield advance and liner placement
3. The tail void or gap
4. The liner support system
5. The shield
6. Support of the soil by slurry or air pressure

In this chapter, the steps taken to simulate these aspects of the tunneling procedure are covered. The verification runs made to test the finite element code are also presented.

4.2 INITIAL STRESSES

In any excavation analysis, in-situ stresses play a significant role in the deformation behavior of the soil mass. In the finite element code, initial stresses can be calculated in two ways:

1. Gravity turn-on --

   a) In this procedure, the so-called primary state of stress within the soil and the corresponding displacements which have already occurred in nature are evaluated. The evaluation is conducted by performing a finite element analysis in which gravity loading is applied to all the elements. The resulting stresses $\{\sigma_0\}$ are the initial stresses. Because the present version of the code is linear elastic, the lateral stresses generated by this procedure are automatically taken as $\sigma_z \nu/(1 - \nu)$. The initial displacements and shear stresses were assumed to be zero.

2. Simplified initial stress calculation.

   a) In this procedure, the initial stresses $\{\sigma_0\}$ are assumed to be due to the weight of the overburden. Assuming a horizontal ground surface, the initial stress in each element is computed directly as a function of depth below the ground surface. In other words,

$$\sigma_z = \gamma H \tag{4.1}$$
$$\sigma_y = K_0 \sigma_z \tag{4.2}$$
$$\sigma_x = K_0 \sigma_z \tag{4.3}$$
$$\tau_{xy} = 0,\ \tau_{xz} = 0,\ \tau_{yz} = 0 \tag{4.4}$$

   where σ_z = Vertical stress

σ_x, σ_y = Horizontal stresses

τ_{xy}, τ_{yx}, τ_{xz} = Shear stresses

γ = Unit weight of soil

H = Depth below ground surface

K_0 = Lateral earth pressure coefficient

This approach allows for the introduction of any level of lateral stresses desired.

4.3 EXCAVATION SIMULATION

In general, excavation may be simulated in the finite element method by applying stresses to the boundary exposed by the excavation so as to create a stress-free surface. From literature on excavation (Dunlop et al., 1968; Clough and Duncan 1969; Christian and Wong, 1973; Chandrasekaran and King, 1974), four steps can be distinguished in the excavation procedure. For a soil mass with initial stresses these four steps are:

1. Calculation of equivalent nodal loads for these stresses, $\{Q_1\}$.

2. Elimination of the stiffness of the excavated elements in order to avoid the interaction with the unexcavated elements.

3. Application of nodal loads equal in magnitude, but opposite in sign to the equivalent nodal loads calculated in step 1 to the nodes exposed by the excavation. (This step ensures a stress-free excavation boundary.)

4. Addition of incremental excavation stresses $\{\Delta\sigma_1\}$ to the initial stresses $\{\sigma_0\}$ to give $\{\sigma_1\}$. Often, a series of steps are used to model the excavation. In such cases, the general recursive formula for the calculation is

$$\{\sigma_i\} = \{\sigma_0\} + \sum_i \{\Delta\sigma_i\}. \tag{4.5}$$

The major difference between the various excavation schemes is the method of determining the equivalent nodal forces. To obtain these nodal forces, the stresses on the excavation boundaries which usually pass between the elements are required. However, in the finite element method, stresses are usually computed at the center of an element. It would appear that for excavation simulation purposes, stresses should be computed at element nodes since they would lie along the excavation boundary. Unfortunately, stresses at the element nodes, if they could be computed, are known to be inaccurate. Thus, the first step in the calculation of the equivalent nodal loads is to find a way to account for the stress gradient between the element center and the excavation boundary.

To determine stresses on excavation boundaries, Dunlop et al., (1968) averaged the stresses in pairs of adjacent elements on opposite sides of the boundaries. Then, they calculated the equivalent nodal forces by assuming that the average stresses were constant between adjacent nodes. This stress averaging technique was shown to be accurate if elements on either side of the excavation boundary were

rectangular and of equal size. For elements of unequal size, Chang (1969) determined the stresses on the boundary by using only the stresses in the elements directly above that boundary. The equivalent nodal forces calculated from these stresses were then corrected for an assumed gravity stress gradient within the element. Both the stress averaging technique and the gravity gradient technique are not generally applicable to the other types of elements and would be inappropriate for three dimensional elements.

Clough and Duncan (1969) proposed a method which is more general. In this scheme, the equivalent nodal forces to be applied to the excavation surface are calculated using nodal stresses. These nodal stresses are interpolated from the stresses at the centers of adjacent elements; four interpolation elements are required. A linear variation of stresses between nodes is assumed. However, even for two dimensional elements, the choice of the best four interpolation elements is not always obvious. Incorporation of this method in a three dimensional analysis would require eight interpolation elements the choice of which can be even more difficult and would create impractical difficulties with data input.

4.3.1 Technique Adapted For This Investigation

The excavation procedure which is used in the finite element code is a variation of a method proposed by Chandrasekaran and King (1974) and developed by Mana (1978). The unique feature of this approach is that the nodal forces required to simulate excavation are computed directly without initially determining stresses on the excavation

boundary. This is done by using the conditions of equilibrium for finite elements. From the static equilibrium condition in a finite element,

$$\{f\} = [k]\{\delta\} \tag{4.6}$$

where

{f} is the vector of element nodal forces

[k] is the element stiffness matrix

{δ} is the vector of element nodal displacements

Alternatively, {f} can be obtained from the equation

$$\{f\} = \int_V [B \text{ Transpose}]\{\sigma\}dv \tag{4.7}$$

where [B] is the strain-displacement matrix for the element, and {σ} is the vector of element stresses. For an excavated element, the values of {f} calculated using either equation 4.6 or 4.7 are equivalent to the forces exerted by the element on the surrounding elements. Thus, for excavation simulation, a finite element analysis is carried out with {f} as the applied forces. These nodal forces {f} with the proper sign are applied to the nodes exposed by excavation. The stiffness of the removed element is neglected in the analysis. This feature results in a cost saving since each element excavated is one less element included in the stiffness matrix. The elimination of the stiffness matrix is carried out by disregarding the contribution of the excavated element during the assemblage of the structure stiffness matrix. Also,the degrees of freedom associated with the nodes eliminated during

excavation are removed from the system of equations by treating them as restrained nodes. For a three dimensional analysis, the saving in storage and computation time resulting from this stiffness elimination, can be substantial.

To compute all the excavation forces {F}, equation 4.7 is used repeatedly. The recursive formula for the general case is given by

$$\{F\} = \sum_{1}^{N} \int_{V} [B \text{ Transpose}]\{\sigma\} dv \qquad (4.8)$$

where

{F} is the vector of nodal forces exerted on the nodes exposed on the excavation surface

[B] is the strain displacement matrix

{σ} is the stress vector, and

N is the number of excavated elements which have common boundary with the remaining ones.

The integral in equation 4.8 is evaluated using numerical integration. The values of [B] and {σ} are those at the Gaussian integration points within each element.

4.3.2 Surfaces Where Excavation Forces Are Applied

In the case of the advancing tunnel, excavation forces are applied to those surfaces from which previously existing confining stresses are removed during a shove. The first of these surfaces is the tunnel face, where the soil is directly excavated. The excavation simulation forces

here are directed inwards away from the face parallel to the tunnel axis. They act to pull the face into the shield.

A second surface which is affected by the advance of the shield is the soil around the periphery of the tunnel through which the shield cuts. In this area, the confinement provided by soil is replaced by the structural support of the shield. Regardless of the presence of the shield, excavation forces are applied to the peripheral soil surface. However, the effects of these forces are picked up primarily by the stiff shield structure. This is as it should be, and the forces act to compress the shield as occurs in the actual case.

Finally, the last surface influenced by shield advance is that exposed in the tail area. Stresses must be removed from this boundary since the support of the shield is lost, and is not replaced by the liner until grout is injected to transfer support to the liner. The forces acting to create a stress free boundary in the tail void area act radially into the tunnel, and serve to pull the soil into the tail void. More detail on the modeling of the tail void is given in a subsequent section.

During simulation of the shield advance and soil excavation, all three sets of excavation forces mentioned are applied simultaneously as depicted in Figure 4.1. Other effects of the tunneling, such as the shove forces, shield and liner weight forces and slurry pressure at the face may be superimposed onto the excavation force system as well, producing a complex interaction situation.

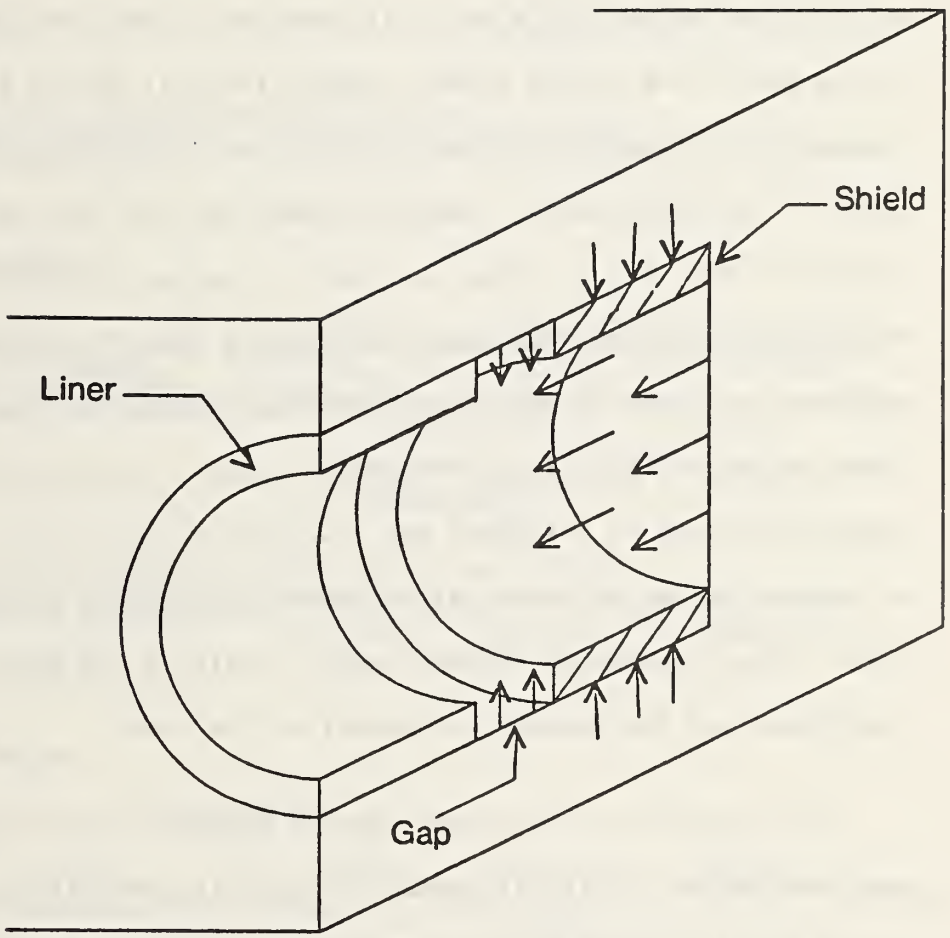

Figure 4.1: Application of Excavation Forces

4.4 LINER-SHIELD AND TAIL VOID SYSTEM

In Figure 4.2a, a schematic diagram of the mechanics of the shield-liner system for a cycle of shove and liner erection is shown. In the field, the shield slides through the soil during a shove, with a ring of liner segments subsequently erected inside the tail of the shield. The thin opening created between the soil and the liner by the advance of the shield is the tail void. The soil in this area moves towards the liner and may come into contact with it, or eventually be supported by grout or pea gravel injected through the liner. While these events are occurring, the shove forces from the shield for the next advance act to influence the system (see Figure 4.2b). They serve to advance the shield while at the same time pushing backwards on the liner. Shear forces in the soil act to restrain the forward movement of the shield and the backwards movement of the liner.

This picture of the shield advance shows it to be complex. In practical terms, it is not possible to exactly simulate this situation in the finite element analyses because of constraints encountered in constructing a finite element mesh. The major problem arises because the tail void, liner and shield are three separate entities which are located in slightly different planes. In a finite element mesh, each of these would require separate sets of elements, elements which would be very thin relative to those used for the surrounding soil. This can create numerical instability with the element type used in the three dimensional program. However, even if this problem did not exist, the

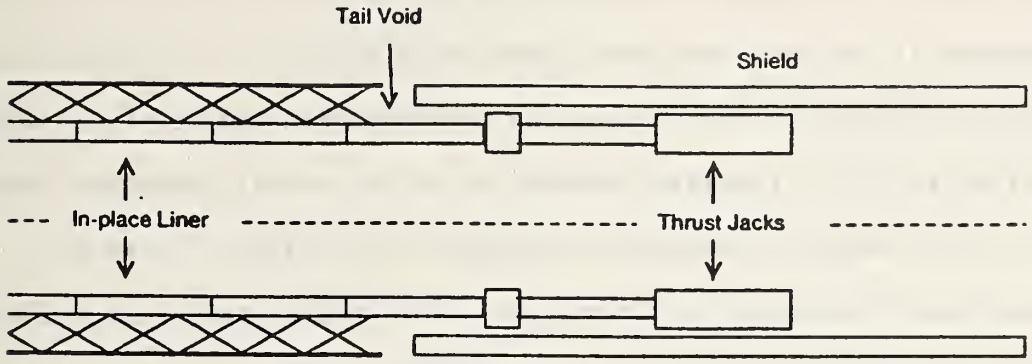

a. Actual System

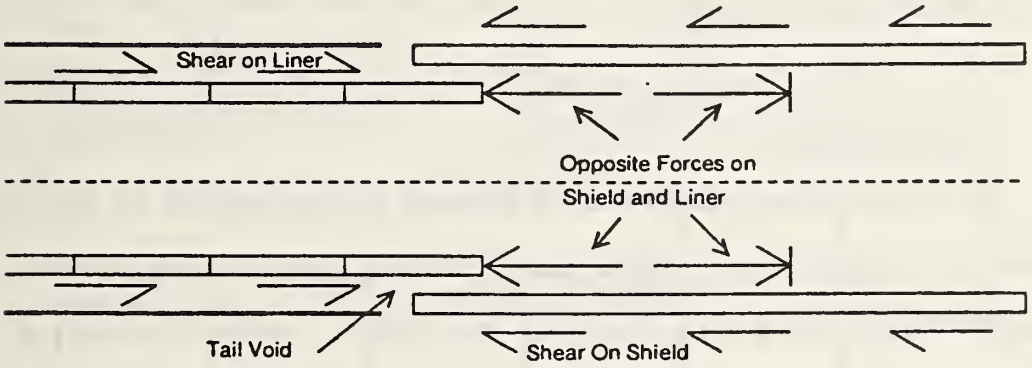

b. Actual Forces

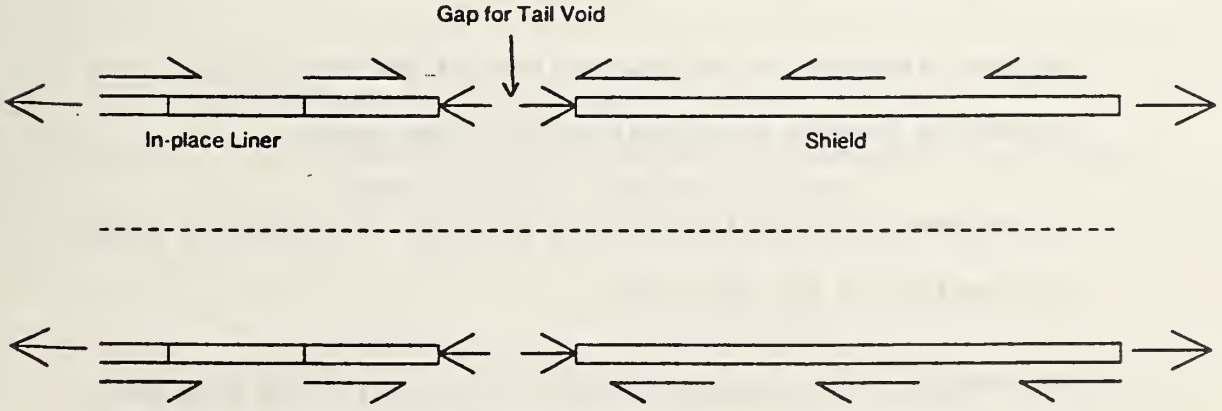

c. Forces Applied In Finite Element Analysis
to Model Shield Thrust Effects

Figure 4.2: Finite Element Modeling of Forces on Liner and Shield

large number of elements required, and the iterative solution needed to determine if the tail void had closed would lead to a very high cost per analysis. Thus, for the present, an approximation was developed which provides for (1) a realistic simulation of the actual mechanics; and, (2) a model which is economical and numerically stable. This is schematically depicted in Figure 4.2c. The shield, tail void and liner system are assumed to lie in a single plane, and to be represented by a set of thin elements of uniform thickness, the stiffnesses of which are varied to suit the situation.

4.4.1 The Tail Void

The tail void is assumed to be created by the advance of the shield as shown in Figure 4.3. In the finite element mesh, a ring of thin elements lies along the periphery of the tunnel. Before the shield arrives, these elements have the properties of the soil. During the shield advance, the following sequence occurs:

1. The soil elements in the new position of the shield have their properties changed to reflect those of the shield.

2. The elements representing the old position of the shield assume the function of the tail void.

3. The elements which were previously in the tail void area have their properties changed to reflect those of the liner.

After the shield advance, the elements in the tail void area are assigned a very low stiffness. In essence, the soil is left unsupported

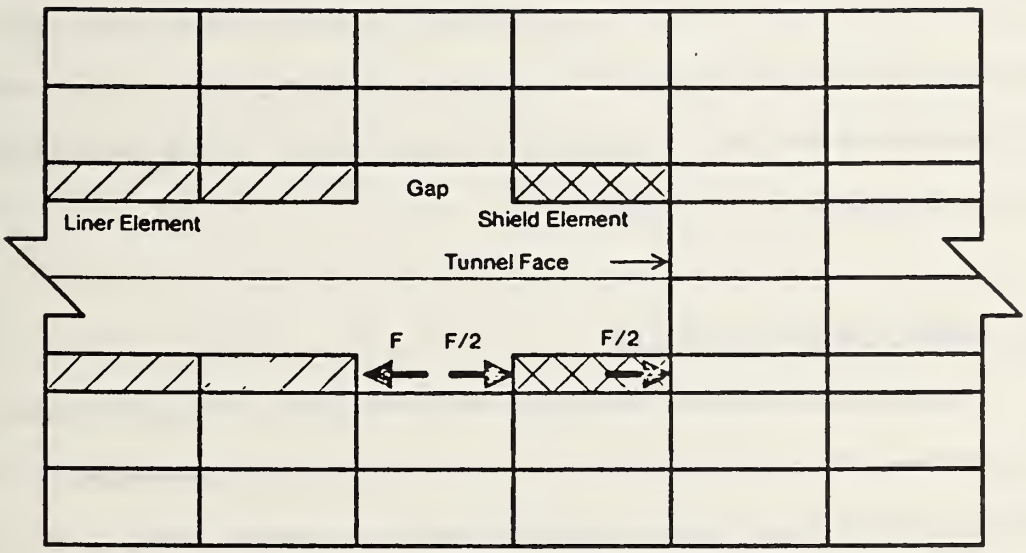

Figure 4.3: Approximate Model of the Shield-Liner-Tail Void System Used in Finite Element Analyses

temporarily, and it is free to move inwards as far as it can. However, because the soil is assumed to behave as a linear elastic material and it is supported on either side by liner and shield elements, the movement into the tail void is limited. And, as will be shown later, the actual calculated levels of movement for the analyses reported herein are realistic. Thus, the effect of the tail void is represented with a simple approximation which is economical and numerically stable. Note also that this method of simulating the tail void provides for a separation of the shield and the in-place liner elements. Thus, the shield shove forces can independently push forward on the shield while pushing backwards on the liner.

4.5 LINER AND SHIELD SYSTEM

The liner is modeled using the variable number of nodes element with 20 nodes. As noted earlier, prior to the advance, elements in the position of the liner have the properties of the tail void. During the advance, these elements are reactivated by changing their properties to that of a liner. The stresses within the element, accumulated while they were soil elements are set to zero on their "birth".

The shield is also modeled using the 20 node element. Like the liner elements, the shield elements undergo two material definitions. Initially, they are soil elements then they are eliminated during excavation, and finally they are reactivated afterwards as shield elements. Both the liner and the shield are modeled as linear elastic materials, but the specified modulus of elasticity, E for the latter is much higher than that for the former.

4.5.1 Modulus For Liner And Shield Elements

The modulus for the liner elements would normally be taken as that of the liner material -- concrete or steel. This value is appropriate if the thickness of the liner element in the analysis is the same as the actual thickness being modeled. However, a major problem encountered in the liner modeling was that using an actual liner thickness in the coarse finite element mesh which had to be used for the analysis led to the generation of very thin, long liner elements. These thin elements have very high aspect ratios and hence caused numerical problems. To resolve this difficulty, the liner elements were made thicker than the actual case. However, in using a larger thickness for the liner than the actual one, the modulus must then be reduced in order to give a proper bending response. The amount of this reduction can be reasonably defined based on the fact that that bending rather than membrane stresses predominate in the liner in shallow tunnels. The modulus for the thicker liner elements were thus reduced according to the relation between the liner thickness and the bending stiffness. (The bending stiffness is inversely proportional to the cube of the liner thickness.) This reduction factor will be subsequently referred to as the thickness reduction factor, TRF. Thus, for example, if the liner element thickness is twice that of the actual liner, one-eighth the modulus of the liner is assigned to the element. Although this procedure is reasonable as a first approximation it may be useful to avoid it in future studies by incorporating a thin shell element into the finite element code.

Another aspect of the liner modulus which merited consideration is the fact that the liner used in the finite element code is continuous whereas that used in practice is segmented. The joints between the liner segments act as hinges allowing greater movement. Thus, the actual liner is more flexible than it would be if assumed continuous. To account for this flexibility, a reduction was applied to the continuous liner modulus. Johnston (1981) has shown that a reduction factor of about 40 yield liner performance similar to that observed in the field. This factor is subsequently referred to as the flexibility reduction factor, FRF.

The aspect ratio problem in the liner modeling mentioned above applies to the shield element also, and it was necessary to use shield elements thicker than the actual skin of the shield. However, in this case there are additional complications since the internal bulkheads and machinery in a shield provide an indeterminate, but substantial additional stiffness to the shield cylinder. Selection of an equivalent modulus to simulate this stiffness is very difficult and required a special set of parametric studies as described in Chapter 5.

4.5.2 Modeling The Shoving Forces

As discussed in Chapter 2, the shield is shoved forward by means of a thrust force applied through hydraulic jacks acting against the in-place liner. The thrust force has the effect of moving the liner backwards independent of the forward movement of the shield. The total required thrust force, F, may be estimated by the equation for the cohesion force around the shield periphery.

$$F = \pi D L C \qquad (4.9)$$

where

D is the tunnel diameter,

L is the length of the shield, and

C is the cohesion of the clay.

These independent jacking forces, whose sum equals the value of F, may or may not be symmetrical or uniform. This is a common practice since unequal thrusting forces are used to correct for shield diving tendencies or misalignment, or to vertically or laterally change course to follow a planned curvature.

The actual tunnel force system to be modeled is shown in Figures 4.2a and 4.2b. It should be noted that the liner segments are installed within the shield, and as they exit the shield they are surrounded by the tail void. Thus, the first few segments are subjected to no shear during the shove. However, liner segments well back from the shield are subjected to a shear by the surrounding soil in a direction opposite to that induced on the shield.

4.6 MODELING THE SLURRY AND EPB SHIELDS

4.6.1 Slurry Shield

The slurry pressure on the face of the tunnel is simulated in the program by subjecting the soil to a surface loading. This pressure can be uniform or variable. In the analyses presented in subsequent chapters, the applied pressure is based on the equation for the overload factor, OF:

$$OF = \frac{P - P_i}{C} \qquad (4.10)$$

where

P is the overburden pressure at the spring line of the tunnel,

P_i is the uniform slurry or air pressure, and

C is the shear strength of the soil.

Thus, for an assumed value of OF, P_i is calculated using equation 4.10.

Two different assumptions can be made concerning the mode of support of the soil around the shield by the slurry pressure:

1. Slurry gets around the shield and supports the soil in the gap and around the shield in addition to supporting the tunnel face.

2. The slurry pressure supports the soil at the face only.

These two assumptions are examined in parametric studies in Chapter 6.

4.6.2 EPB Shield

Most of the tunneling in urban areas takes place under the ground water table. When the EPB shield is used in such a condition, it chews up the soil and water essentially into a slurry exerting pressure on the face of the tunnel. Thus, the EPB shield in actuality is similar to the slurry shield except that the slurry pressure is applied at the face only. In the program, the pressure is assumed to come from shoving forces. The results from the slurry shield analysis are therefore applicable to the EPB shield as well, except that the magnitudes and distributions of pressures may be different.

4.6.3 Shield And Liner Weight

The weight of shields are quite substantial and need to be considered in shield tunnel analysis. Shield weights range from 40 tons (356 kN) to over 300 tons (2670 kN) depending on the size of the shield and the tunnel. In this research, the weight of the shield is modeled using concentrated nodal forces acting downwards vertically. The weight is distributed equally among the nodes constituting the shield elements. A similar procedure is used to model liner weights.

4.7 SUMMARY - SIMULATION OF TUNNELING OPERATIONS

The sequence of operations to model the tunneling operation is as follows:

1. As the shield is shoved forward, the soil elements in the area of advance are excavated.

2. Liner segments are erected where there used to be a gap or tail void before the shield was shoved, and the previous shield position becomes the new position of the tail void.

3. Forces are applied to simulate the effects of excavation, shove forces, shield and liner weight, and slurry pressures as needed.

4. The finite element analysis is carried out to obtain deformations and stresses under the action of forces for one shove of the shield.

5. Additional shoves may be analyzed as needed by repeating this process.

4.8 VERIFICATION OF BASIC ELEMENTS OF THE FINITE ELEMENT CODE

In order to verify the various computational procedures incorporated in the finite element code, a number of problems, for which closed form solutions are available, were analyzed. Results from the finite element analyses were then compared with those predicted by the closed form solutions.

4.8.1 Thick Cylinder Problem

The thick cylinder problem was analyzed to test such procedures in the finite element code as stiffness generation and assembly, displacement and stress computations and the excavation scheme for an assemblage of elements.

The thick cylinder problem is shown in Figure 4.4. The cylinder may be subjected to uniform internal and/or external radial pressures. From the theory of elasticity, the variation of stresses and displacements with the radial distance r is given by (Obert and Duvall, 1967):

$$\sigma_r = \frac{a^2p_i - b^2p_o}{b^2 - a^2} + \frac{a^2b^2(p_o - p_i)}{r^2\ b^2 - a^2} \tag{4.11}$$

$$\sigma_{th} = \frac{a^2p_i - b^2p_o}{b^2 - a^2} - \frac{a^2b^2(p_o - p_i)}{r^2\ \{b^2 - a\}\ 2} \tag{4.12}$$

$$\tau_{rth} = 0 \tag{4.13}$$

$$u = \frac{1 + \nu}{E}\left[\frac{p_ia^2 - p_ob^2}{b^2 - a^2}(1 - 2\nu)r - \frac{a^2b^2(p_o - p_i)}{(b^2 - a^2)r}\right] \tag{4.14}$$

where

σ is the radial distance

σ_{th} is the tangential stress

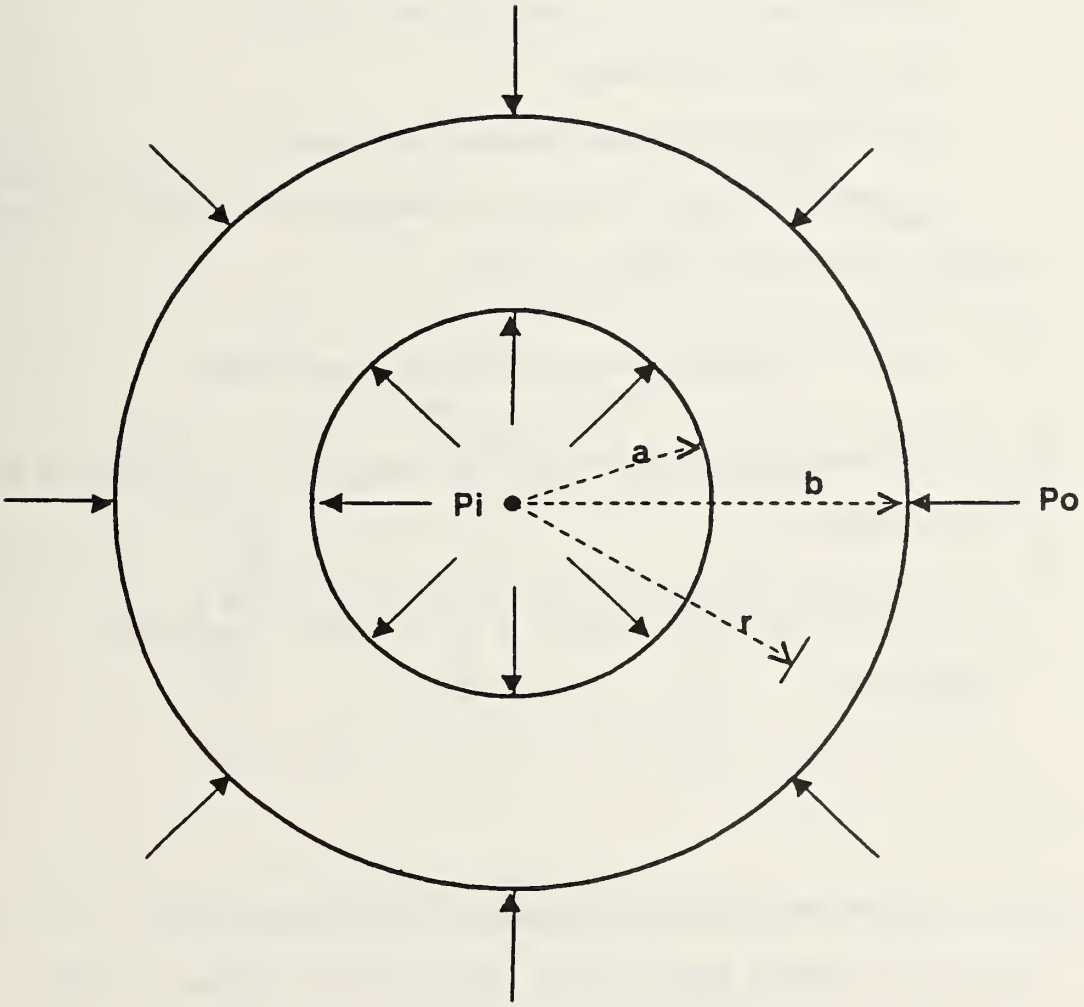

Figure 4.4: Thick Cylinder

P_0 is the uniform external pressure

P_i is the uniform internal pressure

b is the outer radius of the cylinder

a is the inner radius of the cylinder

$\tau_{r\ .th}$ is the shear stress in the $r\theta$ plane

ν is the Poisson's ratio of the cylinder material

u is the radial displacement

E is the Young's modulus of the cylinder material

If $\tau_{r\ .th}$ is identically zero, the polar components of stress, σ_r and σ_{th} are the principal stresses.

Two types of finite element analyses were performed:

1. The cylinder cavity was assumed to be present from the start of the analysis.

2. The cylinder cavity was assumed to have been created by excavation.

4.8.1.1 Cavity Present From The Beginning Of The Analysis

The finite element mesh used in the analysis is shown in Figure 4.5. The mesh consists of 12 variable number of nodes elements. Each element has 20 nodes. The nodes at the top and bottom are restrained in the vertical or Z direction. Symmetry of loading and geometry allowed the representation of the problem by only a quadrant.

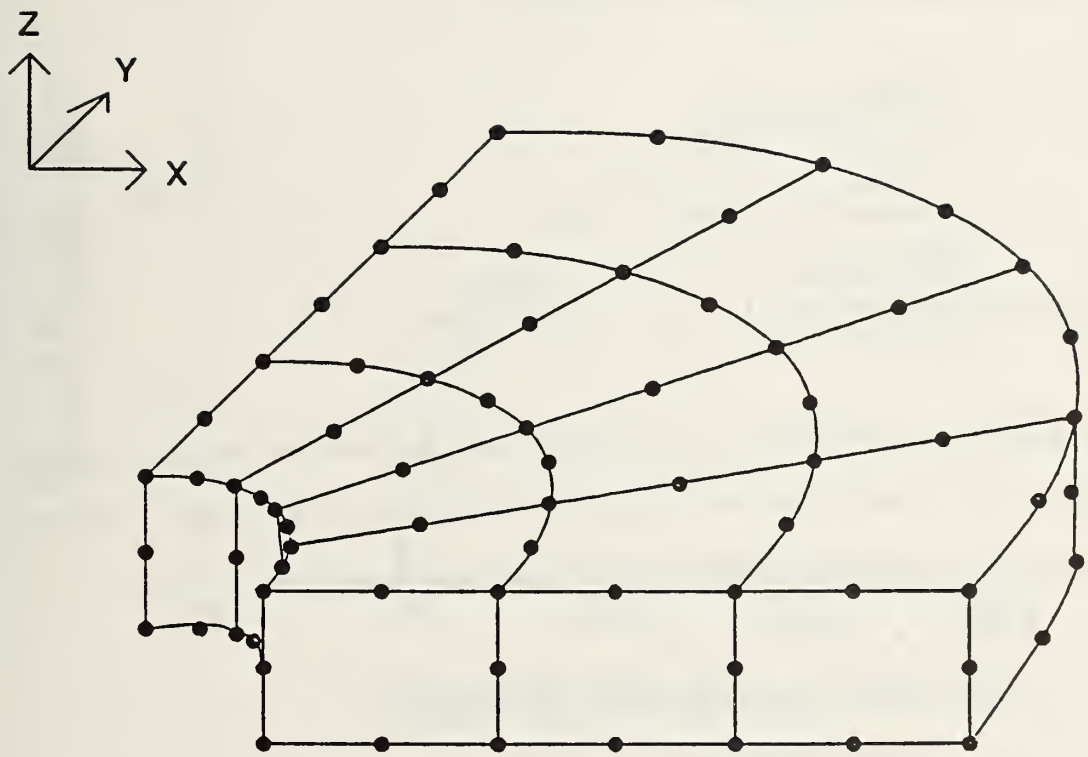

Figure 4.5: Finite Element Mesh for Cylinder with Cavity Present Initially

The problem analyzed is equivalent to that of a thick-walled cylinder subjected to an external pressure and with an internal pressure of zero. It is useful to analyze because it corresponds to the problem of a tunnel in a rock formation under a hydrostatic stress field. For this case, p_i in the closed form equations 4.11, 4.12, and 4.14 is zero. The three equations therefore reduce to

$$\sigma_r = \frac{-b^2 p_0}{b^2 - a^2}\left[1 - \frac{a^2}{r^2}\right] \tag{4.15}$$

$$\sigma_{th} = \frac{-b^2 p_0}{b^2 - a^2}(1 + a^2/r^2) \tag{4.16}$$

$$u = \frac{1 + \nu}{E}\left[\frac{-p_0 b^2}{b^2 - a^2}(1 - 2\nu)r - \frac{a^2 b^2 p_0}{(b^2 - a^2)r}\right] \tag{4.17}$$

The problem is simulated by applying a uniform surface pressure, p_0 of 25 psi (172.5 kN/m^2) on the outer circumference of the mesh. The values of the other parameters used in the analysis are:

Poisson's ratio ν = 0.3

Young's modulus E = 30 x 10^6 psi (20.7×10^7)

a = 5 inches (12.7 cm)

b = 20 inches

The stresses from the finite element analysis and theory are compared in Figures 4.6 and 4.7; the displacements are given in Table 4.1.

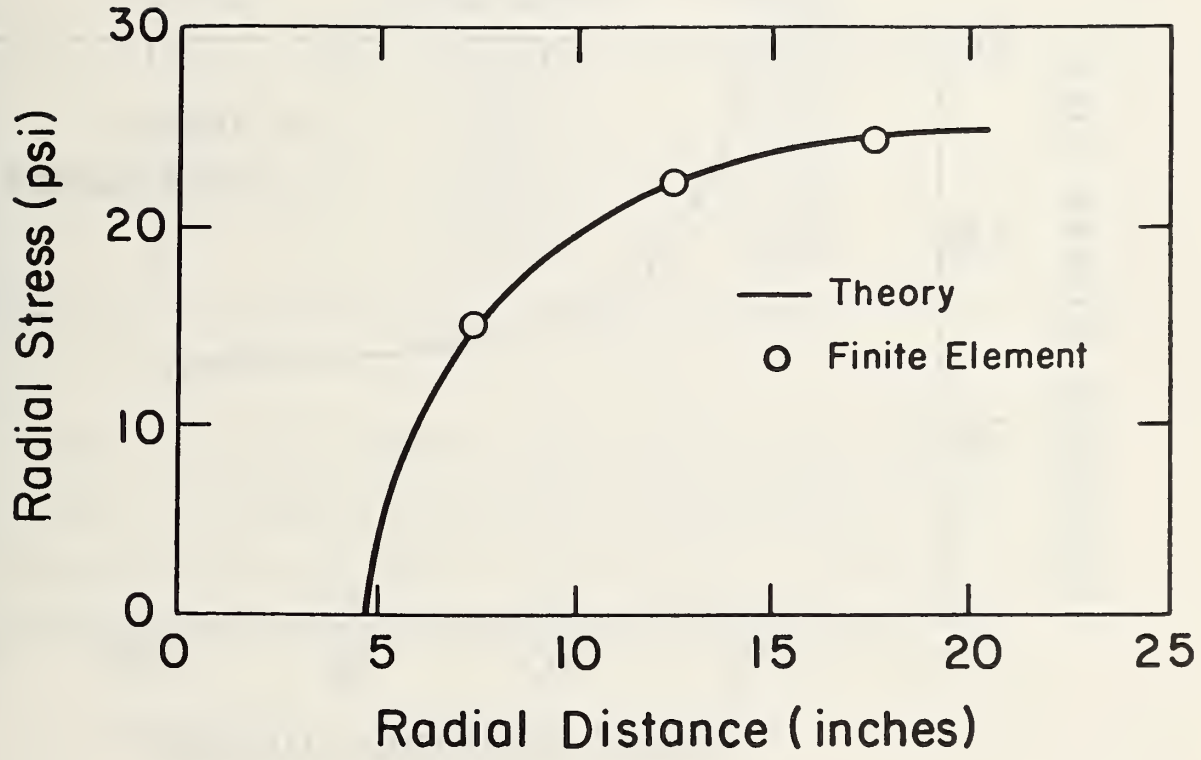

Figure 4.6: Variation of Radial Stress with Radius (Cavity Present Initially)

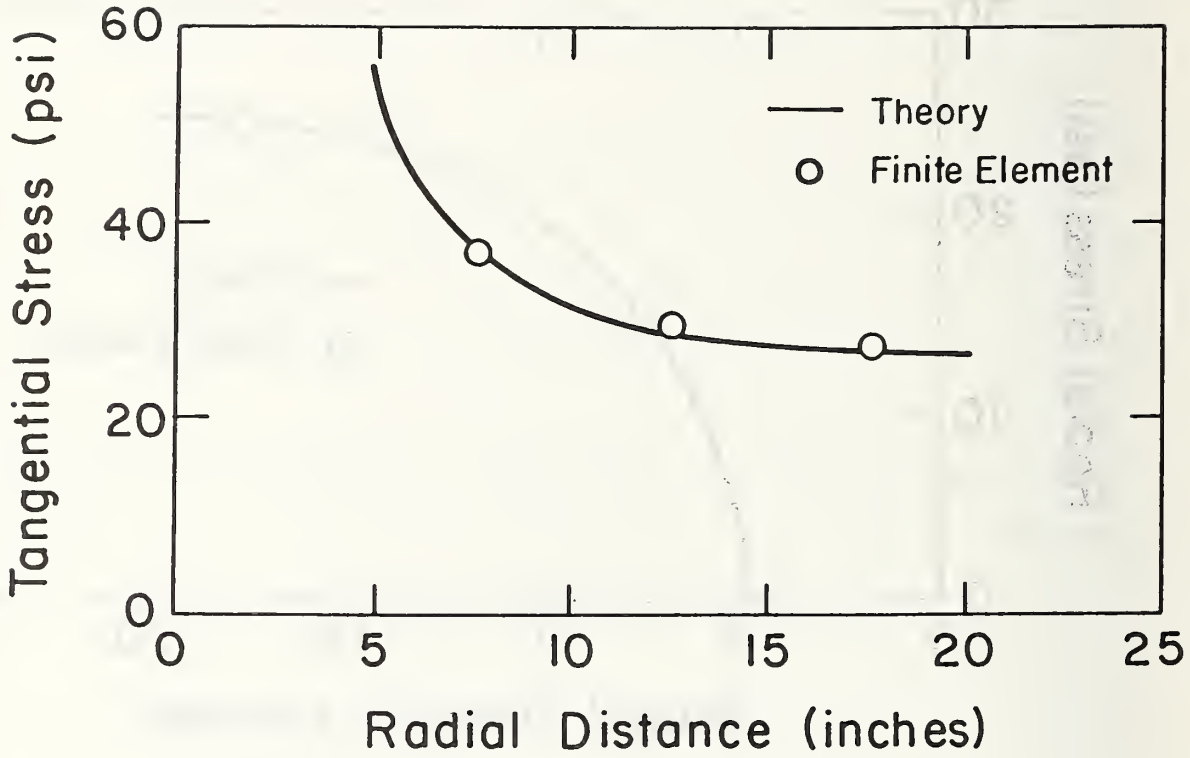

Figure 4.7: Variation of Tangential Stress with Radius (Cavity Present Initially)

TABLE 4.1

Displacements - Cylinder With Cavity Initially

RADIAL DISTANCE (Inches)	DISPLACEMENTS X 10^{-6} INCHES FINITE ELEMENT	THEORY
5	8.09444	8.08889
7.5	7.31643	7.31852
10	7.51381	7.51111
12.5	8.08910	8.08889
15	8.85948	8.85926
17.5	9.73956	9.73968
20	10.68930	10.68889

There is excellent agreement between the two sets of results for the radial and tangential stresses and the displacements. This indicates that basic procedures in the code such as stiffness matrix generation and the solution of equation are accurate.

4.8.1.2 Cavity Created By Excavation

The mesh used in the finite element analysis is shown in Figure 4.8. Only a quadrant of the mesh is needed due to symmetry in loading and geometry. The mesh consists of 14 elements and each element has 20 nodes. The nodes at the top and bottom are restrained in the vertical or Z direction. Elements 1 and 2 are excavated to create the cavity required. To use the excavation routine, it is necessary to have initial stresses within the elements to be excavated. In this problem, all the elements were each subjected to an initial isotropic state of stress of 25 psi (172.5kN/m^2). In terms of the closed-form theory, the

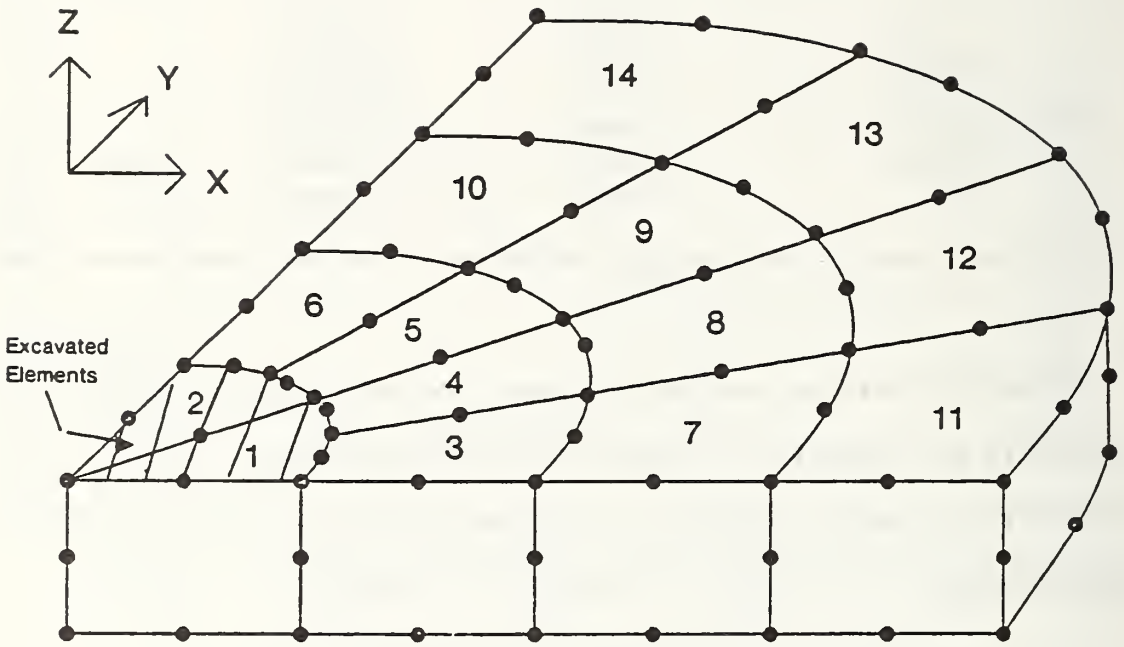

Figure 4.8: Finite Element Mesh for Cylinder with Cavity Created by Excavation

problem is equivalent to that of a thick cylinder with an internal pressure, P_i=25 psi (172.5 kN/m^2) 25 psi and an external pressure, P_o=0. Equations 4.11, 4.12 and 4.14 therefore reduce to:

$$\sigma_r = \frac{a^2 p_i}{b^2 - a^2} + \frac{a^2 b^2 \ (-p_i)}{r^2 \{b^2 - a^2\}} \tag{4.18}$$

$$\sigma_{th} = \frac{a^2 p_i}{b^2 - a^2} - \frac{a^2 b^2 \ (-p_i)}{r^2 \{b^2 - a^2\}} \tag{4.19}$$

$$u = \frac{1 + \nu}{E}\left[\frac{p_i a^2}{b^2 - a^2}(1 - 2\nu)r + \frac{a^2 b^2 p_i}{(b^2 - a^2)r}\right] \tag{4.20}$$

The same values of a, b, ν and E as defined in Section 4.7.1.1 are used in this problem.

The results from the finite element analysis and theory are compared in Figures 4.9 and 4.10. The corresponding displacement data are given in Table 4.2.

TABLE 4.2

Displacements - Cylinder With Cavity Created By Excavation

RADIAL DISTANCE (Inches)	DISPLACEMENTS X 10^{-6} INCHES FINITE ELEMENT	THEORY
5	5.92777	5.92222
7.5	4.06643	4.06852
10	3.18048	3.17778
12.5	2.67244	2.67222
15	2.35948	2.35926
17.5	2.15623	2.15635
20	2.02265	2.02222

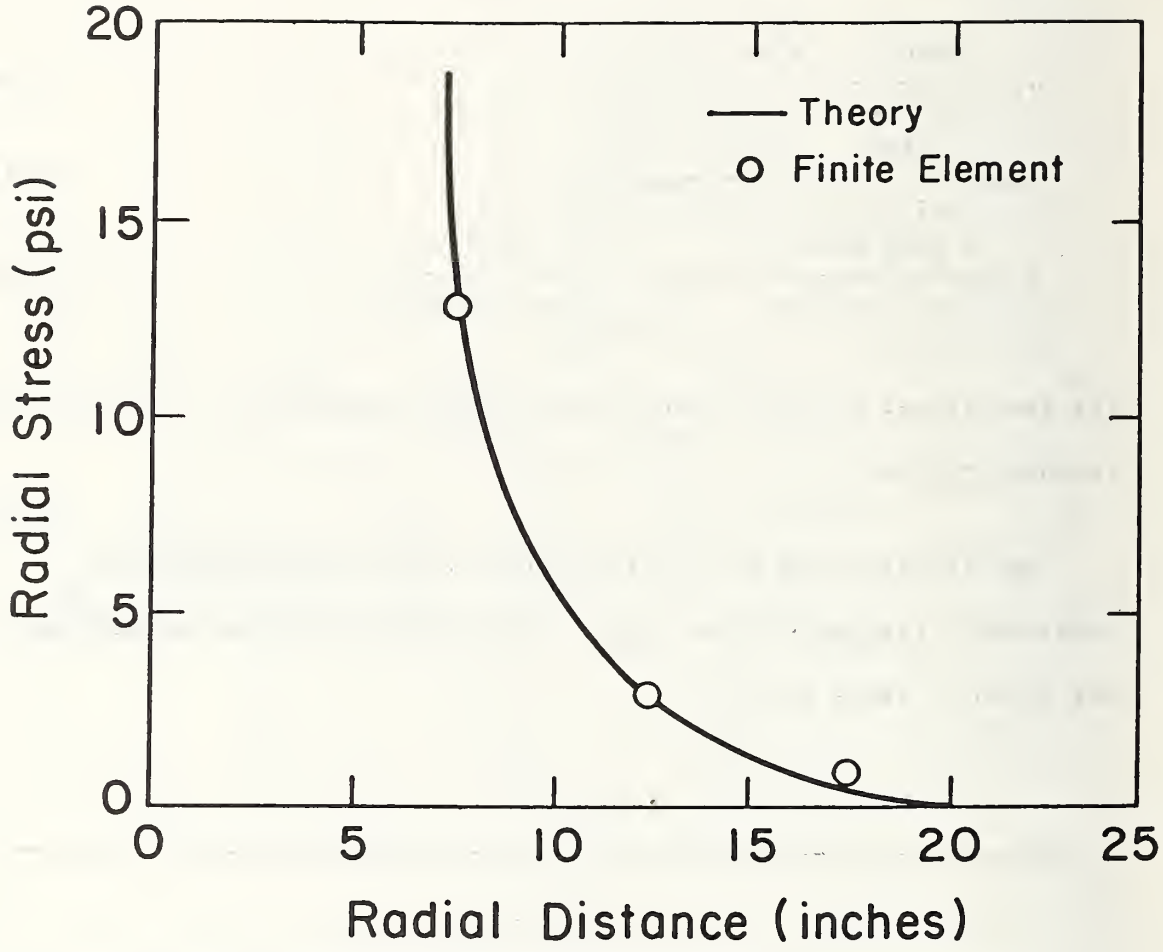

Figure 4.9: Variation of Radial Stress with Radius (Cavity Created by Excavation)

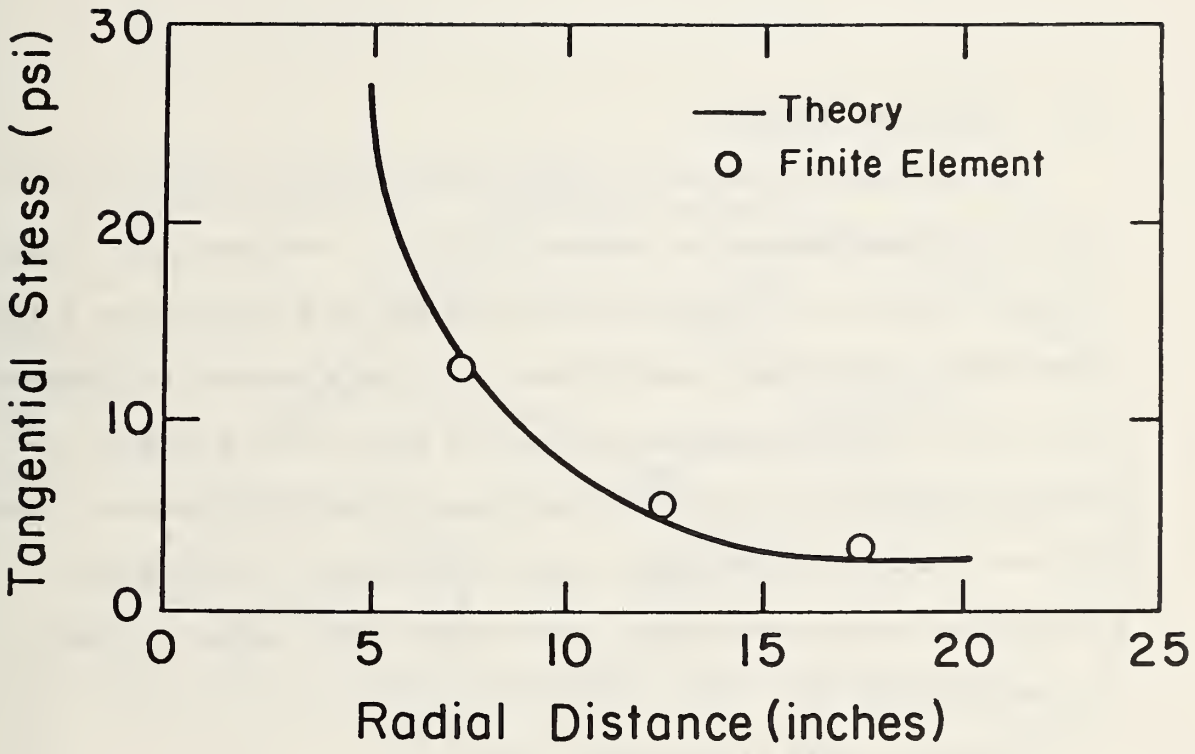

Figure 4.10: Variation of Tangential Stress with Radius (Cavity Created by Excavation)

The data show excellent agreement, attesting to the accuracy of the excavation procedure incorporated in the finite element code.

4.8.2 The Liner Problem

This problem is similar to that of the thick wall cylinder with cavity created by excavation (Section 4.7.1.2). The mesh used in the analysis is shown in Figure 4.11. It consists of 9 elements and a total of 96 nodes, each element has 20 nodes. All the elements were subjected to an initial isotropic state of stress of 25 psi (172.5 kN/m^2). In this case, elements 1 through 3 were excavated and then elements 2 and 3 were reactivated to constitute a liner and assigned a modulus much greater than that of the medium. The values of the parameters used in the analysis are:

Poisson's ratio of medium, $\nu_m = 0.3$

Poisson's ratio of liner, $\nu_l = 0.3$

Elasticity modulus of medium, $E_m = 30{,}000$ psi

Elasticity modulus of liner, $E_l = 30 \times 10^6$ psi

Thickness of liner, t = 5 inches (12.7 cm)

To obtain a liner interaction curve, the excavation forces were applied in two steps: one-third of the forces was applied initially without the liner, and then the rest were applied with the liner in place. The liner interaction curve shown in Figure 4.12 was developed as follows:

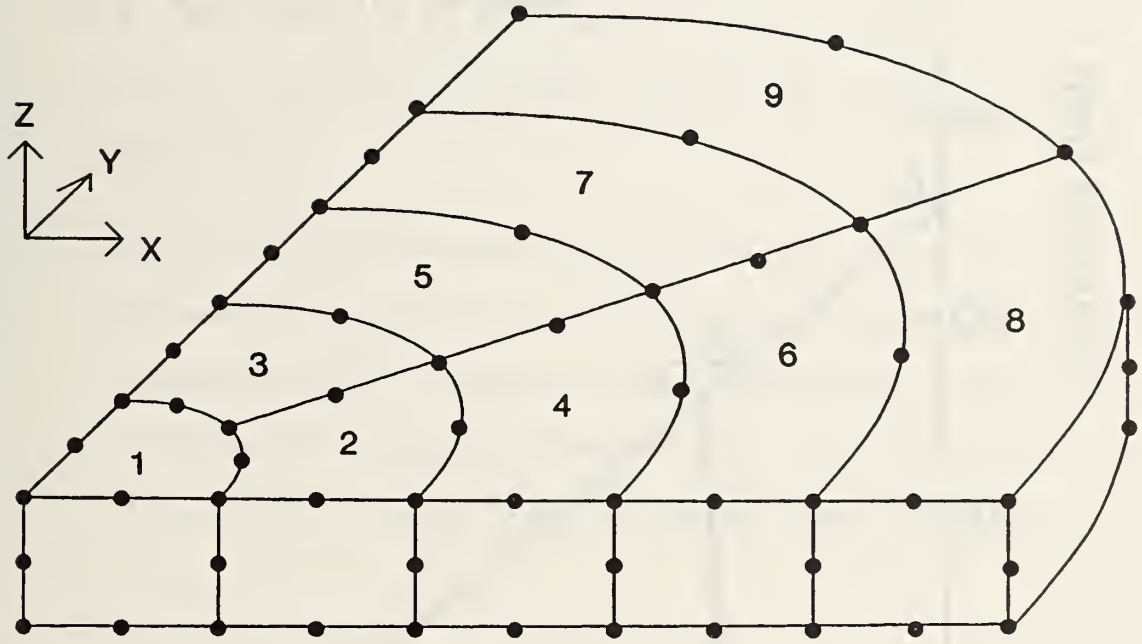

Figure 4.11: Finite Element Mesh for the Liner Problem

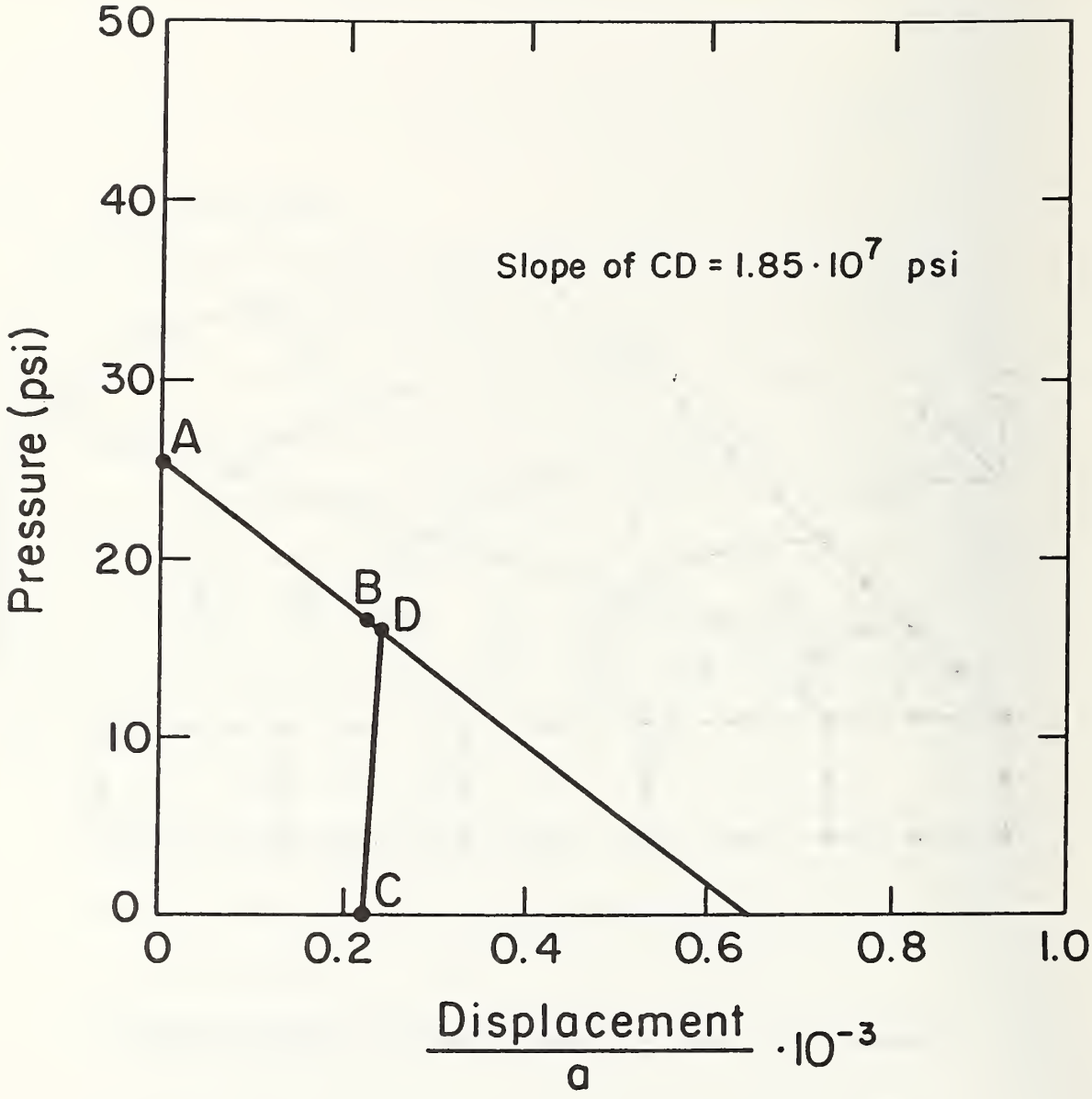

Figure 4.12: Liner Interaction Curve

1. Since there is an isotropic stress of 25 psi (172.5 kN/m^2) before the excavation (i.e., for zero displacement), point A can be obtained.

2. The displacement after the application of the first part of the excavation forces corresponds to C. Thus, knowing C and the residual pressure at that displacement (two-thirds the total pressure), point B can be obtained. Since A and B lie on a straight line, they are enough to define the response curve of the medium.

3. When the remaining excavation loads are applied, the liner is deformed. With C as the origin, this liner displacement is set off and using the fact that the liner response curve meets that of the medium at that displacement, point D can be plotted. The slope of line CD is equivalent to the stiffness of the liner.

From theory, the stiffness of the liner, S is given approximately by (Deere et al., 1969):

$$S \simeq \frac{E[a^2 - (a - t)^2]}{a^2 + (a - t)^2} \qquad (4.21)$$

where

a is the outer radius of the liner

t is the thickness of the liner

E is the Young's modulus for the liner material

The slope of CD was estimated using a second approximation. This gave a value of S of 1.85×10^7 psi which is very close to the value of 1.80×10^7 psi given by equation 4.21.

4.9 SUMMARY

The procedures used to model different aspects of the shield tunneling technique are presented in this chapter. Also verification runs made to test the accuracy of these modeling procedures are covered. The test runs indicate that the basic modeling procedures in the finite element code are accurate.

Chapter V

TUNNEL SIMULATION STUDIES - CONVENTIONAL SHIELD

5.1 INTRODUCTION

In the preceding chapter, the basic three-dimensional finite element code was described and verified. Also, general procedures to model tunneling were discussed. In this chapter, the program is applied to a series of actual tunnel problems where various aspects of the finite element approach are refined, and the influence of a number of important parameters are investigated. To accomplish these objectives, a typical large diameter tunnel driven with a shield in a homogenous clay layer is analyzed. Issues including the following are examined:

1. The proper stiffness for the shield elements in order to obtain a realistic behavior.
2. The effect of shield weight.
3. The effects of the application of shoving forces.
4. The effects of the tail void.

5.2 PROBLEM DEFINITION

5.2.1 Finite Element Mesh

An important consideration in the preparation of the finite element mesh is the constraint of available computer storage. The dual objectives in preparation of the mesh is to ensure accuracy and minimize the amount of storage required. The finite element mesh used in the analyses is shown in Figure 5.1. Symmetry in geometry and loading allows the use of half the entire mesh. The mesh consists of 238 three-dimensional elements and 660 nodes. The shield and the liner are represented by 20 node elements, and the soil by 16 node elements close to the tunnel opening, and 12 node and 8 node ones elsewhere. A typical cross-section of the finite element mesh between the portal and the tunnel face is shown in Figure 5.2; a similar cross-section between the face and the boundary is shown in Figure 5.3.

The tunnel has a diameter of 23 ft. (7 m) and a crown depth of 23 ft. (7 m). It is located in a 72 ft. (22 m) deep soil deposit underlain by a rigid layer. The face of the tunnel is positioned 3 diameters from the boundary at the portal and 4 diameters from the opposite boundary. These mesh dimensions were selected to avoid the interference of the boundaries with the stresses and displacements around the tunnel face. Ranken and Ghaboussi (1975) showed that the zone of three-dimensional stress and strain around an advancing tunnel extends out to approximately 1-1/2 diameters behind the face of the shield and about 2 diameters ahead of the face. Thus, the dimensions chosen for the mesh in this study should be adequate to avoid boundary effects. The boundary effects are examined further in Section 5.8 of this chapter.

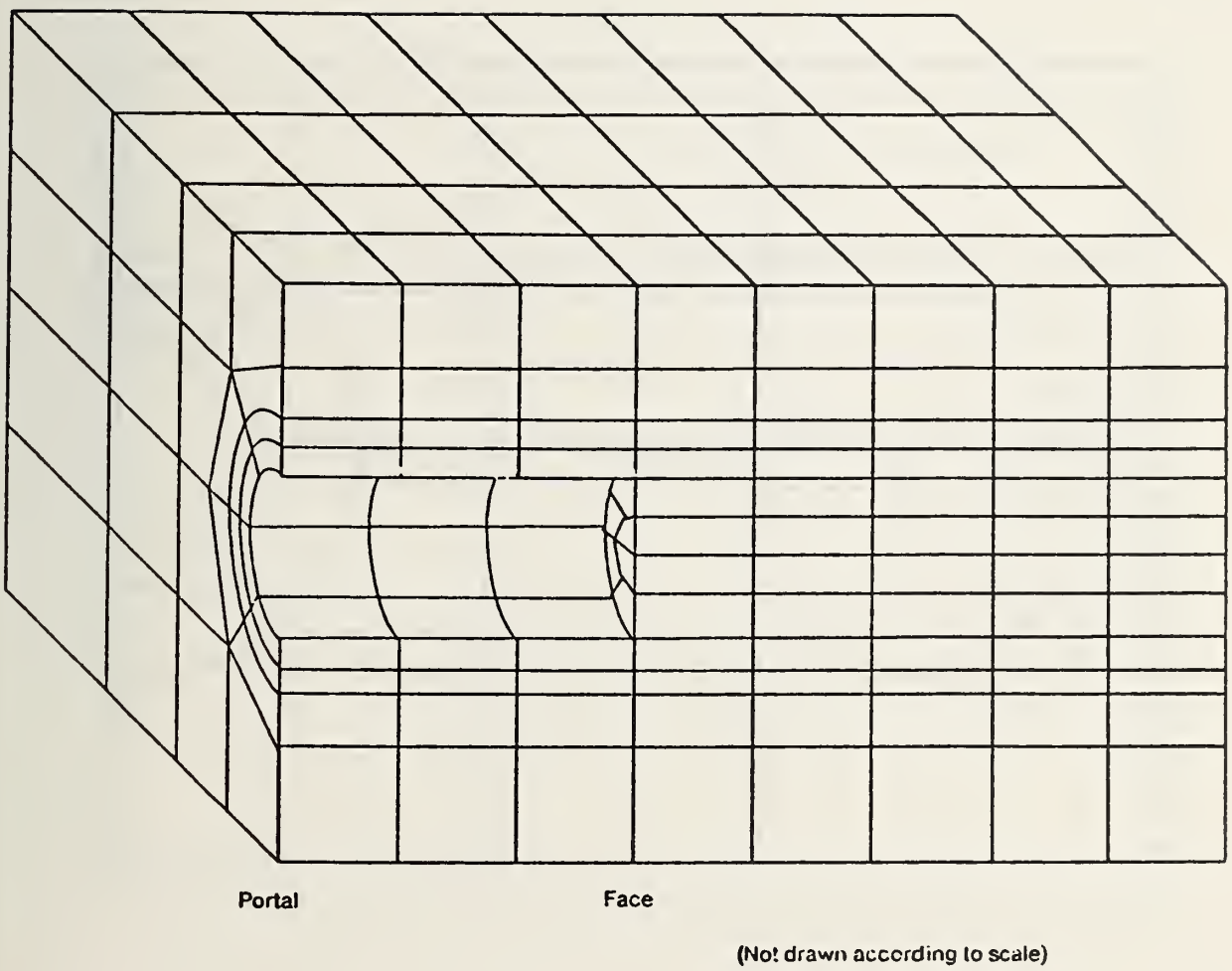

Figure 5.1: Finite Element Mesh for the Analysis of Tunnel

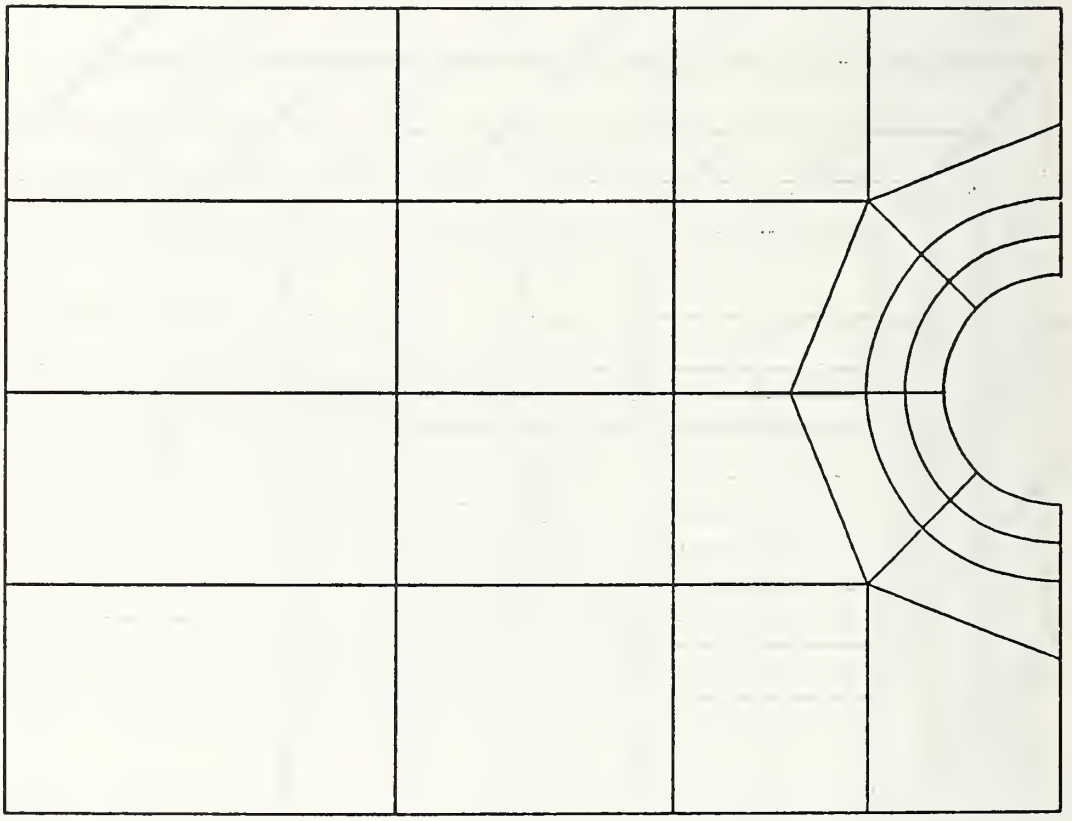

Figure 5.2: Typical Cross-Section Between Portal and Face

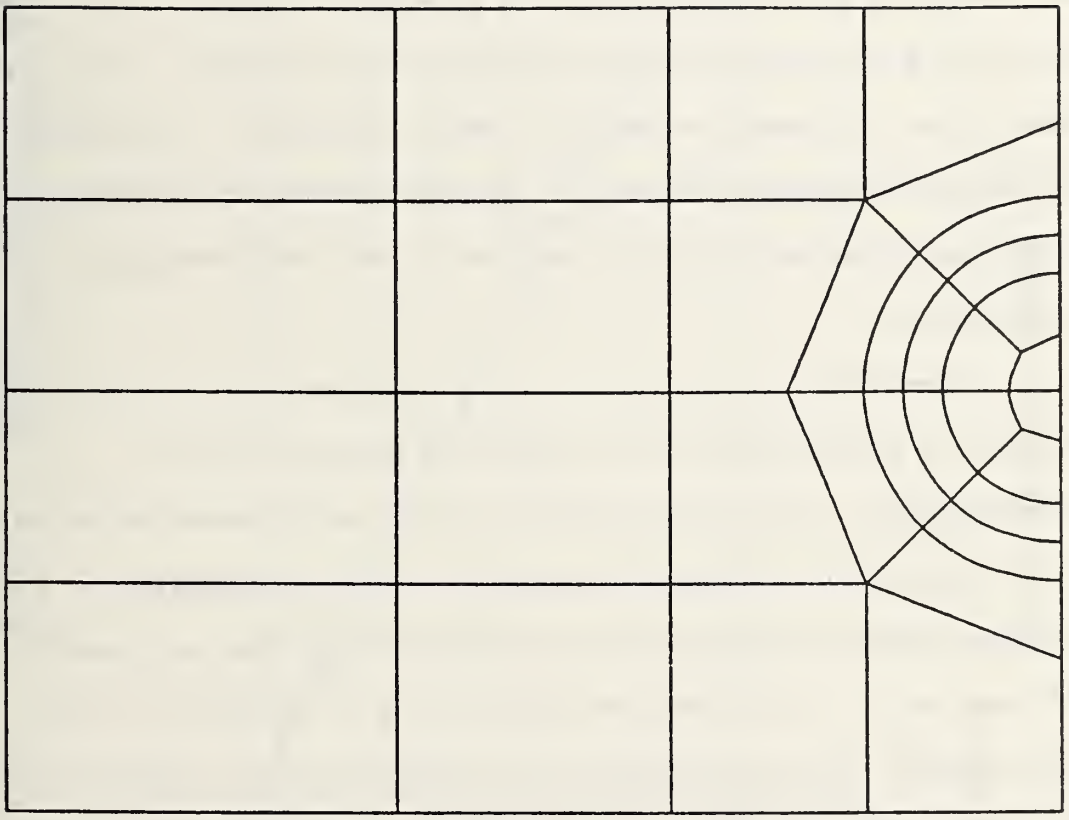

Figure 5.3: Typical Cross-Section Between Face and Boundary

5.2.2 Soil Parameters

The soil deposit is assumed to be a homogenous soft clay layer as might be encountered in an urban area where advanced shields might be used. A typical undrained shear strength profile for such a soil is as shown in Figure 5.4. The soil down to a depth of 10 feet (3.1 m) consists of a dessicated crust with uniform shear strength. Below this depth, the soil strength increases linearly with depth. It has been shown that for undrained conditions, the secant modulus E for such conditions is typically a simple multiple of the undrained shear strength S_u or

$$E = MS_u$$

where M is a constant multiplier which is a function of soil characteristics. For a soft to medium near normally consolidated soil, a value of M of 300 would appear reasonable based on laboratory and field experiences with tunneling and excavations (Clough and Schmidt, 1977; Ladd et al., 1974; Mana and Clough, 1976). This value yields a secant modulus for the soil which in an approximate way reflects the effects of nonlinear soil response which would occur upon yielding as the stresses created by the tunneling act on the soil. The soil density is taken as 115 pcf (18 kN/m^3) and the coefficient of earth pressure at rest is assumed to be 0.5. All the soil elements were assigned a Poisson's ratio of 0.45.

It should be noted that while the soil model employed in the analysis is linear elastic the soil tunneling problem addressed can be

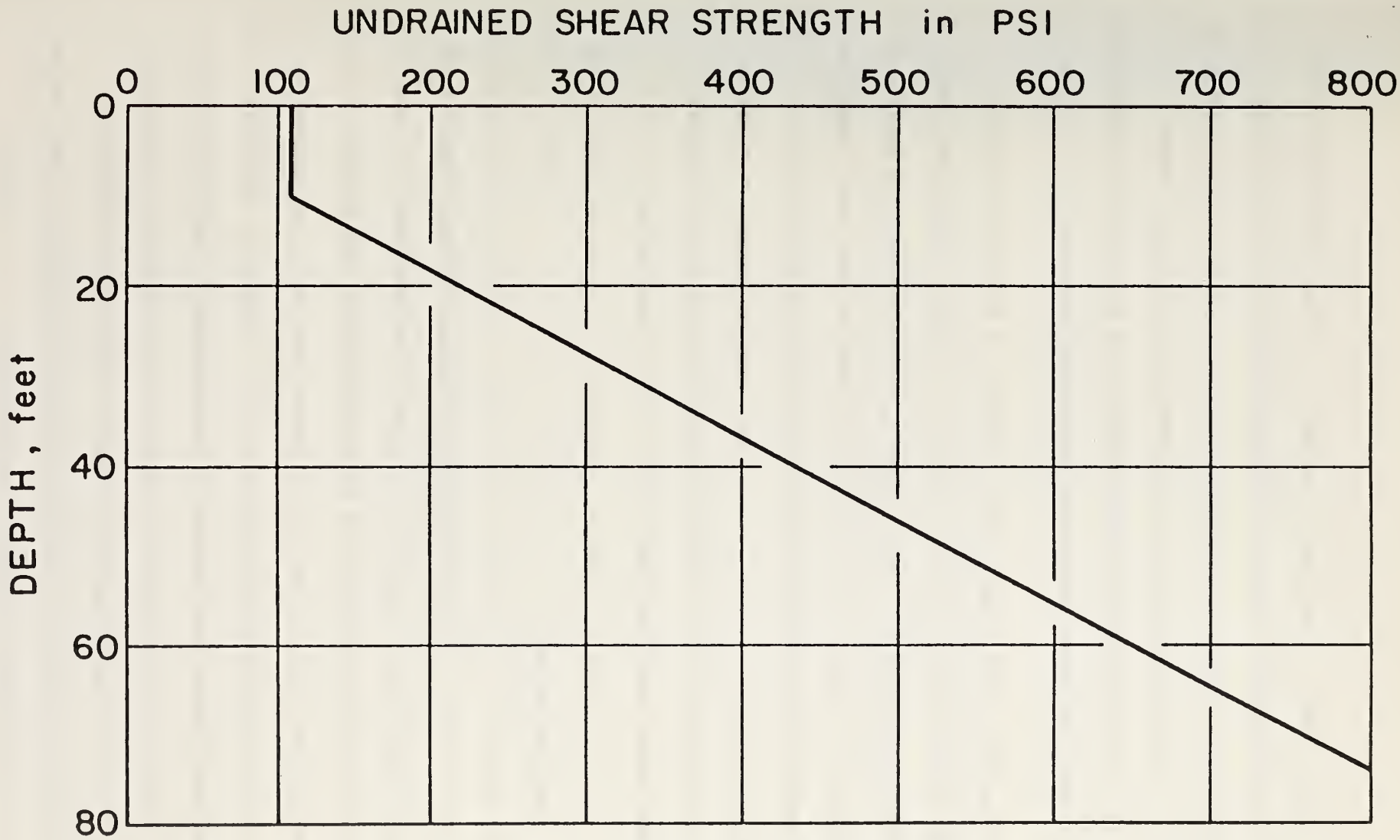

Figure 5.4: Shear Strength Profile

classified via the overload factor concept. The overload factor is the ratio of the overburden pressure at the springline to the undrained shear strength at that point (assuming no air or slurry pressure is present). It is used as an index of potential tunneling problems. Values of six or above indicate that significant movements are likely to occur towards the tunnel face for a conventional shield.

Of course, in the present case, there is no defined value of cohesion, per se, since the soil is linear elastic. However, as noted, the modulus value used was found assuming a certain undrained shear strength profile (Figure 5.4). Using this profile, the shear strength at the spring line is 3.7 psi (26 kN/m^2), and the overload factor calculates as 7.3. According to data presented by Clough and Schmidt (1977), the volume of the settlement trough created by conventional tunneling could reach about 10% of the tunnel cross-section.

5.2.3 Liner and Shield

For purposes of the analyses, the tunnel is assumed to be supported by a concrete liner with a thickness of 15 inches (0.4 m), a density of 144 pcf (24 kN/m^3) and a modulus of 30,000 ksi (207000 kN/m^3). To avoid aspect ratio problems relative to adjacent elements, the elements representing the liner in the finite element mesh were increased to 35 inches (0.9 m) thickness (see Section 4.5.1). Because of the larger than actual thickness and the need to increase the flexibility of the liner to allow for the effects of segment connections, the modulus used for the liner in the analysis was reduced. Applying both of these adjustments following the procedures outlined in Chapter 4, the final value of liner modulus is 3300 ksi (23000 kN/m^2).

As noted in Chapter 4, selection of a modulus for the elements representing the shield presents problems in that the flexibility of the shield is affected by not only the skin of the shield, but also the internal bulkheads and structural supports. This presents an indeterminate structural problem which is examined by means of parametric studies in subsequent sections of this chapter.

The shoving force F is applied uniformly away from the face to the last liner segment erected. On the shield, the shoving force is split into halves and applied uniformly to the front and rear of the shield (see Figure 4.3). The reason for the split in the case of the shield is that in the actual case, the hydraulic jack thrust is applied about midway along the shield length. The value of F used in subsequent analysis was 213 tons (1900 kN). This value is slightly higher than that estimated using equation 4.9. The higher value was used to ensure that the shoving force was high enough to move the shield forward as is done in practice. This force is applied as described in Chapter 4.

5.2.4 Boundary Conditions and Initial Stresses

Consider the block shown in Figure 5.5 as representing the finite element mesh and the faces of the block are as defined in the figure and as follows:

Face 1 - Portal

Face 2 - Artificial boundary located far enough not to influence problem.

Face 3 - Ground surface.

Face 4 - Boundary representing an underlying hard layer.

Face 5 - Artificial boundary located far enough not to influence problem.

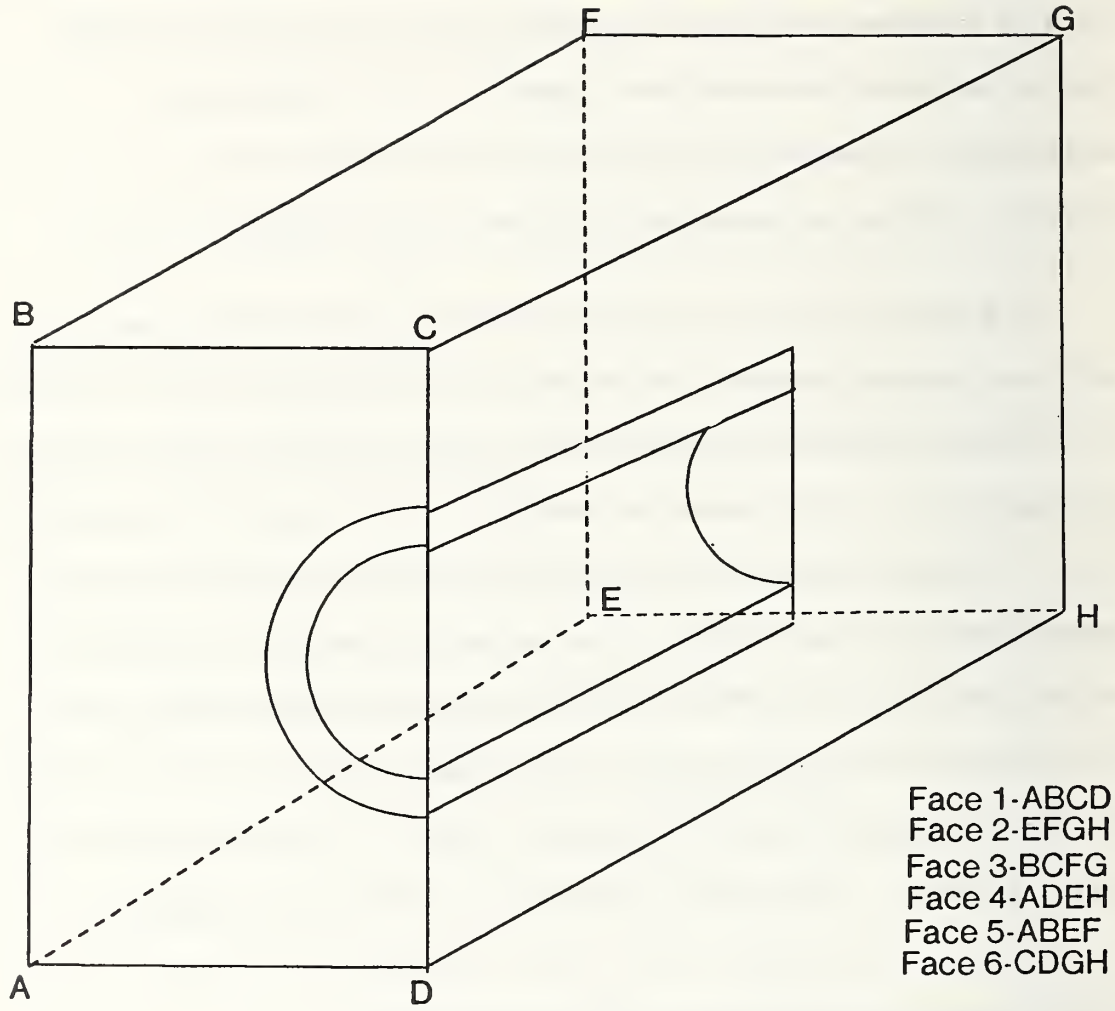

Figure 5.5: Block Showing Finite Element Mesh Boundaries

Face 6 - Plane of symmetry along the centerline of the tunnel axis and the soil mass.

The nodal restraints on each face follow from the conditions required for each face:

1. Nodes on face 4 are restrained against all movements due to the presence of the rigid layer.

2. Nodes on face 1 except those on edges AB, AD and CD are restrained against movement in the Y direction only. Nodes on AB and CD are restrained in the X and Y directions. AD is part of face 4 mentioned in (1).

3. Nodes on face 2 except those on edge EH are restrained against movement in the X and Y directions. EH is part of face 4 mentioned in (1).

4. Nodes on face 3 except those on the edges are not restrained. The corner nodes are restrained. Nodes on edge BC are restrained against movement in the Y direction and nodes on edges FG and BF are restrained against movement in the X and Y directions. Nodes on edge CG are restrained against movement in the X direction only.

5. Nodes on face 5 except those on edge AE are restrained against movement in X and Y directions. AE is part of face 4 mentioned in (1).

6. Nodes on the same plane as face 6 except those on edges CD, GH and DH are restrained against movement in the x direction only. Nodes on edges CD and GH are restrained against movement in the X and Y directions. DH is part of face 4 mentioned in (1).

7. The rest of the nodes are not restrained.

Initial gravity stresses are calculated using the simplified computation procedure described in Section 4.2.

5.3 ADVANCING SHIELD

A major emphasis in this research is the study of the displacement pattern due to an advancing shield. For a linear elastic analysis, this pattern can be derived from the results for one shove of the shield.

Consider the section shown in Figure 5.6. Assume the shield front is at position 3 initially, and r is the reference position at which displacement is being monitored. We want to determine the vertical displacement at r as the shield front advances from position 3 to 8. When the shield front is at position 4, it is at a distance of - 26 ft. (-8 m) from the reference point. At position 5, the distance is -13ft. (-4 m) and at positions 6 and 7 the distances are 13 ft. (4 m) and 26 ft. (8 m), respectively.

After the first shove, the shield front is at position 4 and the vertical displacement at r is that given by the single shove analysis from positions 3 to 4. From the results for the first shove, the

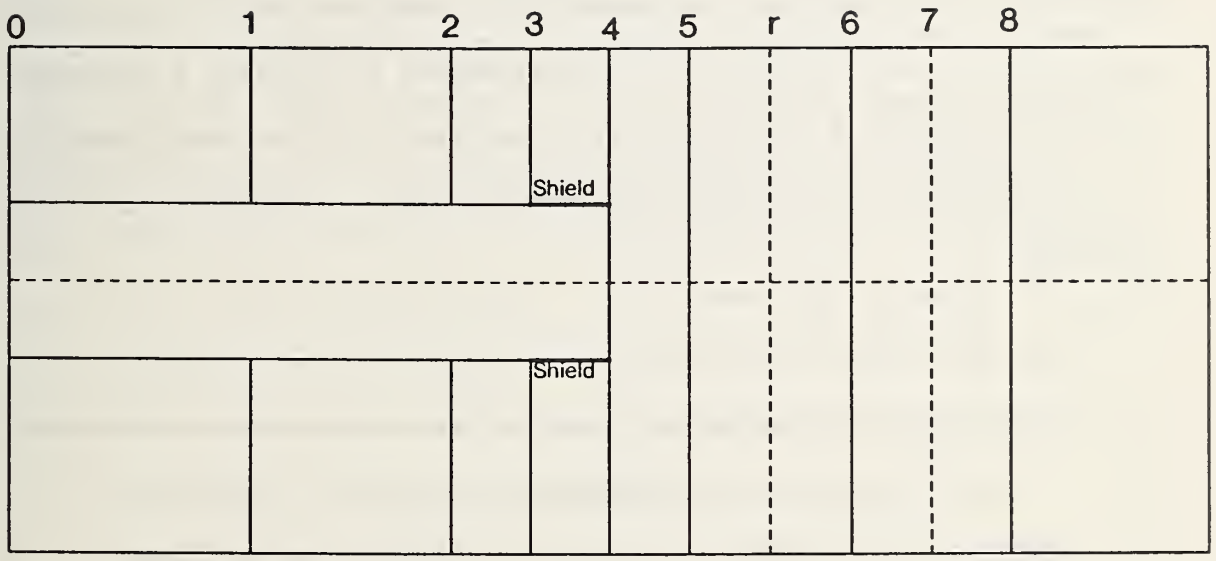

Figure 5.6: The Advancing Shield Problem

vertical displacement for subsequent shoves can now be derived. If the program were to be used to model the shove from position 4 to 5, the vertical displacement at r would be the same as that which occurred at position 5 due to the shove from position 3 to 4. The total vertical displacement at r when the shield front is at position 5, d_{r5}, is therefore given by

$$d_{r5}=d_{r4}+d_{54}$$

where d_{r4} is the vertical displacement at r when the shield front is at position 4 and d_{54} is the vertical displacement at position 5 when the shield front is at 4. Using a similar procedure for the other shield front positions, the vertical displacements given in Table 5.1 are obtained.

TABLE 5.1

Vertical Displacement for Various Positions of Shield Front

Position of Shield Front	Distance From Reference Position (feet)	*Vertical Displacement at Reference Position
4	-26	$d_{r4}=d_{r4}$
5	-13	$d_{r5}=d_{r4}+d_{54}$
r	0	$d_{rr}=d_{r5}+d_{44}$
6	13	$d_{r6}=d_{rr}+d_{34}$
7	26	$d_{r7}=d_{r6}+d_{24}$
8	52	$d_{r8}=d_{r7}+d_{14}$

* d_{ij} = Vertical displacement at i when the shield front is at j.

5.4 SELECTION OF PROPER SHIELD STIFFNESS

As mentioned previously, the definition of the shield modulus poses a problem since it must reflect the effects of the shield skin as well as any internal support system. A parametric study was therefore performed to determine a realistic value for the modulus. Two different conditions were considered:

1. The shield is assumed to consist only of a circular cylinder with no internal bracing due to bulkheads and reinforcing elements. In this case, the selection of a modulus value depends upon the modulus of the shield material and the relative thicknesses of the shield skin and that of the elements used to represent it in the finite element program. As for the liner elements, it is not possible to use a thickness in the finite element mesh which is the same as the actual shield. For purposes of numerical stability, a greater thickness must be used, and, thus a reduction in modulus is required in order to obtain a proper structural response. In the analyses, the shield material is assumed to be steel (E=30000 ksi) and the liner element thickness in the mesh is 35 inches (0.9 m). Applying a modulus reduction factor, calculated as described for the liner, the resulting modulus for the shield elements is 5200 ksi (36,000 kPa). Because this system is relatively flexible, this case is referred to as the low stiffness shield.

2. The shield is assumed to be heavily braced internally by the presence of bulkheads and other structural elements. The modulus

for the 35 inches (0.9 m) thick finite elements representing the shield is set at 30,000 ksi (207,000 kPa), or that of steel with no reduction factor. This produces a shield which for practical purposes is inflexible, and it is referred to as the high stiffness shield.

Aside from the stiffness of the shield, other factors are kept the same in order to allow a direct comparison of the two cases. For both analyses, the shield is assumed to be a conventional type with an open face and a total weight of 200 tons (1780 kN)

The validity of the computed results is judged by comparisons with certain established field behavior trends. These include:

1. The form and shape of the surface settlement bowl. Schmidt (1969) has shown that most field surface settlement data follow the shape predicted by the Gaussian error function, and this can be used to test the predicted behavior.

2. The form and shape of the settlement profile created by the movement of a given point on the tunnel center line as the shield approaches and then advances beneath the point. Observations reported by Cording and Hansmire (1975) have established what this profile should look like for conventional shield operations noting it is influenced by movements into the face, over the shield, and into the tail void.

The comparison between the finite element results for the two shield stiffnesses with the Gaussian error function is shown in Figure 5.7. As expected the flexible shield case yielded larger deformations than the stiff one. More importantly, the settlement at the centerline above the flexible shield is about six times larger than that for the stiff case, emphasizing the significance of shield stiffness on the tunnel analyses. Comparison of the theoretical error function to the predicted profiles shows that both cases have settlement curves in reasonable agreement to theory, although the results for the stiff shield give the best fit. This comparison does not permit a definitive conclusion to be drawn however as to which shield stiffness is more reasonable.

The second test of the predicted data is the nature of the settlement profile created by an advancing shield. A qualitative comparison is made between the finite element results and field data from the Washington, D.C. Metro (Cording and Hansmire, 1975) in Figure 5.8. This case is used since it is suggested by Cording and Hansmire (1975) to be typical for properly operating conventional shield in soils. The results clearly show that the high stiffness shield give a more realistic behavior. The actual field data demonstrate that settlements primarily are developed after the face of the shield has passed the reference point (face of shield greater than 10 feet (3.1 m) passed the reference point). A similar response is obtained using the high stiffness shield. Both the form and general magnitude of settlements predicted by the analysis are correct. The low stiffness shield on the other hand causes significant settlements to occur before

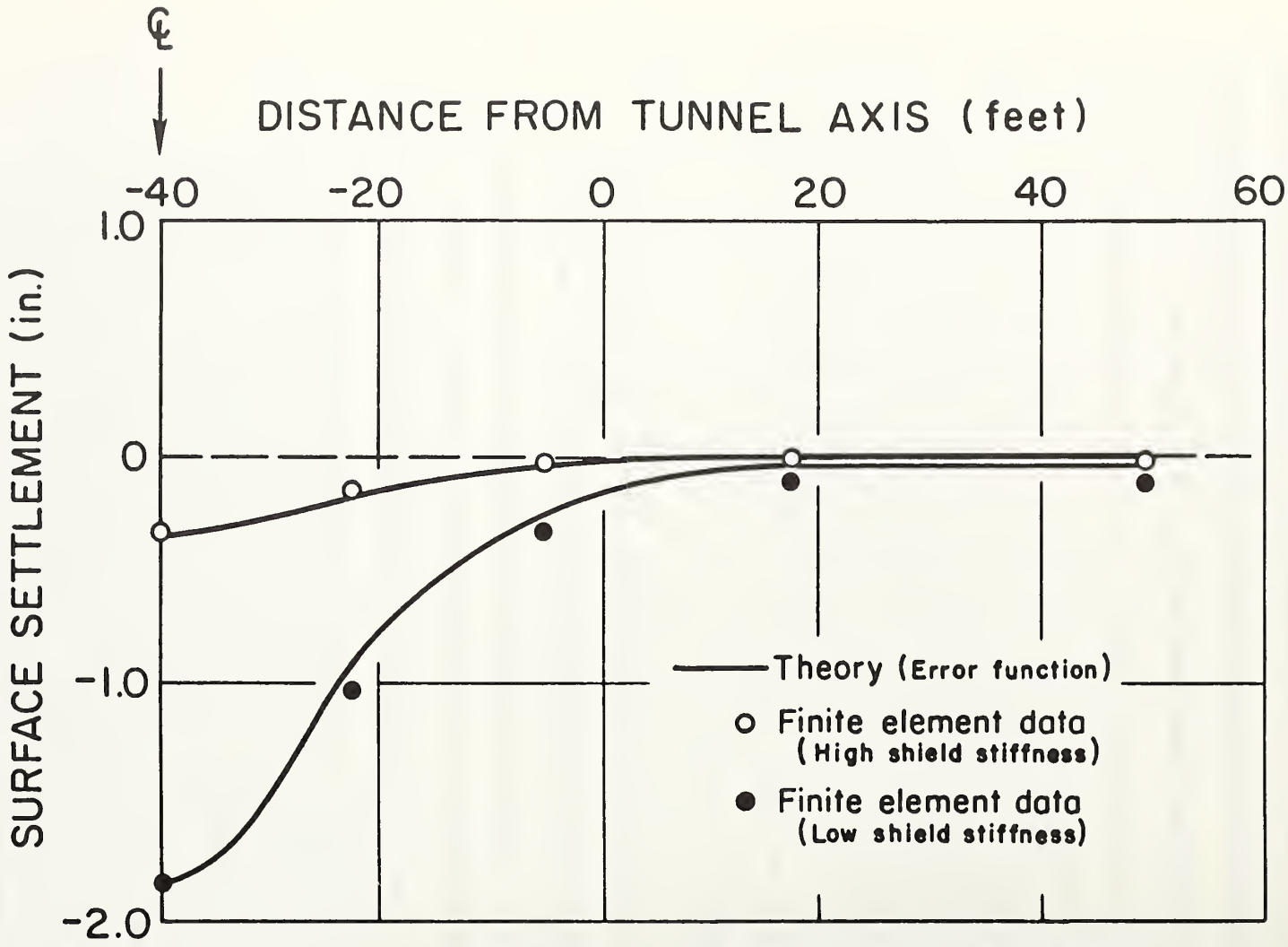

Figure 5.7: Comparison of Finite Element Data With Error Function

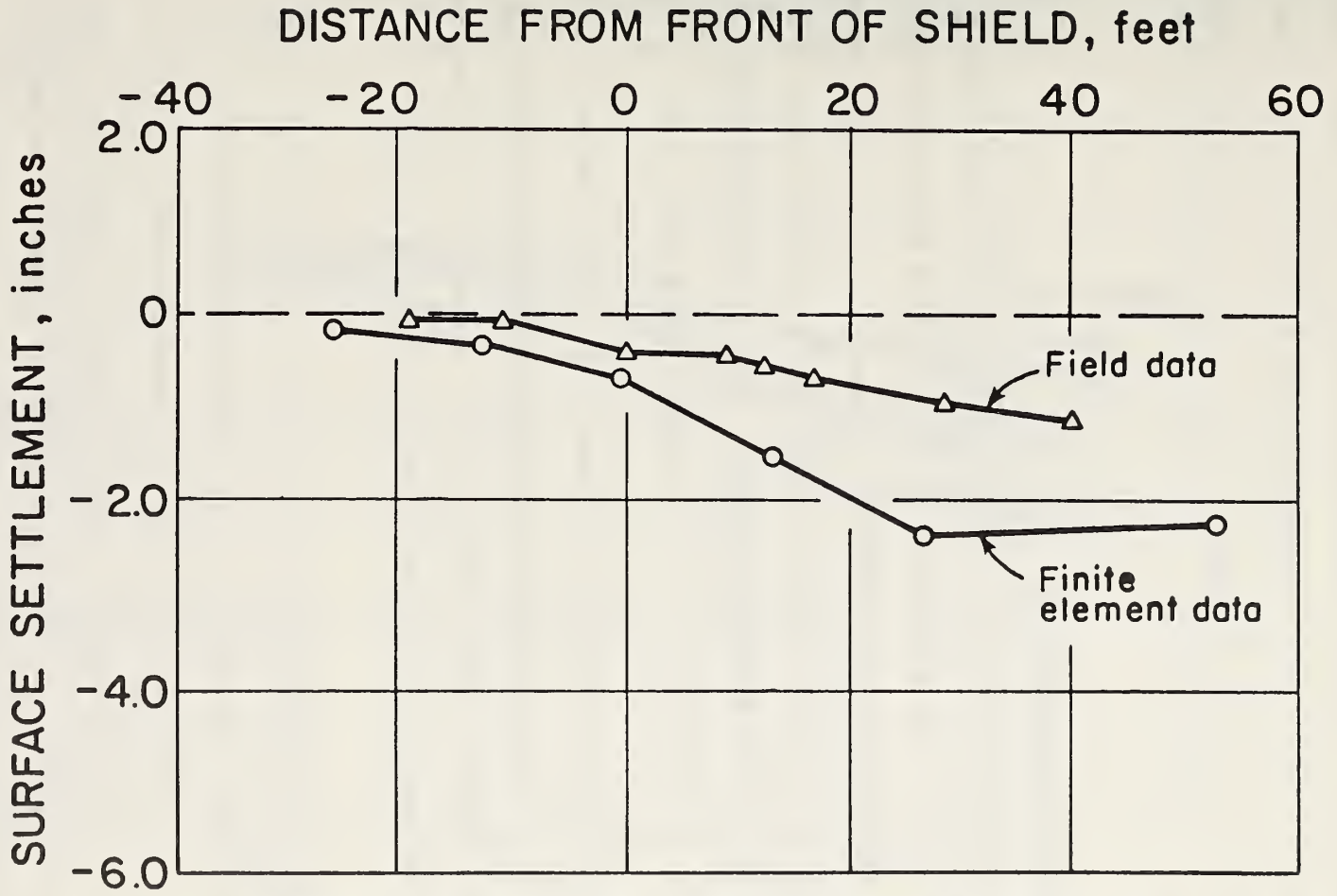

Figure 5.8: Comparison of Field and Finite Element Data

the tail void effect occurs. This is due to the compression of the flexible shield, a behavior which does not occur in the field. Thus, it is clear that the correct representation for the shield is the high stiffness case. In all subsequent analyses, the high stiffness shield is used.

5.5 EFFECT OF SHIELD WEIGHT

Shield weight can vary from 40 to 300 tons (356 to 2670 kN) depending on the size and type of shield. In this study, the typical value is taken as 200 tons (1780 kN), however it is useful to consider the effect of different values in order to evaluate the significance of shield weight on the predicted results. Runs were performed using values for the weight of 0, 40, 80 and 240 tons (0, 356, 712, 2136 kN).

Results for the analyses are shown in the form of advancing shield plot in Figure 5.9. As expected, the heavier the shield, the larger the settlement since the weight pushes the soil downwards. It is obviously important to include the weight of the shield in the analyses.

5.6 EFFECT OF LINER WEIGHT

To determine the effect of the liner weight on the deformation pattern of an advancing shield, two runs were made with and without the addition of the liner weight. The liner weight for each shove of the shield is the weight of the liner segment last erected. The addition of the liner weight is effected by applying concentrated vertical loads equivalent to the weight of liner segment to the nodal points constituting the segment. In this analysis, a liner weight of 6.5

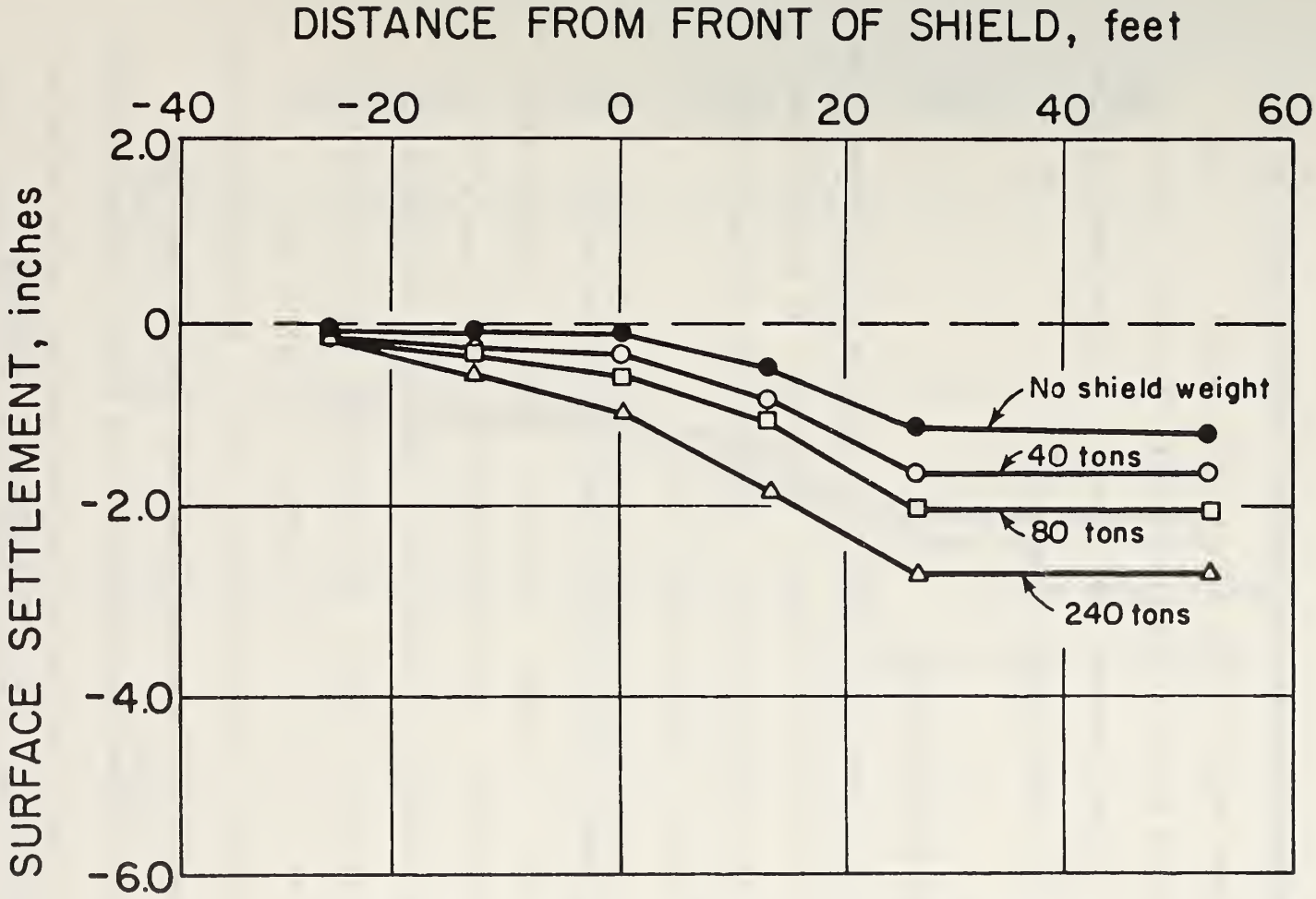

Figure 5.9: Effect of Weight of Conventional Shield

tons/linear feet (191.5 kN/linear feet) of liner was used. This is based on the weight of a liner segment 15 inches (38 cm) thick and made of concrete with a density of 144 pcf (22.5 kN/m^3).

The deformation patterns for these two cases are shown in Figure 5.10. The figure shows that the effect of the weight of the liner segment considered herein is not significant. This conclusion may not be true for a thicker concrete liner segment. In subsequent analyses, the weight of the liner segment is neglected.

5.7 EFFECT OF SHOVING FORCES

The shoving forces serve primarily to move the shield forward. In addition, they help prevent dipping of the shield. To ascertain their importance on the predicted behavior, runs were made with and without the shoving forces on the conventional shield.

The displacement vector plot at a section parallel to the longitudinal axis of the tunnel is shown in Figure 5.11 for the case without shoving forces. The corresponding plot for the case with shoving forces is shown in Figure 5.12. Figure 5.11 indicates that where shoving forces are absent, the displacement component parallel to the longitudinal axis of the tunnel across the tunnel face is approximately uniform. Also, the shield itself is shunted backwards and settles or dives below its original position. For the case where shoving forces are present however, there is a bulge in the displacement profile at the face reflecting the fact that the soil in the center of the face moves into the tunnel axis more than the edge adjacent to the

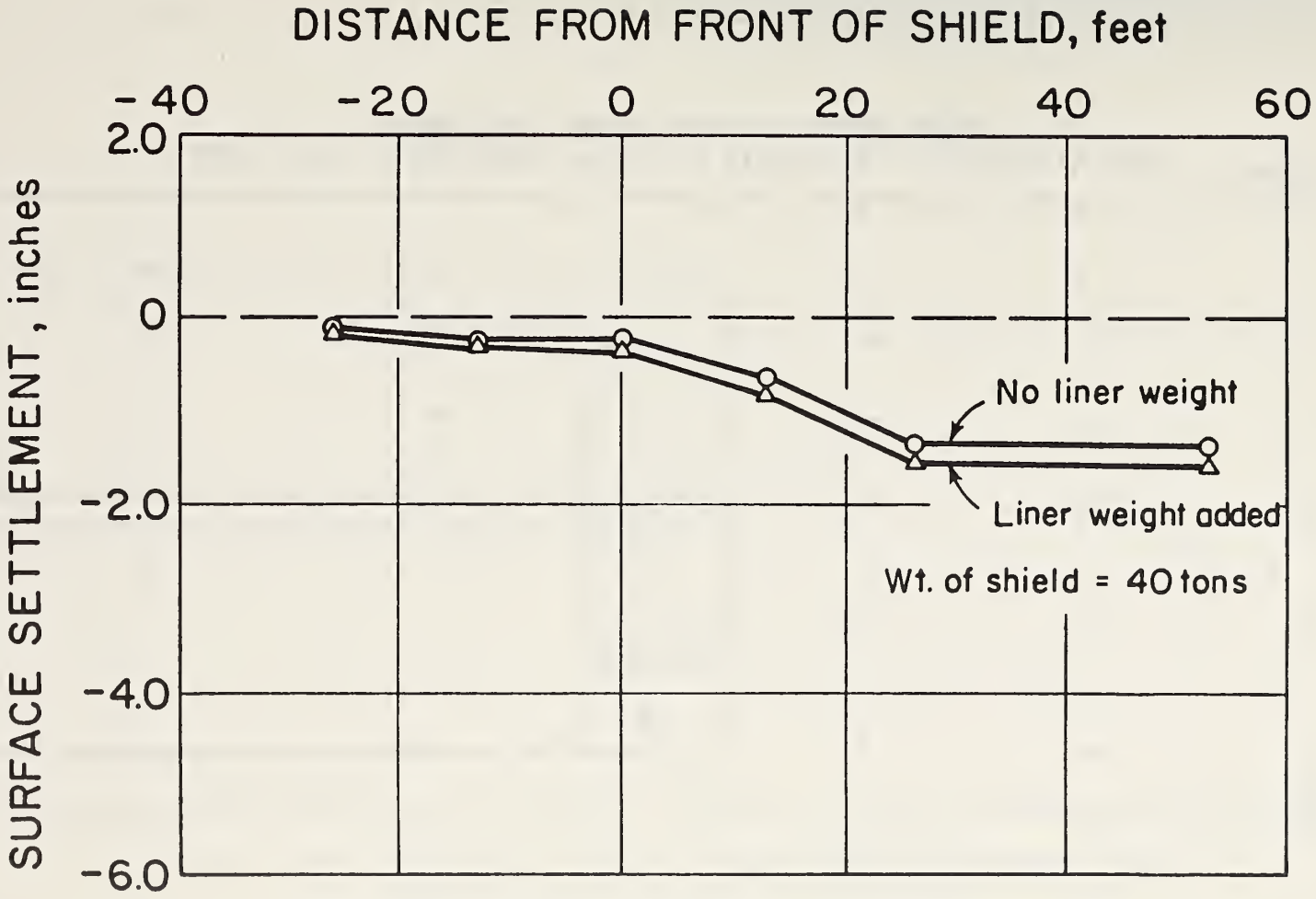

Figure 5.10: Effect of Liner Weight - Conventional Shield

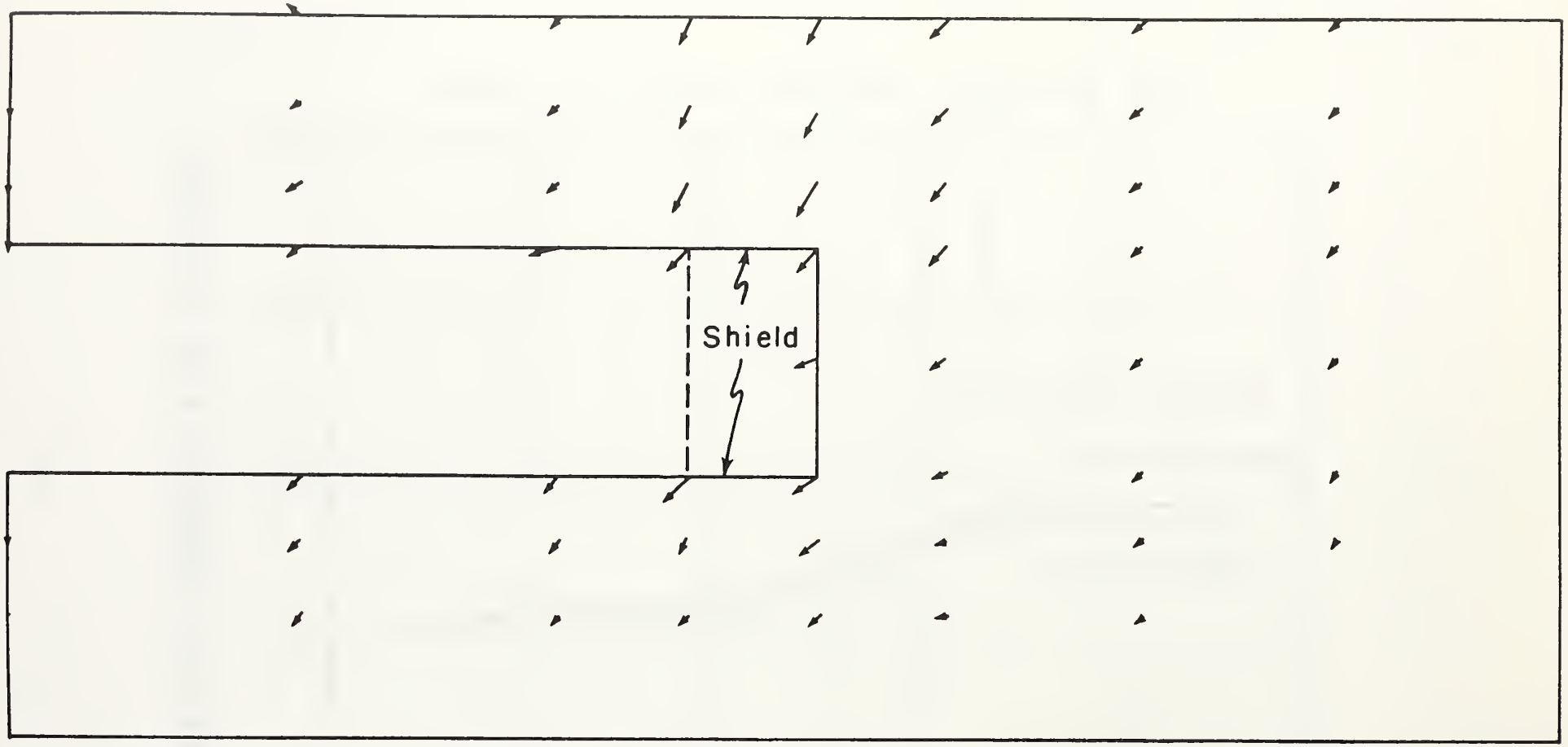

Scale 1 in. = 0.66 ft.

Figure 5.11: Displacement Vector on Plane Along Longitudinal Axis - Conventional Shield With No Shoving Forces

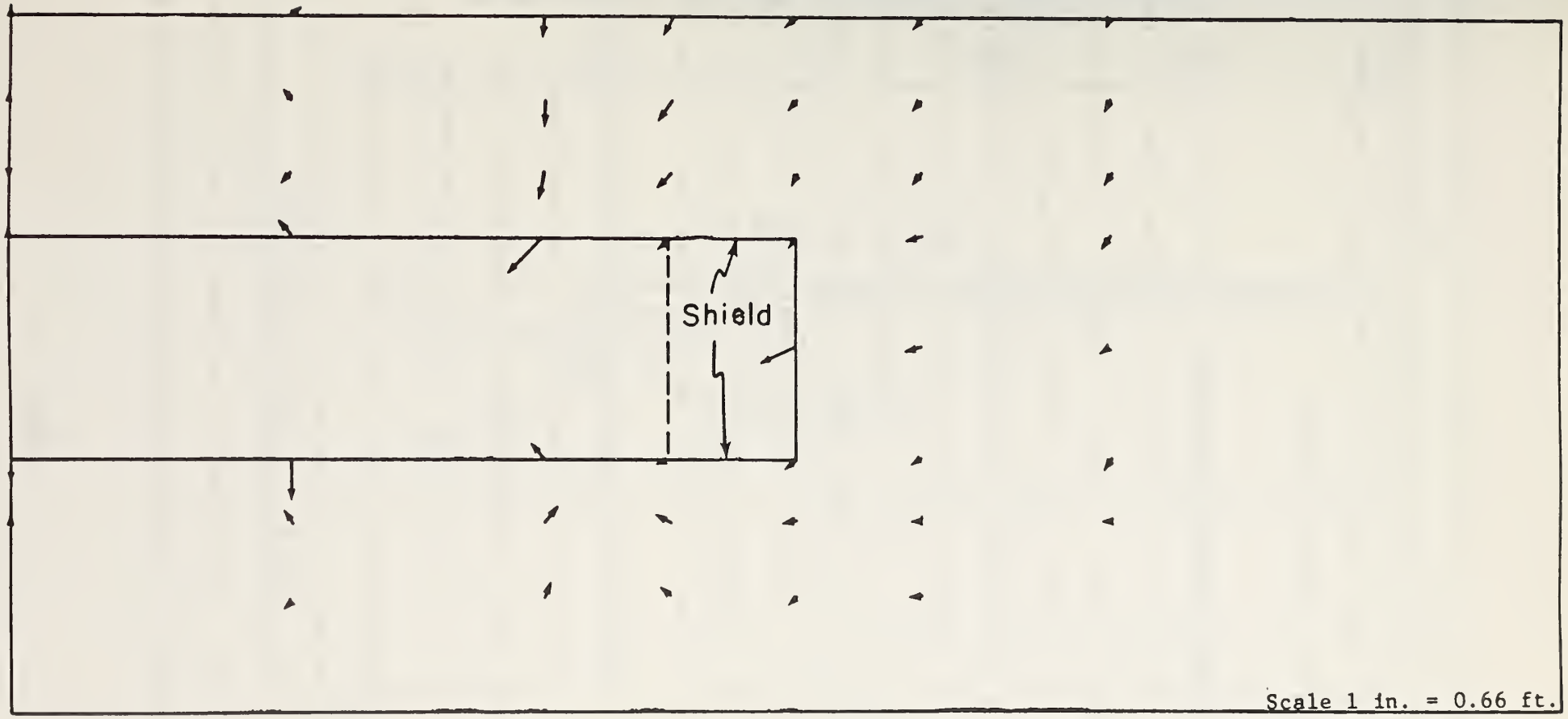

Figure 5.12: Displacement Vector on Plane Along Longitudinal Axis - Conventional Shield with Shoving Forces

shield. In addition, the general pattern of shield movement is changed, and in particular, the diving of the shield is eliminated (see Figure 5.12). Thus, the application of shoving forces leads to much more realistic results as would be expected.

5.8 VERIFICATION OF BOUNDARY CONDITIONS

As noted earlier in this chapter, the positions of the left, front and rear boundaries (faces 1, 2 and 5 in Figure 5.5) of the finite element mesh were chosen to avoid influencing displacements and stresses around the face of the shield. The appropriateness of the boundary positions can be examined using the results of a conventional shield run. For this purpose, a plot is prepared of the settlement bowls at the face of the tunnel and about 12 feet (4 meters) behind the face after one shove of the shield. The settlement bowls are shown in Figure 5.13. Also, the displacement profile at a section parallel to the longitudinal axis after one shove of the shield is shown in Figure 5.14.

Figures 5.13 and 5.14 show that the displacements at points close to the boundaries are very small and constant. The displacement profiles indicate that the boundaries are far away enough not to significantly affect the displacement pattern around the opening.

The stress patterns around the opening after one shove of the shield is examined by plotting the vertical stress values on a section at the tunnel face and those on a section parallel to the longitudinal axis of the tunnel. The stresses are non-dimensionalized by dividing the vertical stress at the center of the element after the shove by the

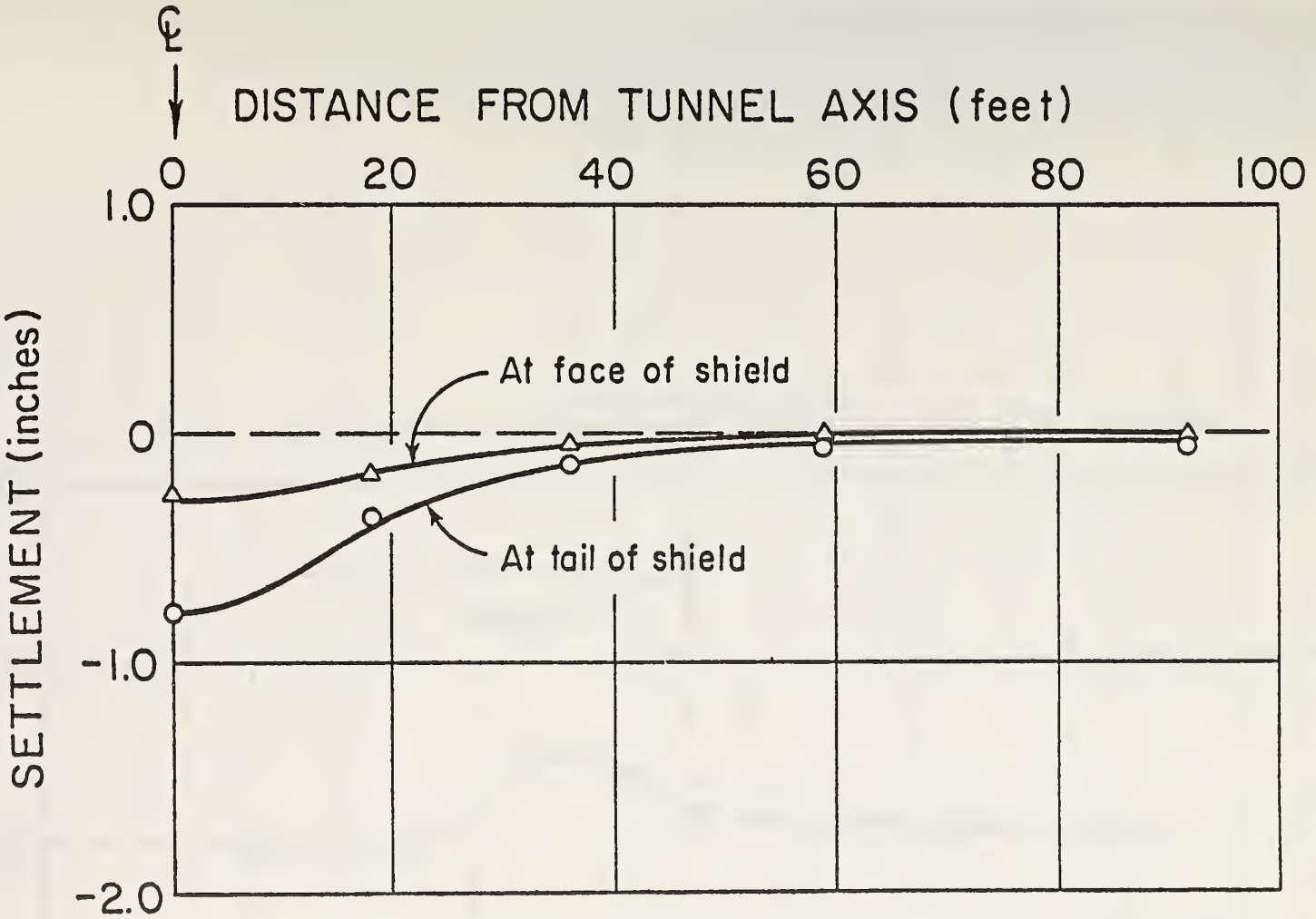

Figure 5.13: Settlement Bowl After One Shove of Conventional Shield

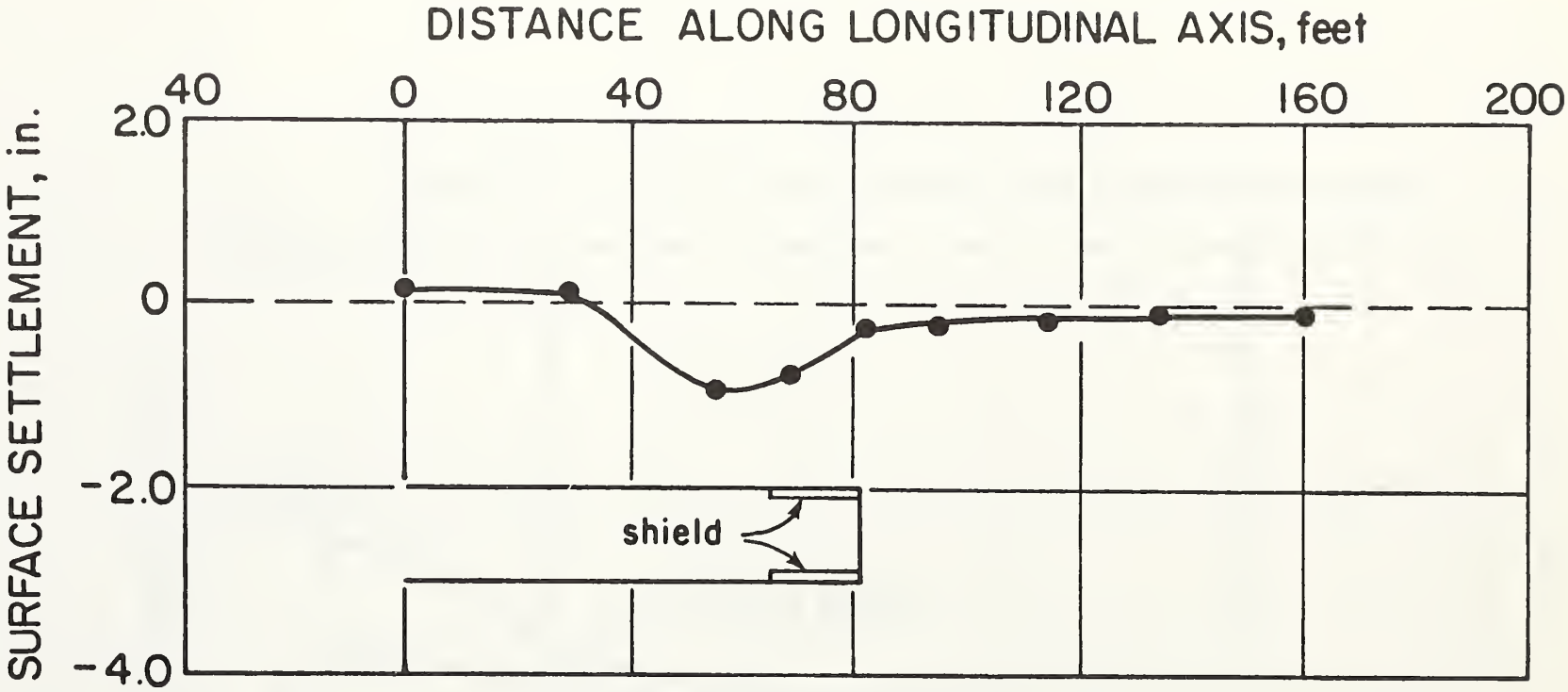

Figure 5.14: Surface Settlement Along Longitudinal Axis After One Shove Of Conventional Shield

initial or gravity stress in the element. If the boundaries are properly located, the stresses in each element near them should be essentially unchanged by the tunneling process. Non-dimensional stresses on a cross-section at the tunnel face and along the tunnel axis are given by Figures 5.15 and 5.16, respectively. The results show that there is little change in vertical stress close to the boundaries. This conclusion confirms the earlier observation made from the displacement pattern plots. Thus, the boundaries do not affect the displacement and stress patterns around the opening and are properly located.

The plots show that in general, the vertical stresses in the zones below and above the tunnel opening are reduced from their initial values whereas the stresses are increased at the springline. The magnitude of these stress changes are affected by the level of decompression which takes place in the conventional shield.

5.9 SUMMARY

The following points which are relevant in subsequent analyses to be performed were deduced from the parametric studies presented in this chapter:

1. The weight of the shield is added for each analysis. For this work, the assumed shield weight is 200 tons (1780 kN), a value typical for the size of opening studied herein.

2. The shield itself is assumed to be very stiff and not to compress or distort under the action of the soil pressure.

3. The shoving forces are applied to the shield and the in-place liner in order to properly model the shield tunneling procedure. The value of the total shoving force, F is taken as 213 tons (1900 kN); it is based on the force required to overcome the adhesion on the shield circumference.

4. The finite element mesh is designed to take advantage of the symmetry which exists about the vertical axis of the tunnel. Only a half mesh is used with the plane along the vertical axis of the tunnel serving as a plane of symmetry.

5. The left, front, and rear boundaries of the finite element mesh are positioned so as to have little influence on the predicted results around the tunnel face. The right boundary is the plane of symmetry, the upper boundary the ground surface, and the lower boundary the top of an assumed very stiff underlying soil or rock layer.

Perhaps the most important conclusion drawn from the parametric studies is that each time a step was taken to use modeling procedures closer to actual practice, the more realistic the predicted behavior became.

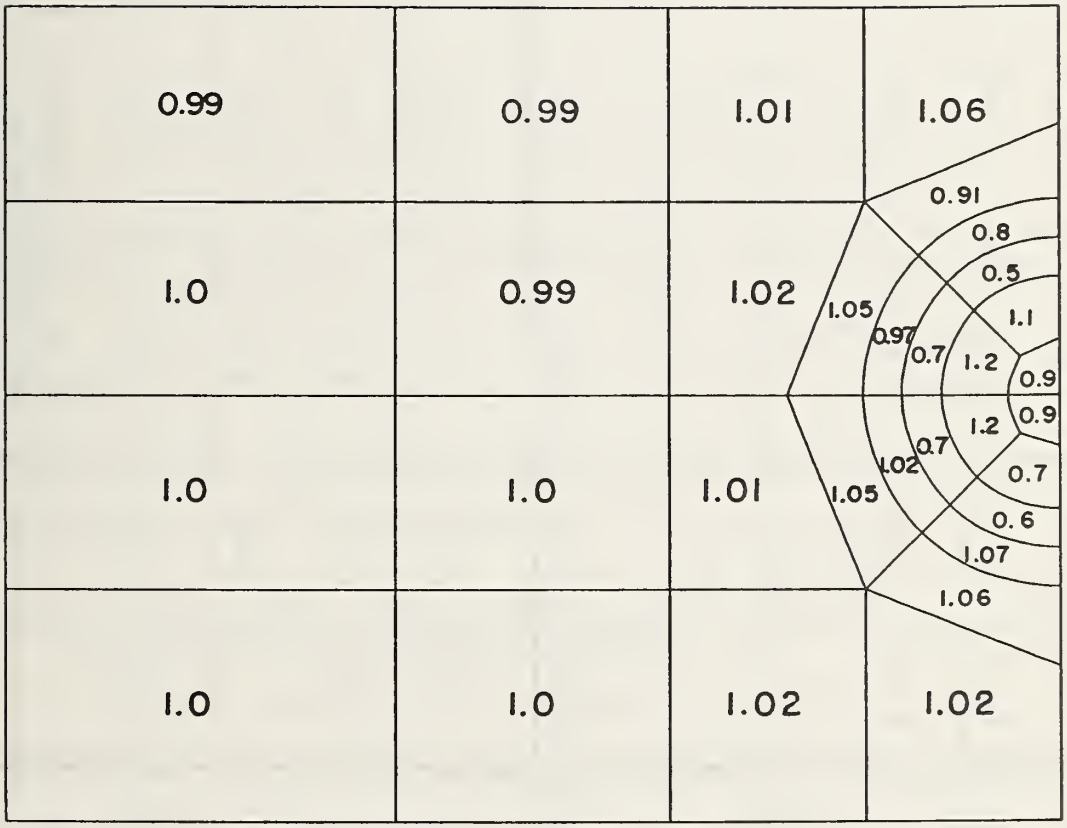

Figure 5.15: Non-Dimensionalized Vertical Stresses on Cross-Section at Tunnel Face-Conventional Shield

FACE

↓

1.01	0.96	1.20	0.93	1.06	1.01	1.03	1.0
1.44	1.60	1.30	1.60	0.91	1.03	1.05	1.01
1.20	0.80	1.20	1.10	0.80	1.0	1.03	1.06
1.40	1.10	1.10	1.12	0.50	0.90	0.97	0.90
1				1.1	1.08	1.08	1.06
1.0	1.20	1.10	1.24	0.90	1.05	1.02	1.0
1.0	1.32	0.98	1.13	0.90	1.07	1.02	1.0
1.30	0.45	0.94	0.80	0.70	1.07	1.05	1.01
				0.60	0.79	0.90	0.90
1.30	0.94	0.90	0.90	1.06	1.06	1.07	1.07
1.24	1.30	0.84	1.1	1.06	0.98	0.99	0.98
1.01	0.96	0.98	1.1	1.01	1.0	1.0	1.0

Figure 5.16: Non-Dimensionalized Vertical Stresses on Plane Along Longitudinal Axis - Conventional Shield

Chapter VI

CONVENTIONAL AND ADVANCED SHIELDS

6.1 INTRODUCTION

Based on the results described in Chapters 4 and 5, the groundwork has been established for comparative analyses involving the three different shield types considered in this study namely, the conventional, slurry and EPB shield machines. For the conventional shield, results from section 5.4 will be used. These are felt to represent the most realistic modeling of the normal open-faced soil tunneling shield. Corresponding results for the slurry and EPB shields are presented later in this chapter.

6.2 PARAMETERS USED IN SUBSEQUENT ANALYSES

The analyses presented in this chapter were made using the same finite element mesh and soil parameters used for the conventional shield as described in Chapter 5. For all cases, the same liner modulus, shield weight and shield stiffness are assumed.

6.3 MODELING OF ADVANCED SHIELDS

The general modeling procedures used for the advanced shields were described in Chapter 4. The main difference between them and the conventional shield is that pressures are exerted on the face of the tunnel and possibly in the tail void area which help reduce movements in

the soil. In the following sections, several alternative pressure distributions and locations are considered for these support pressures.

6.3.1 Soil Support by the Slurry Shield

In the slurry shield, the slurry is brought into the bulkhead area at the face of the shield and forced out against the soil face through the open slits in the cutter head. The soil itself is presumably not in contact with the cutterhead, but rather is separated from it by a layer of pressurized slurry. This type of support at the face is unquestioned. However, there is a debate over the issue of whether the slurry migrates around the shield and thence supports the soil in the tail void area. There is no direct published data to support this type of behavior. Discussions with manufacturer representatives suggests that it may or may not happen depending on the soil type. In order to examine the importance of this issue, two possibilities were considered in the analyses:

1. The slurry pressure was assumed to support the soil around the shield, in the tail void and on the face of the tunnel.

2. The slurry pressure was assumed to support the soil on the face of the tunnel only.

It was assumed that the slurry exerted a high enough pressure to reduce the overload factor to 3 for the tunnel opening. To calculate the overload factor, the soil is assumed to have a shear strength profile as shown in Figure 5.4. The overload factor is defined as the

ratio between the overburden stress at the springline less the slurry pressure divided by the undrained shear strength of 3.7 psi (26 kN/m^2) at the springline. The resulting slurry pressure is 16.1 psi (114 kN/m^2). For the first case, the pressure is applied to all the elements exposed on the face, around the shield and at the tail void. For the second case, the pressure is applied to the face only.

Ground settlements for the two analyses are presented in Figure 6.1 in the form of the advancing shield diagram. Movements which occur at the ground surface on the tunnel axis are depicted for shield positions from 33 feet (10 m) in front of the reference point to 50 feet (15 m) ahead of it. Significantly, in both cases, the slurry pressures at the face cause a slight heaving of the ground surface as the shield approaches. Once the shield is past the reference point, and the tail void effects show up, the ground surface settles. This general behavior is consistent with that monitored for several advanced shield projects (see Kitamura et al., 1981 and Clough, et al., 1982).

The significant difference between the two cases is reflected in the settlement which occurs due to the tail void. Where the slurry pressure is assumed to act in the tail void area, the ground settlements are five times less than those where they do not. Obviously, the presence of slurry pressure support in the tail void is a very positive factor. However, based on limited published data about ground movements associated with slurry shields (Takahasi and Yamazaki, 1976 and Miki, et al., 1977), the settlements predicted for the case without pressure in the tail void are the more reasonable. Only with future research will

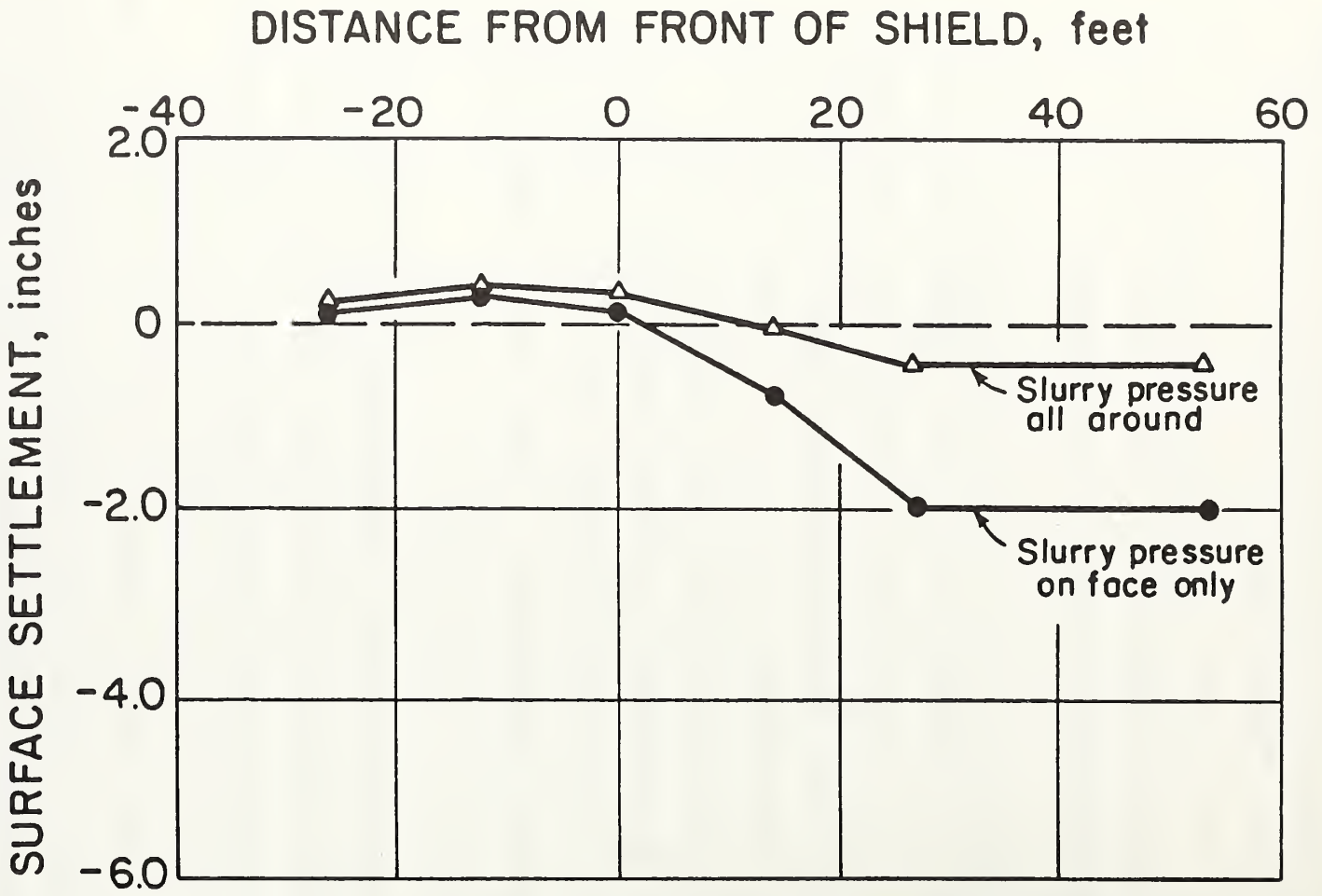

Figure 6.1: Comparison of Soil Support Schemes in Slurry Shield

the actual mechanics of the problem be fully understood. For the present, it appears that the second case of slurry support where pressure is applied at the face only is the more representative of the actual situation. In subsequent comparisons of behavior between shield types, this case will be used.

6.3.2 Soil Support By The EPB Shield

In Chapter 2, the fundamental support mechanisms for the EPB shield were reviewed. The actual nature of the stress exerted by this shield to support the soil at the face will depend upon the balance maintained between the amount of soil taken into the bulkhead area by the rotating cutterhead and the amount removed by the screw auger. Should these amounts be exactly balanced, then, in theory, the soil at the face is relatively undisturbed since no net outward or inward stress gradient exists. On the other hand, should less soil be removed by the screw auger than attempts to enter via the cutterhead, then the soil around the face will be subjected to an outward pressure, the amount of which could be extremely large if the shield operates by taking no soil into the bulkhead. In this case, it would be akin to shoving the shield "in the blind". Finally, if the screw auger should remove soil from the bulkhead area at a greater rate than it is brought in by the cutterhead, then a void can develop in the bulkhead area, and soil at the face may flow into the shield in an uncontrolled manner.

In fact, the evidence is, based on published data for ground movements, that the EPB shield is normally operated in such a manner as to some degree to heave the soil during its passage (Kitamura, et al.,

1981 and Clough, et al., 1982). Thus, there is a net positive pressure exerted at the face, which is of a magnitude large enough to push the soil away from the shield. Neither the exact amount or distribution of this pressure is known at this time. For this work, two distributions of the pressure at the face of the EPB shield are considered:

1. Triangular

2. Uniform

In both cases, the pressure is taken as that which would occur when the thrust jacks for the shield push off of the in-place liner. The pressure due to this thrust force is applied to the face elements exposed by excavation. For the triangular pressure distribution, the pressure is taken to be zero at the crown and 4.3 psi (30 kN/m^2) at the invert. This is equivalent to a situation where the banks of jacks below the springline are activated to shove the shield forward. For the uniform pressure distribution, a uniform pressure of 2.1 psi (15 kN/m^2) was applied to the exposed face elements. This second assumption implies that pressure is exerted uniformly over the tunnel face through the excavated soil in the bulkhead. Note that the pressure levels for the EPB shield are considerably less than those used for the slurry shield analyses (16 psi or 114 kN/m^2).

The advancing shield plots for the two assumptions are shown in Figure 6.2 The results are virtually identical, indicating that the pressure distribution at the face has relatively little effect on the final behavior.

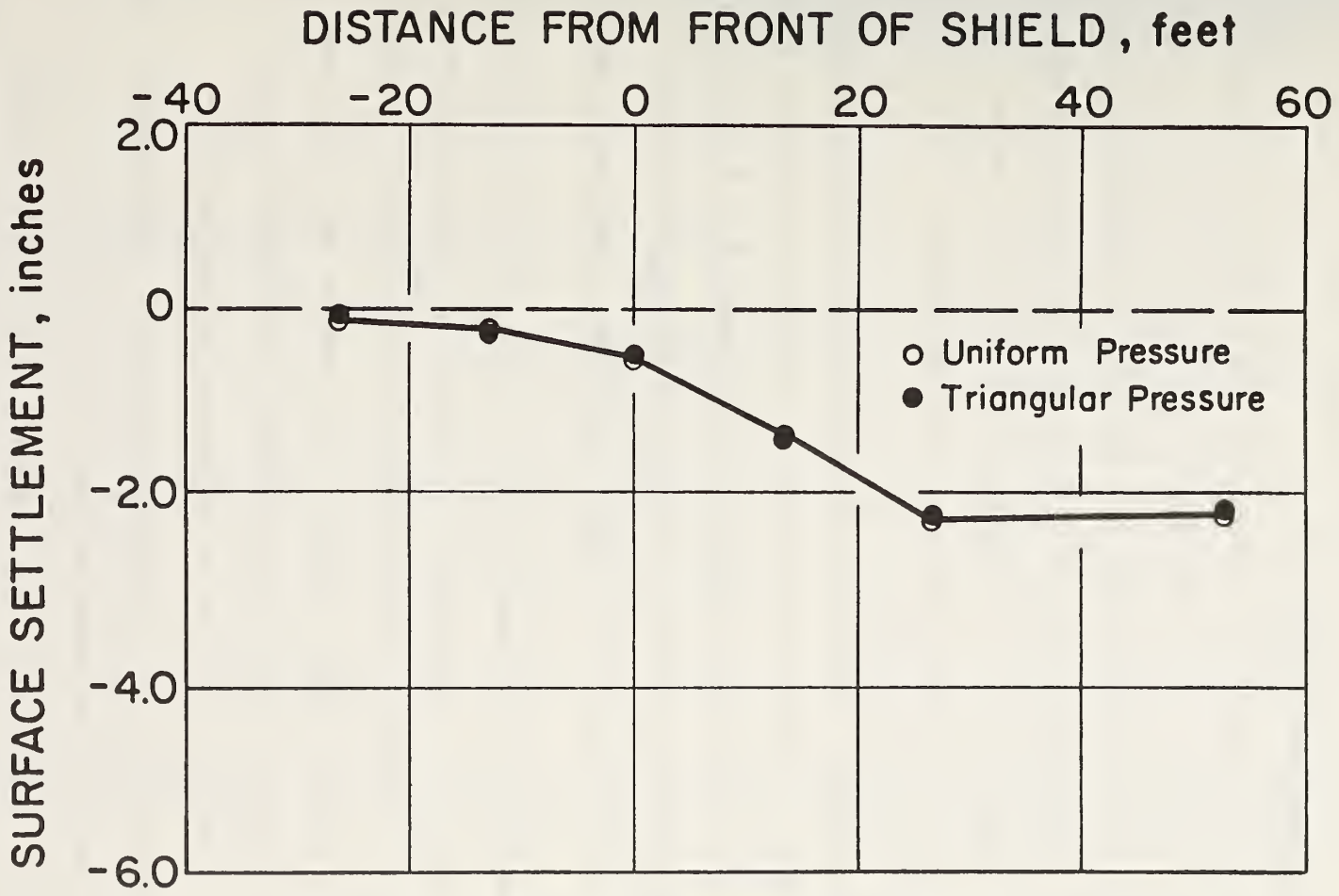

Figure 6.2: Pressure Distribution at the Face - EPB Shield

6.4 DISPLACEMENT PATTERNS

6.4.1 Along Longitudinal Axis

In order to understand the reasons for the predicted differences between the different types of shield, it is useful to examine in detail the development of the displacements. Data will be presented for the cases of the conventional and slurry shield (slurry pressure at the face only). The results for the EPB shield fall about halfway between the other two, and will only be covered later in the chapter.

The displacement vectors at a section parallel to the longitudinal axis induced by one shove of the conventional shield are shown in Figure 5.12. There are significant movements towards the tunnel opening in the tail void area and at the face. At distances greater than one and one-half diameters ahead of the tunnel, negligible displacements occur.

The comparative displacement vector plot for the slurry shield is shown in Figure 6.3. At the face of the tunnel, the slurry pressure actually counter-balances the inward movement tendencies and forces the soil outward from the tunnel opening. This leads to the ground heave effect which occurs as the shield approaches a reference point (see Figure 6.1). However, in spite of the heaving at the face, the movements into the tail void area are significant. These movements lead to the settlement of the ground surface as the shield passes a given reference point (see Figure 6.1). As noted earlier in this chapter, control of movements in the tail void area are crucial to helping reduce ultimate ground settlements.

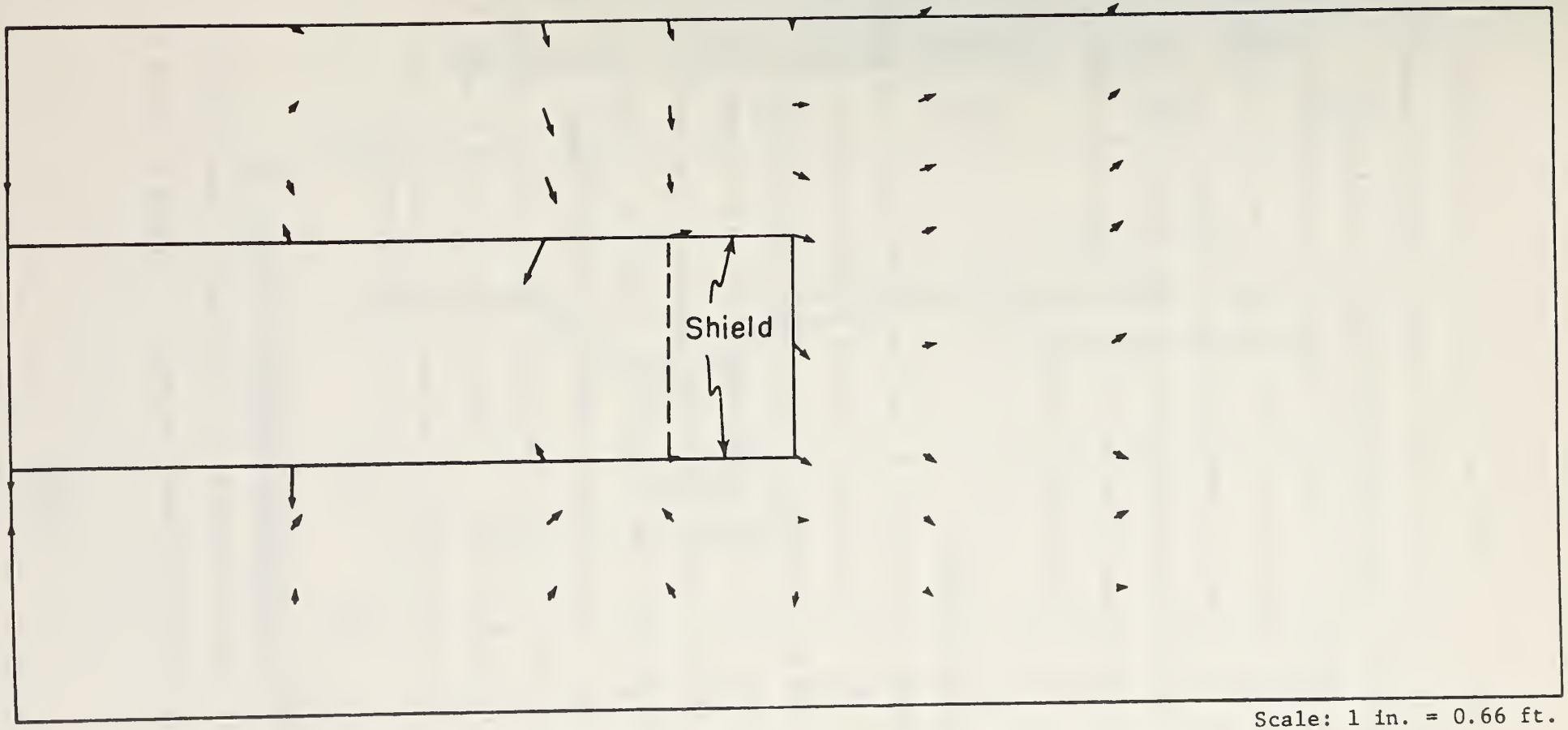

Scale: 1 in. = 0.66 ft.

Figure 6.3: Displacement Vector on Plane Along Longitudinal Axis - Slurry Shield

Another view of the effects of the single shove on the ground surface is shown in Figure 6.4, a plot of surface settlement generated along the longitudinal tunnel axis by the advance. The figure illustrates the significant movement at the tail for the conventional and slurry shields. Interestingly, these movements are slightly larger for the slurry shield than the conventional shield. Ahead of the shield, the situation is reversed since the ground surface for the slurry shield is heaved upwards as the shield approaches while the opposite occurs for the conventional shield.

6.4.2 Around Tunnel Opening

The displacement vector plot at a section at the tail of the shield for the same shove of the conventional shield is shown in Figure 6.5. The plot shows that soil movement due to the tunneling activity is towards the center of the tunnel cross-section. The displacement pattern has the effect of making the tunnel cross-section slightly elliptical in the deformed state compared to the original circular shape. This movement into the tunnel opening confirms the same observation made earlier from the displacement vector plot at a section parallel to the longitudinal axis. A similar observation can be made for the slurry shield based on the corresponding plot shown in Figure 6.6.

6.5 LATERAL MOVEMENTS DURING SHIELD PASSAGE

The predicted lateral movements at a cross-section perpendicular to the tunnel axis during shield advance are shown in Figures 6.7 and 6.8

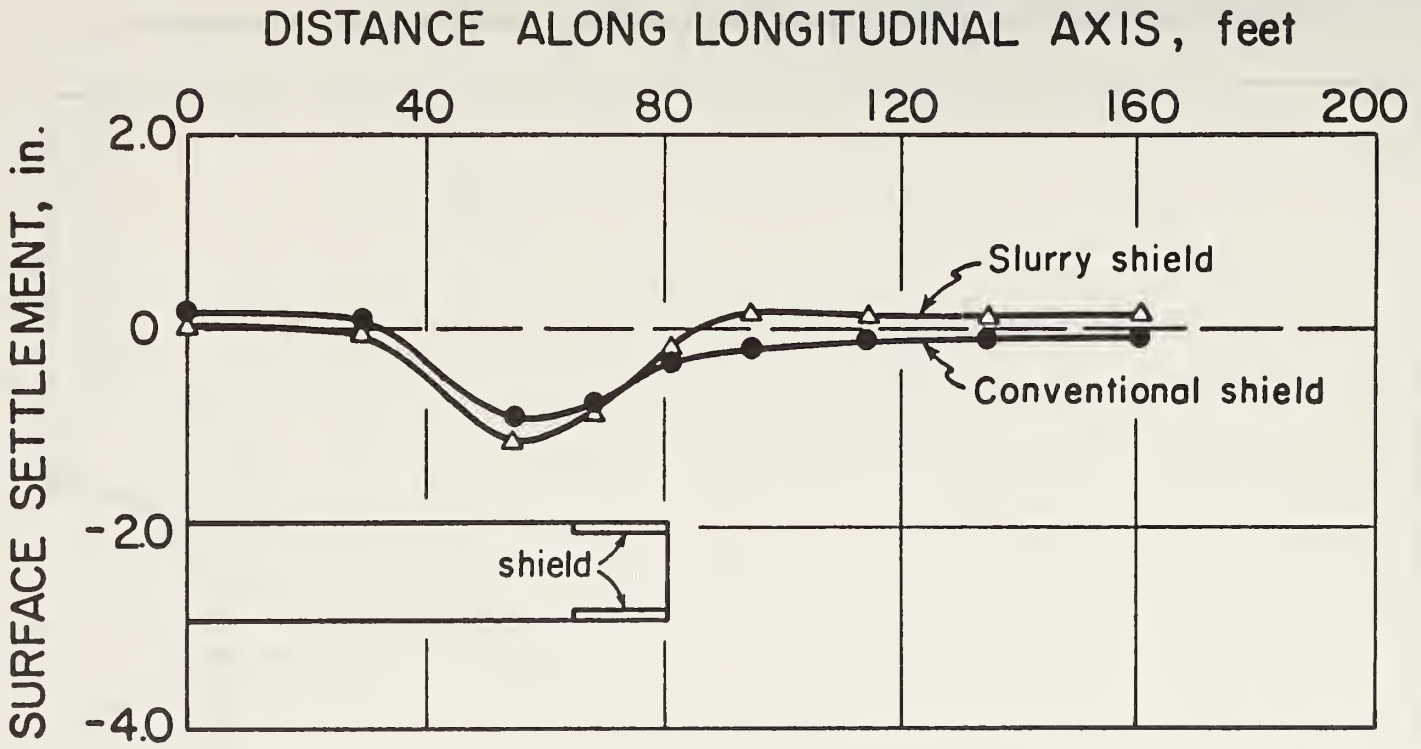

Figure 6.4: Surface Settlement Along Longitudinal Axis After One Shove of Shield

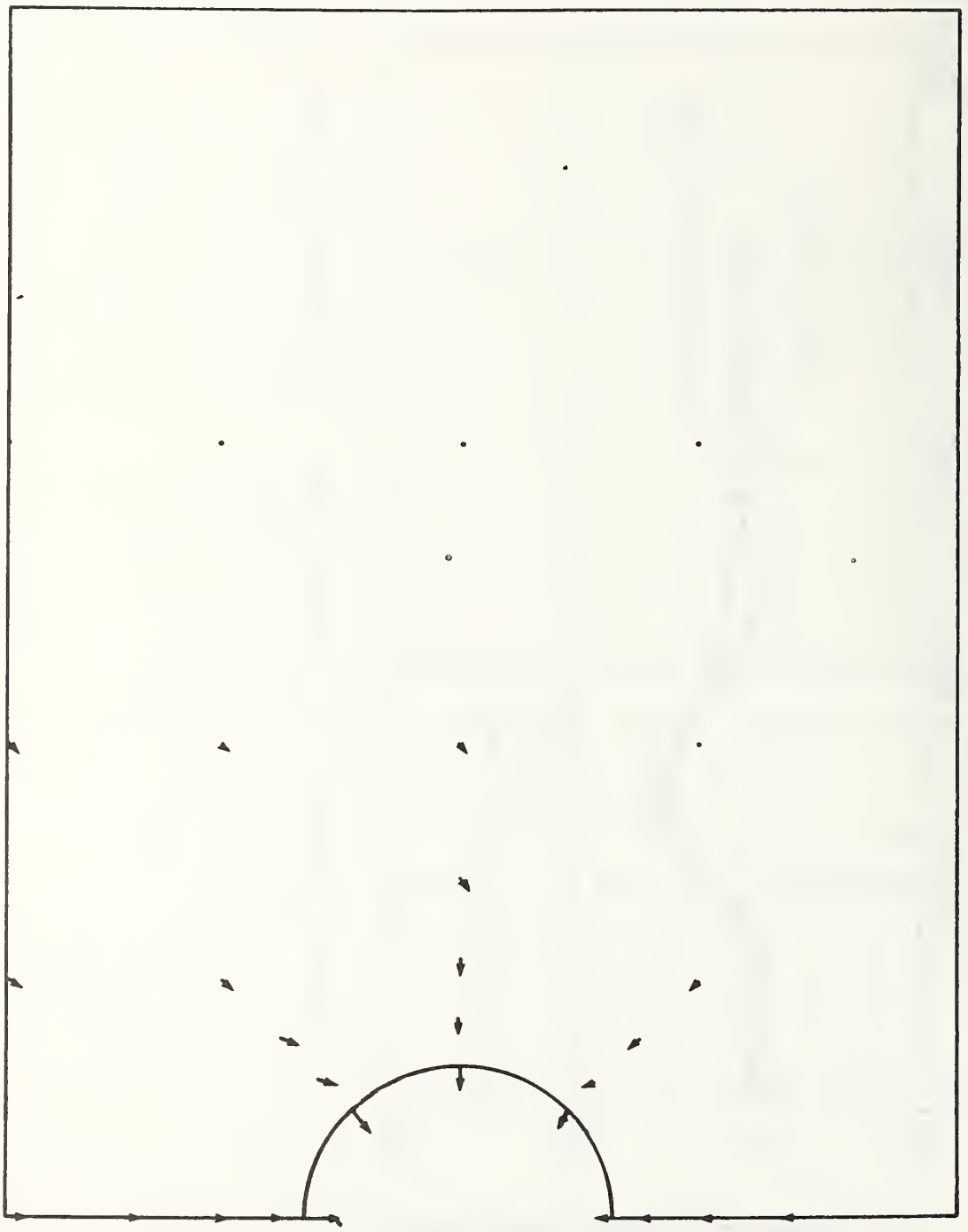

Figure 6.5: Displacement Vector at a Cross-Section Conventional Shield

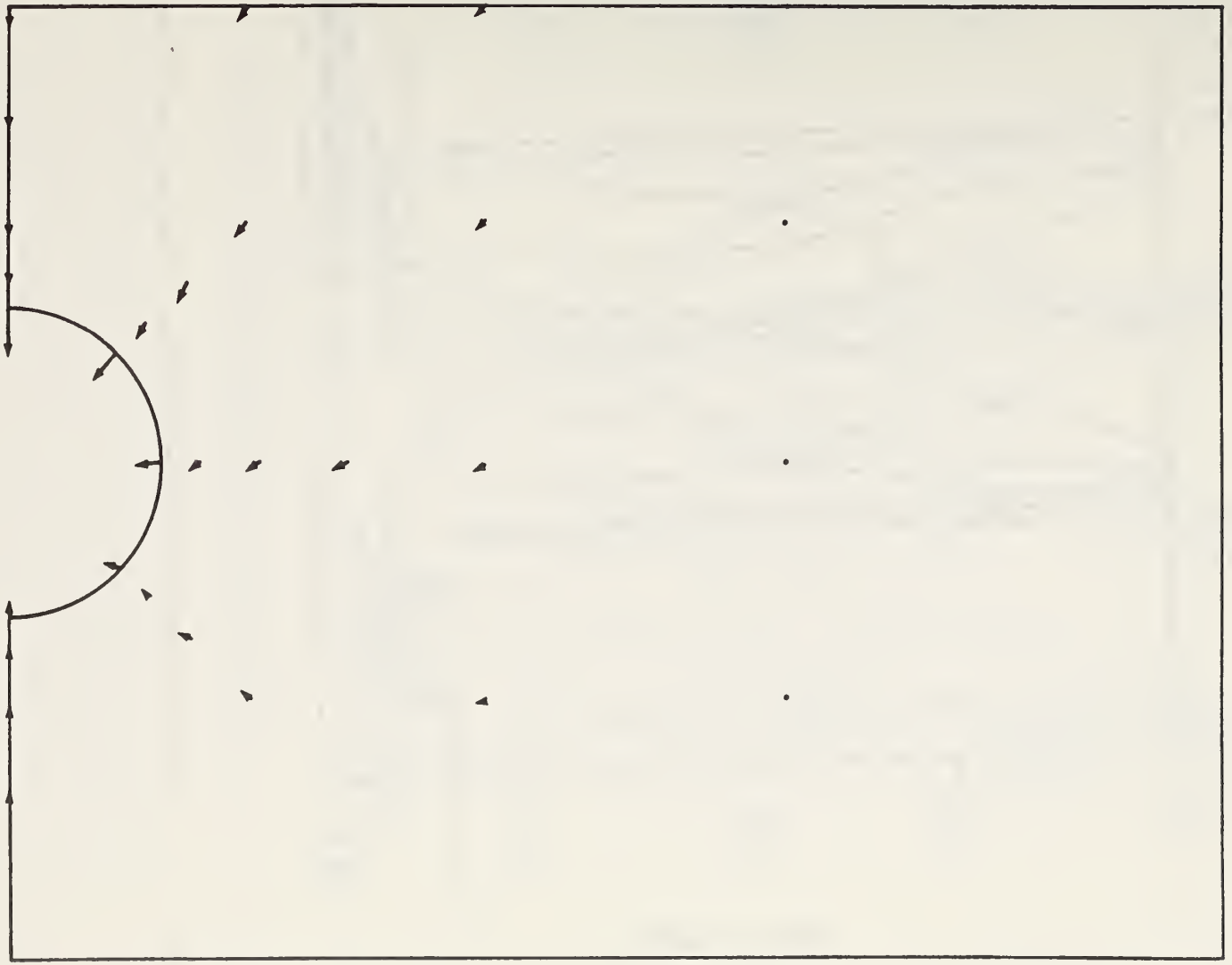

Figure 6.6: Displacement Vector at a Cross-Section - Slurry Shield

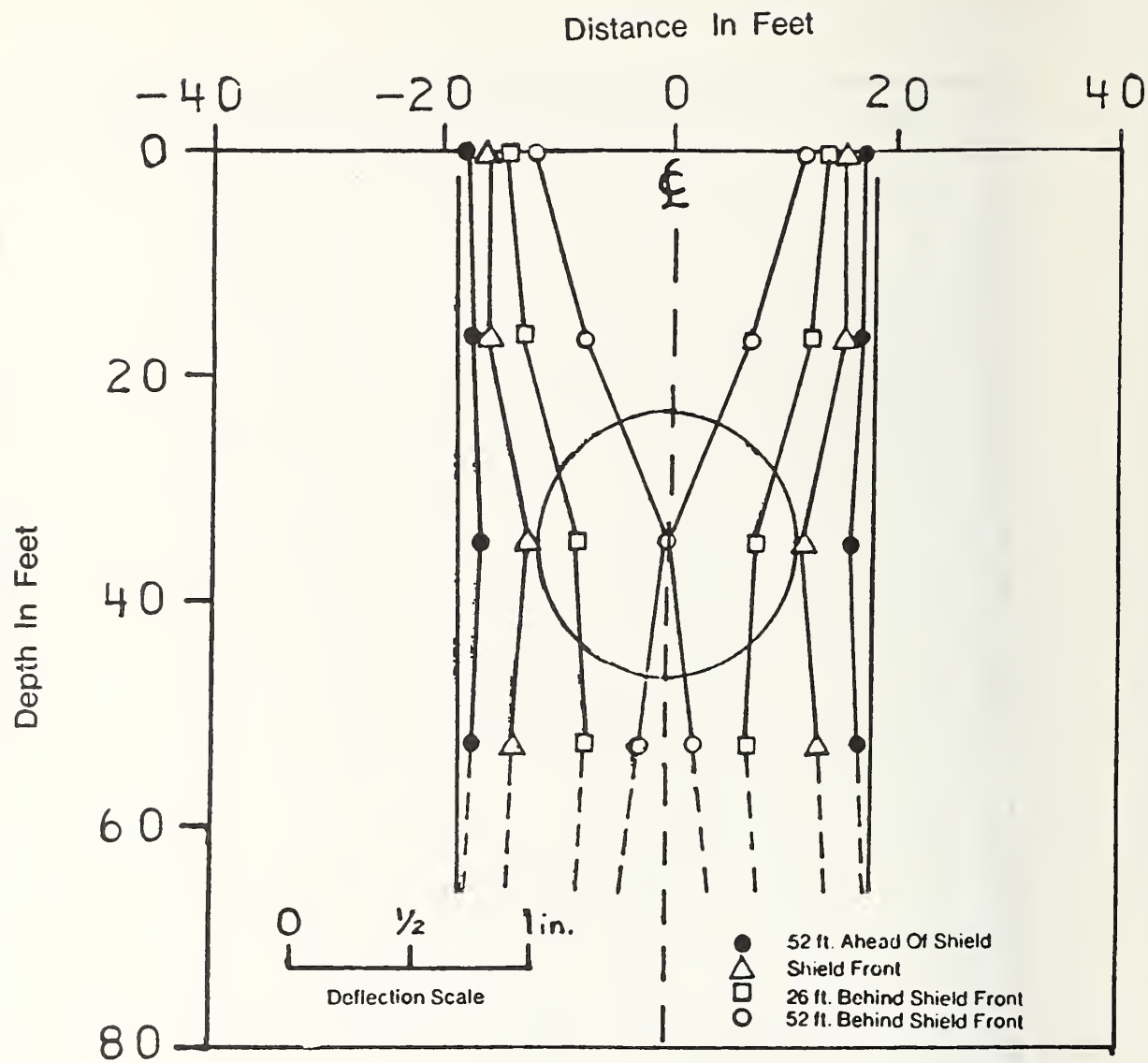

Figure 6.7: Lateral Movement At A Cross-Section - Conventional Shield

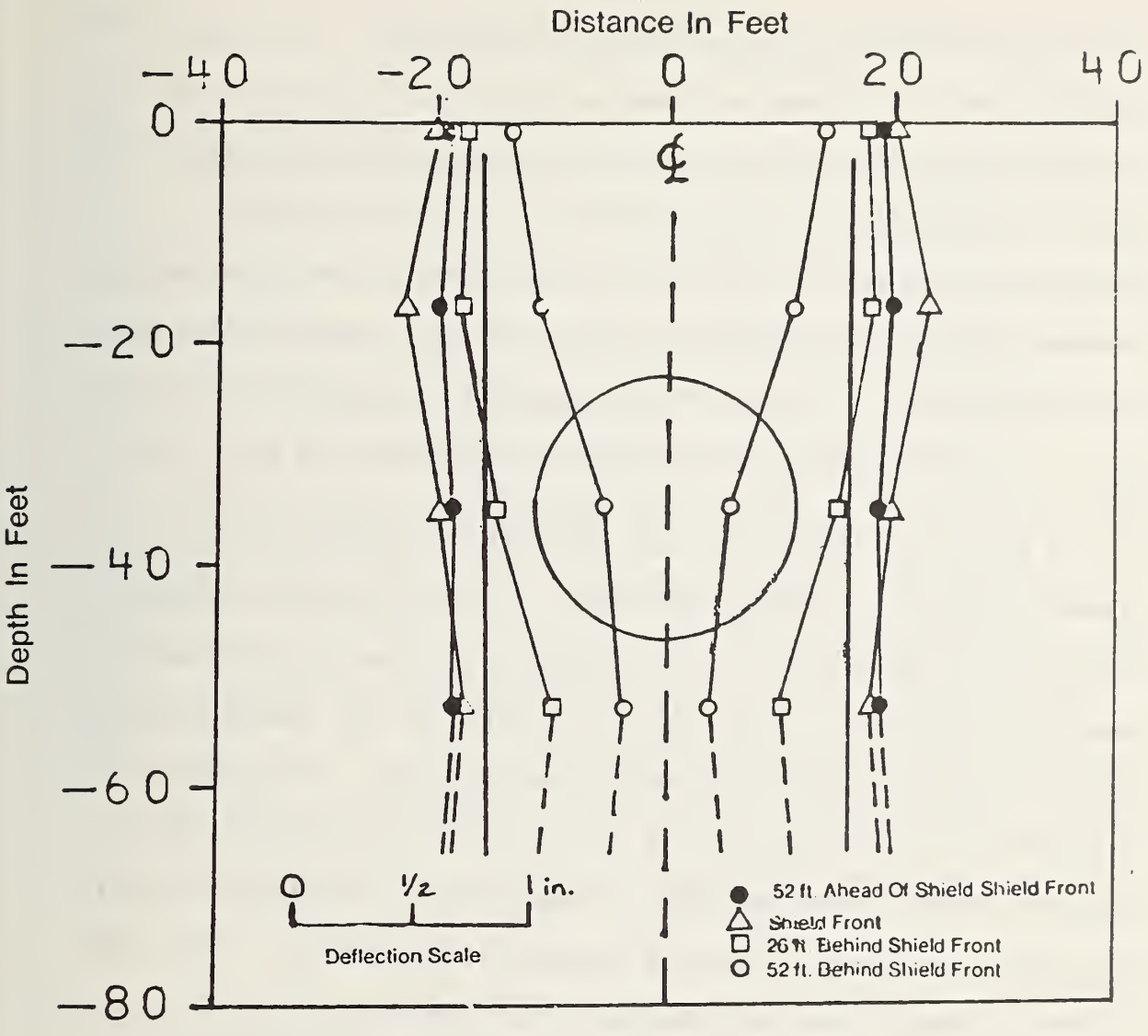

Figure 6.8: Lateral Movement at a Cross-Section - Slurry Shield

for the conventional and slurry shields, respectively. The lateral movements that are plotted are those calculated for a vertical line located some 18.2 feet (5.5 m) from the vertical axis of the tunnel. In the field, similar types of movements are sometimes measured by installing inclinometers in the ground and observing them during shield passage. The lateral movements are shown for the situations where the face of the shield is 52 feet (15.8 m) away from the reference line, at the line, and past it by 26 feet (7.9 m) and 52 feet (15.8 m).

As the conventional shield approaches the reference line, the lateral movements are towards the tunnel. This is evident even before the shield reaches the line. These movements are due to displacements towards the open face. After the shield passes by, the inward movements are accelerated due to the presence of the tail void. This behavior is in contrast to that for the slurry shield, where initially the lateral movements are away from the tunnel. Subsequently, the lateral movements are towards the tunnel, reflecting passage of the tail void. This exact pattern of behavior has been observed for an EPB shield where the soil was forced away from the shield during shield passage (Clough, et al., 1982).

6.6 LONGITUDINAL MOVEMENTS ON THE TUNNEL AXIS PRIOR TO SHIELD PASSAGE

In this case, attention is directed towards the lateral movements which occur ahead of the shield. Such movements could be measured in the field if an inclinometer casing were installed on the centerline of the tunnel and measurements of lateral movements made as the shield approached. These measurements or observations define the type and

amount of displacement which occur towards or away from the front of the shield.

The calculated movements for the conventional, slurry and the EPB shields are shown in Figures 6.9, 6.10, and 6.11, respectively. Values are given when the face of the shield is 52 feet (15.8 m), 26 feet (7.9 m), and 0 feet (0 m) from the reference line. For the conventional shield, the movements are always towards the face with the amount increasing as the shield front approaches and passes the reference line. For the slurry shield, the movement is initially towards the shield, but as it gets closer, the soil near the tunnel centerline begins to move away from it. The slurry pressure at the face gradually overcomes the general pattern for inward movements as the face comes close to the reference line. The movement along the longitudinal axis of the tunnel for the EPB shield is similar to that for the conventional shield except that in the former case, the maximum displacement at the face is less than that for the latter.

6.7 SETTLEMENT BOWLS

The calculated surface settlement bowls at a reference cross-section as the conventional shield approaches and passes the line are shown in Figure 6.12. The settlement pattern is consistent, with surface displacements increasing steadily throughout shield passage. The curvature of the bowl is increased sharply as the effect of the tail void is felt. The maximum settlement reaches 1.5 inches (3.8 cm) after the shield clears the reference line.

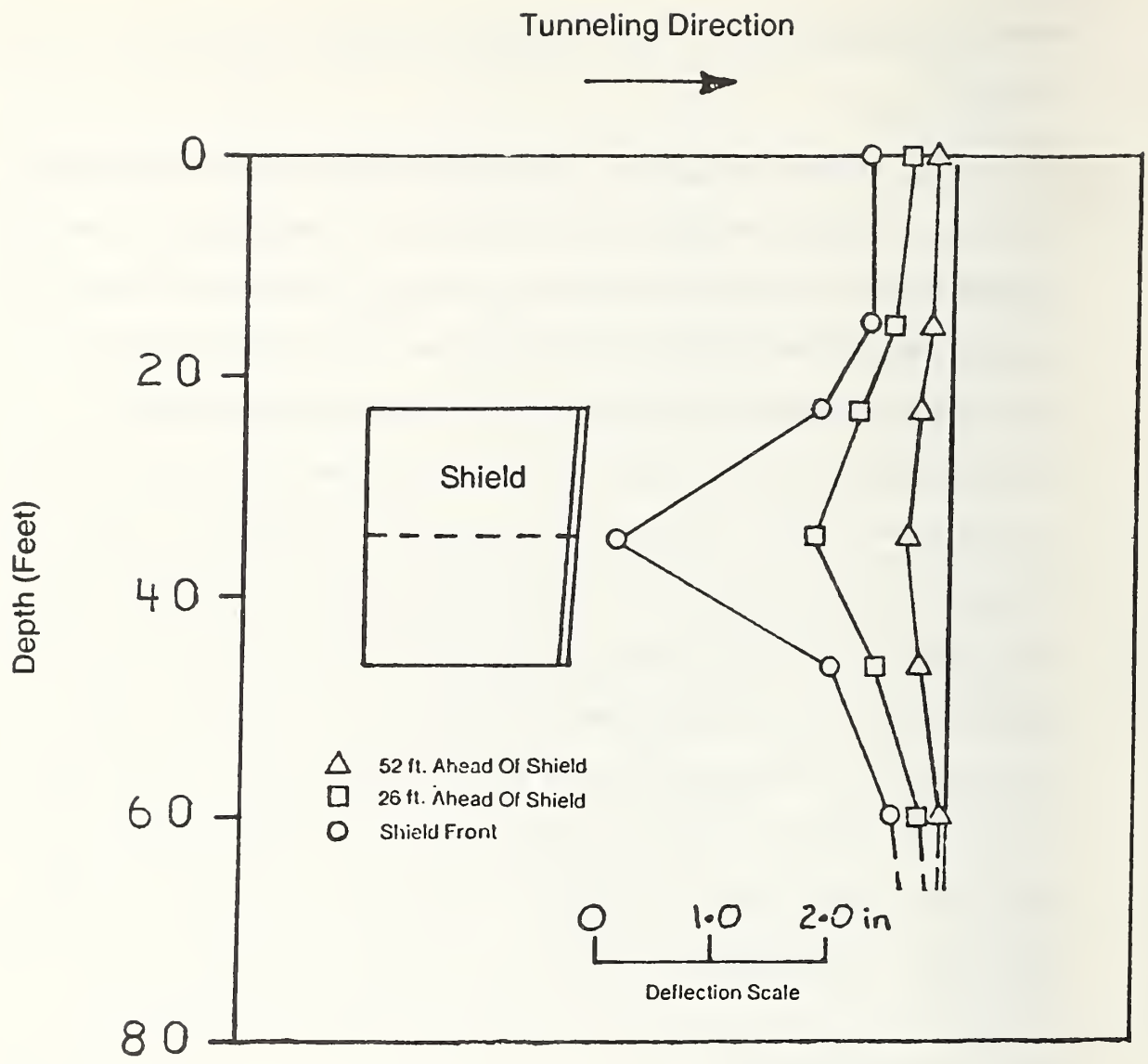

6.9: Lateral Movement At The Face of Conventional Shield

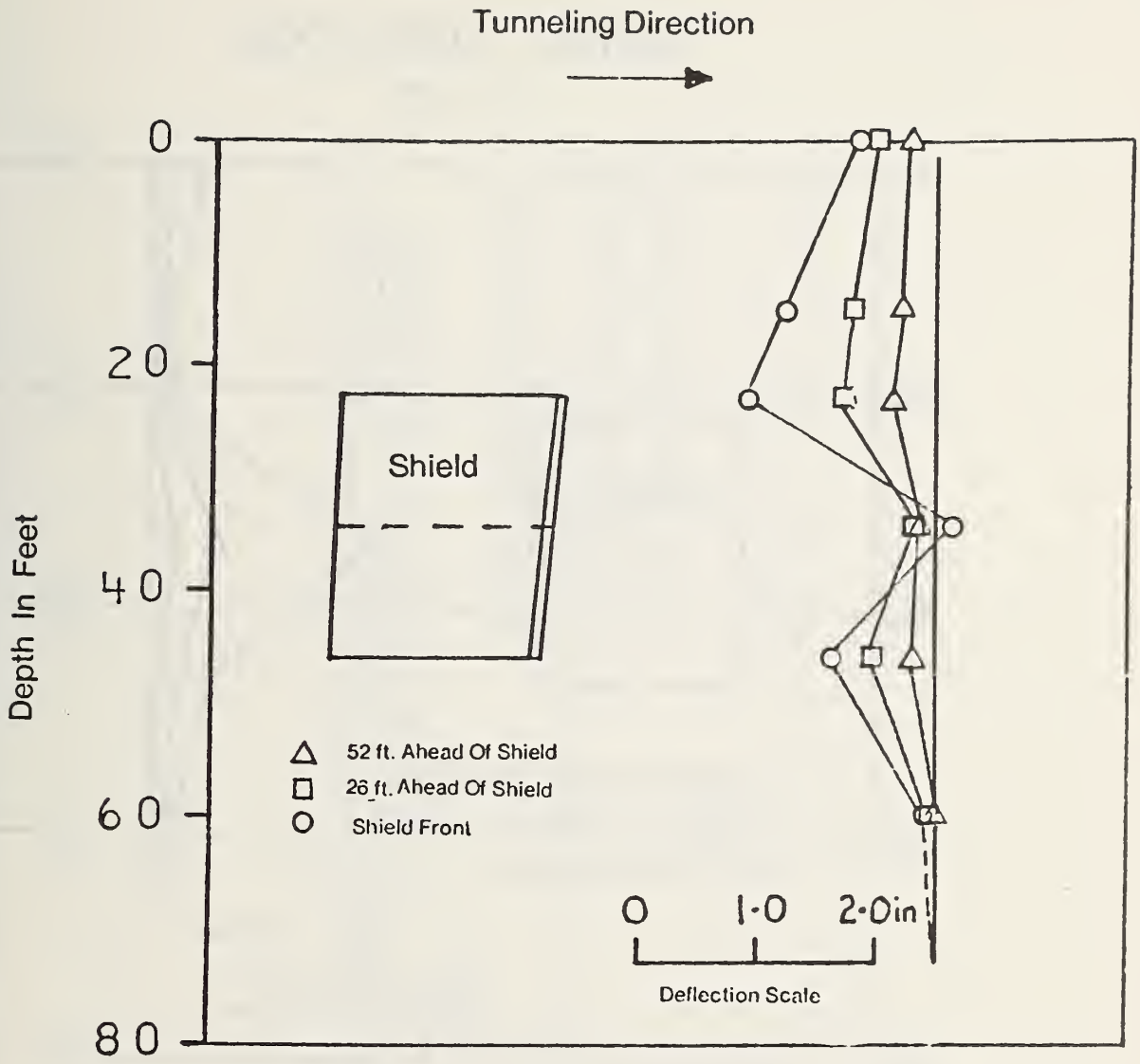

Figure 6.10: Lateral Movement at the Face of Slurry Shield

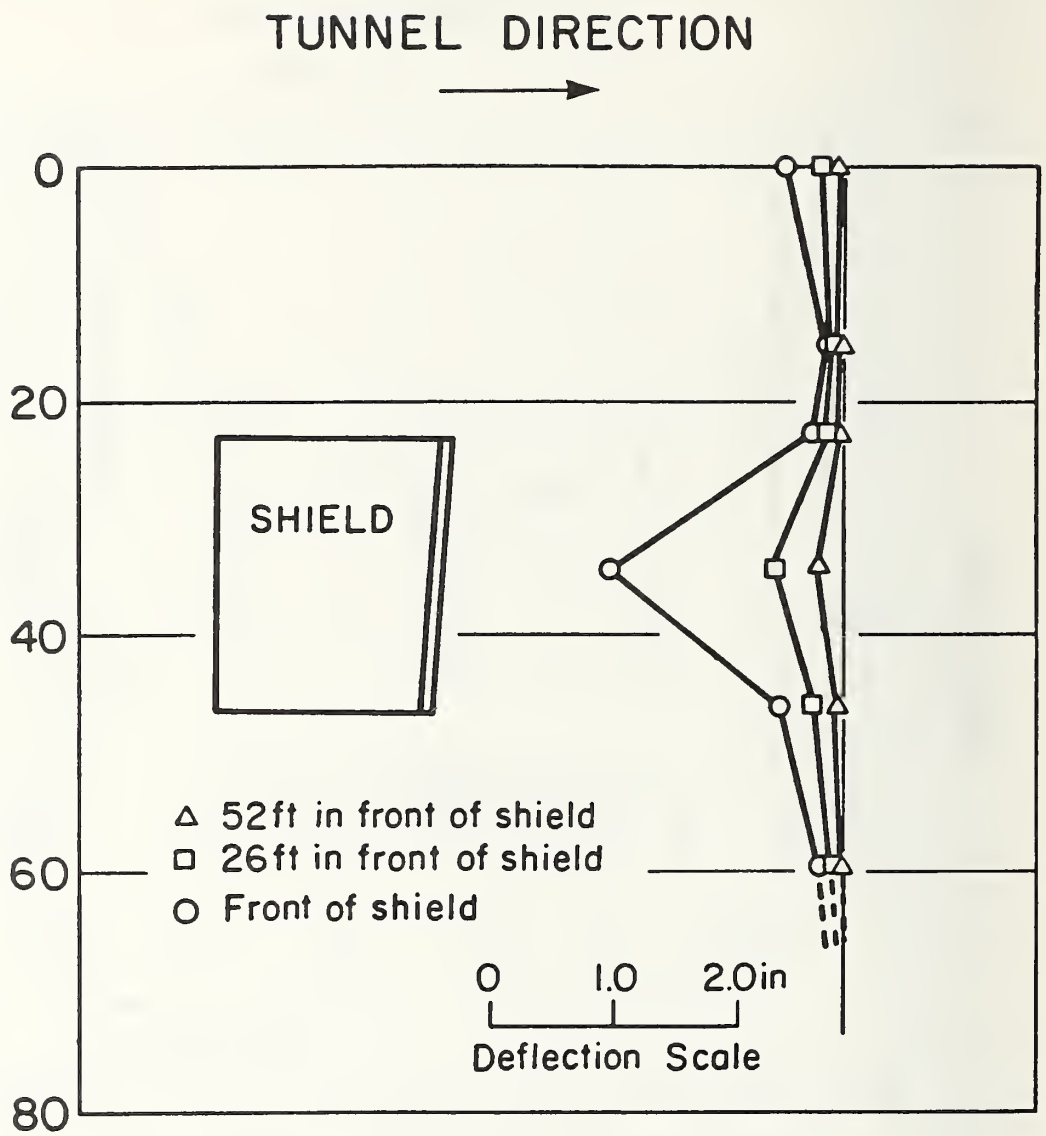

6.11: Lateral Movement At The Face of EPB Shield

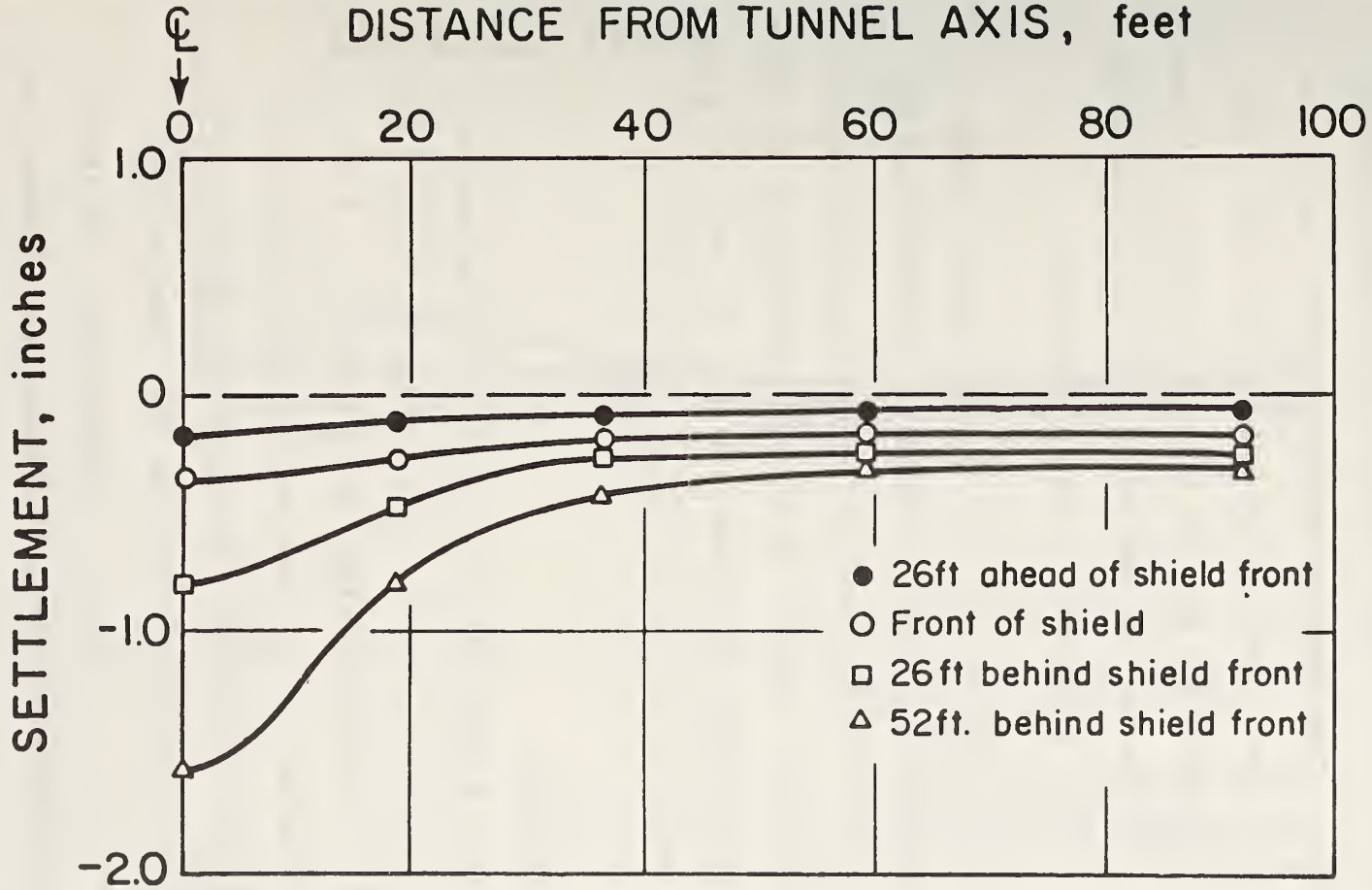

Figure 6.12: Settlement Bowls Due to Advancing Conventional Shield

The corresponding settlement bowl for the slurry shield is given in Figure 6.13. In contrast to the conventional shield, the reference line heaves upward during the approach of the shield. Settlement occurs after shield passage. These behaviors obviously reflect the relative effects of the slurry pressure at the face and the tail void. In the end, the shape of the settlement bowl for the slurry shield is the same as that of the conventional shield, however, the maximum settlement is only 0.9 inches (2.3 cm) in the case of the slurry shield.

The corresponding settlement bowl for the EPB shield is shown in Figure 6.14. The settlement pattern is similar to that described for the conventional shield, with surface displacement increasing steadily throughout shield passage. However, the maximum settlement for the EPB shield after the shield clears the reference line is 1.1 inches (2.8 cm) compared to 1.5 inches (3.8 cm) for the conventional shield.

6.8 SETTLEMENT AT DEPTH

The settlement at a depth below the ground surface can also be examined for the conventional, slurry, and EPB shields. Plots of the settlement profile at the ground surface and at a depth of 8.9 feet (2.7 m) below the ground surface for an advancing shield were prepared for the three shield types. The plot for the conventional shield is given by Figure 6.15 and the corresponding plots for the slurry and EPB shields are given by Figures 6.16 and 6.17, respectively. The figures show that for the three shield types, the ground surface settlement lags behind that at a depth of 8.9 feet (2.7 meters) probably due to three dimensional spreading of settlement away from the source of lost ground.

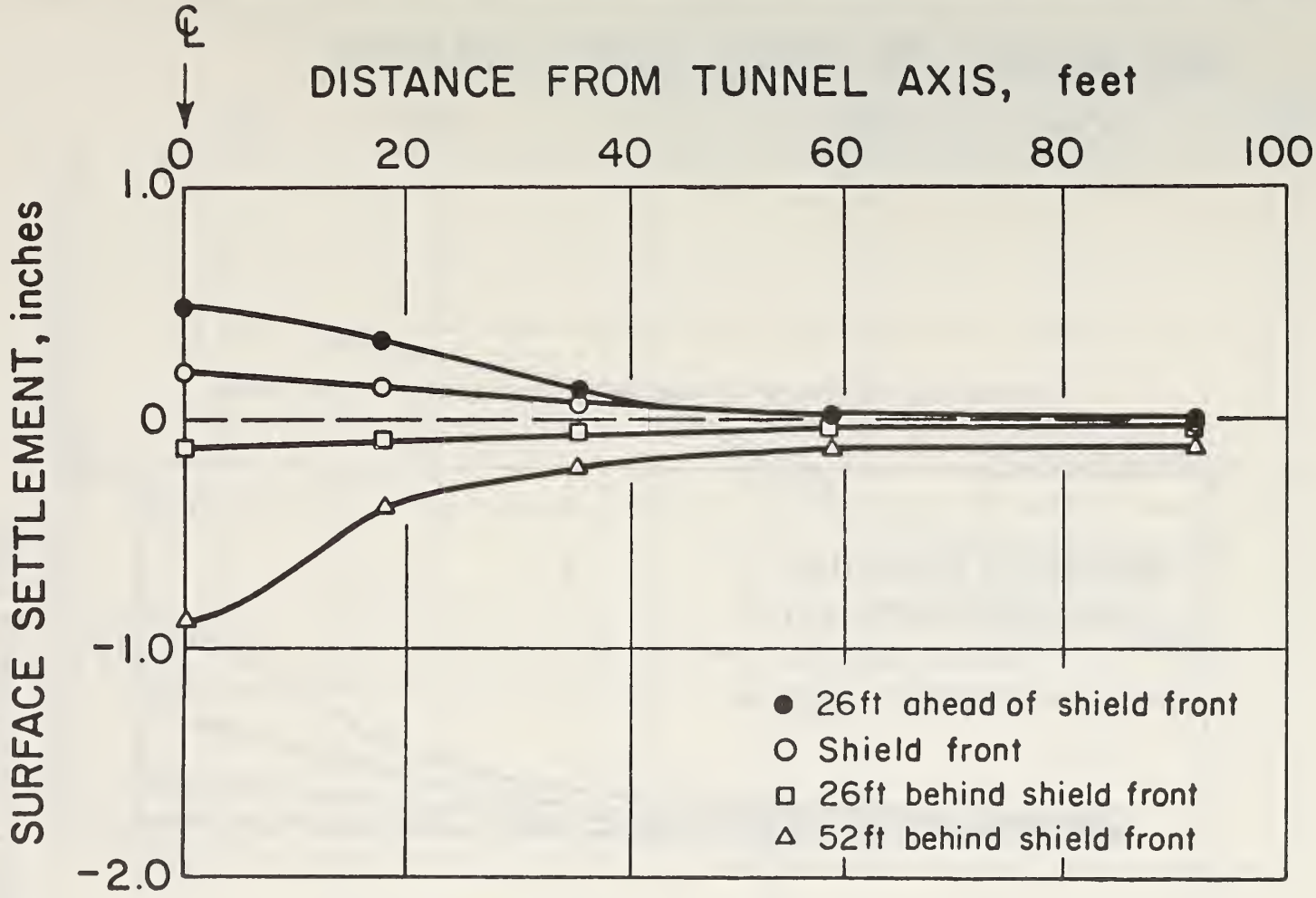

Figure 6.13: Settlement Bowls Due to Advancing Slurry Shield

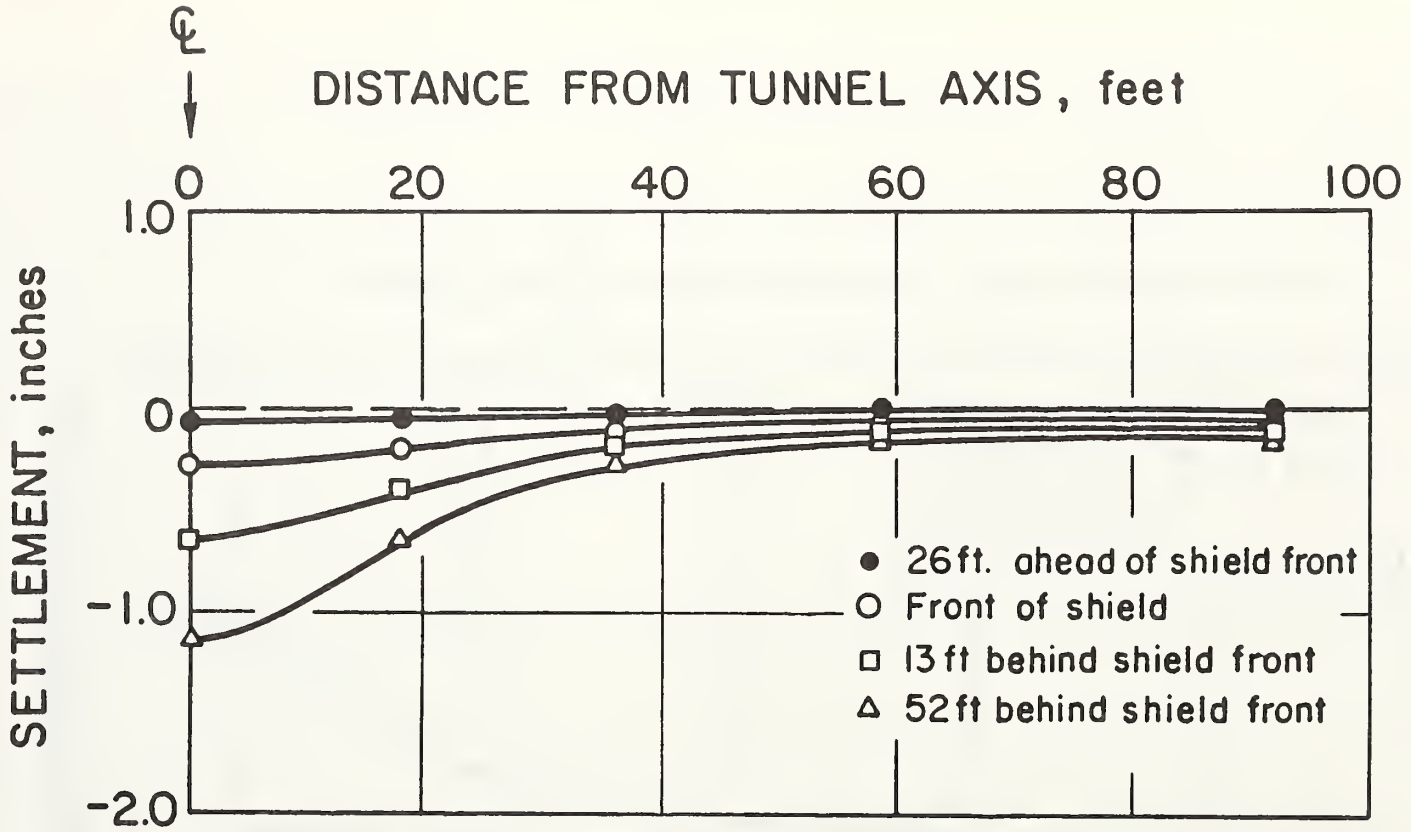

Figure 6.14: Settlement Bowls Due to Advancing EPB Shield

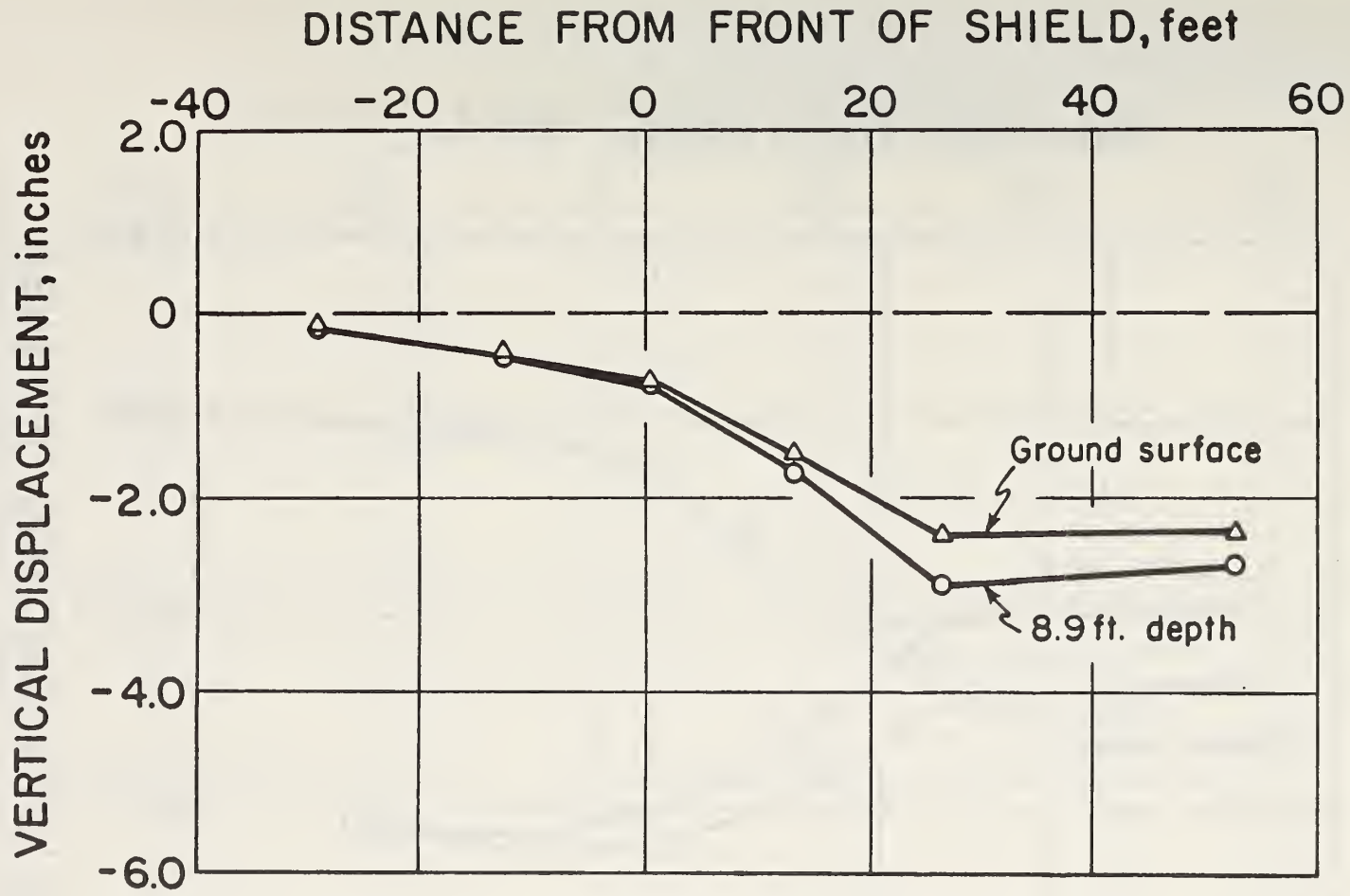

Figure 6.15: Settlement at Depth - Conventional Shield

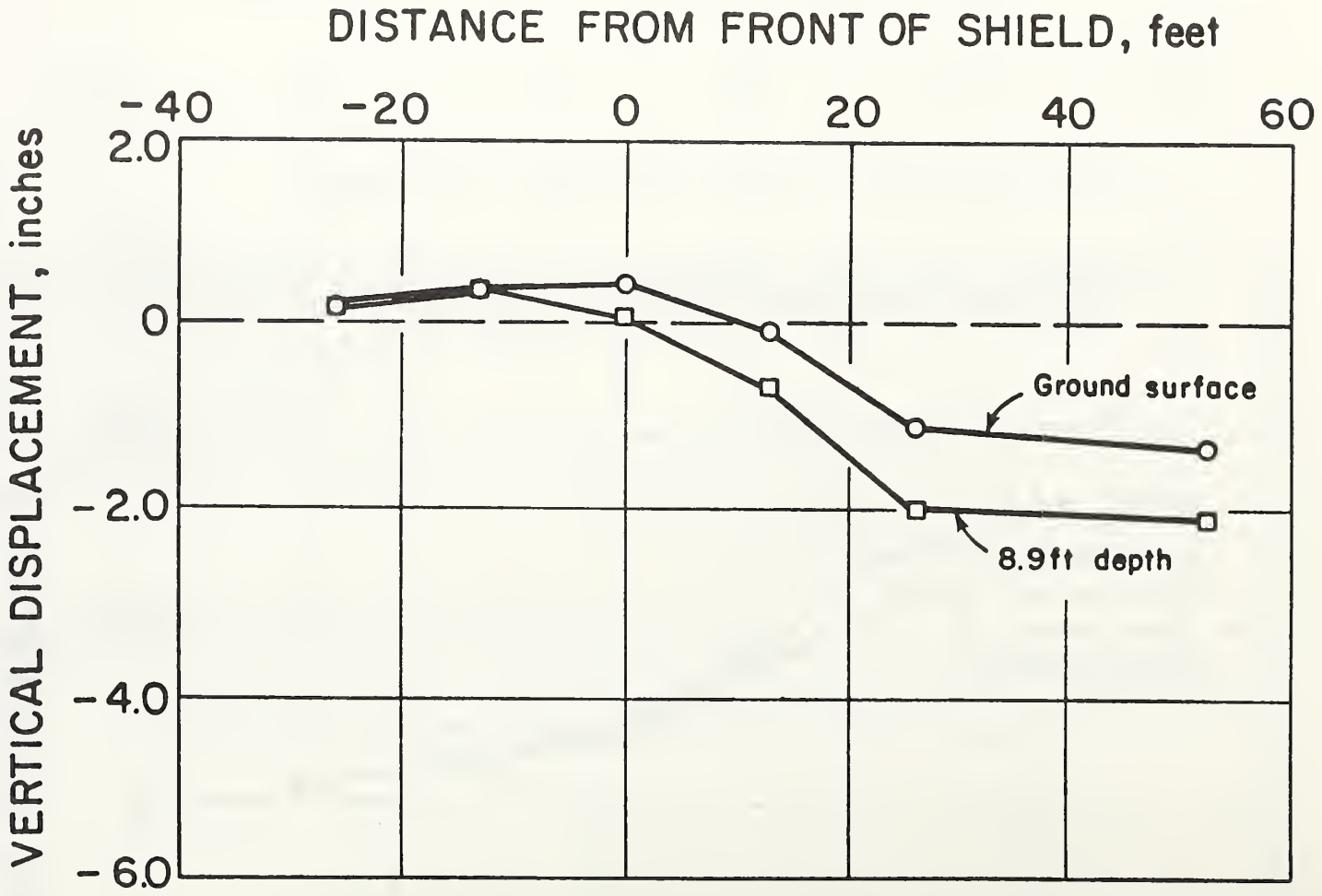

Figure 6.16: Settlement at Depth - Slurry Shield

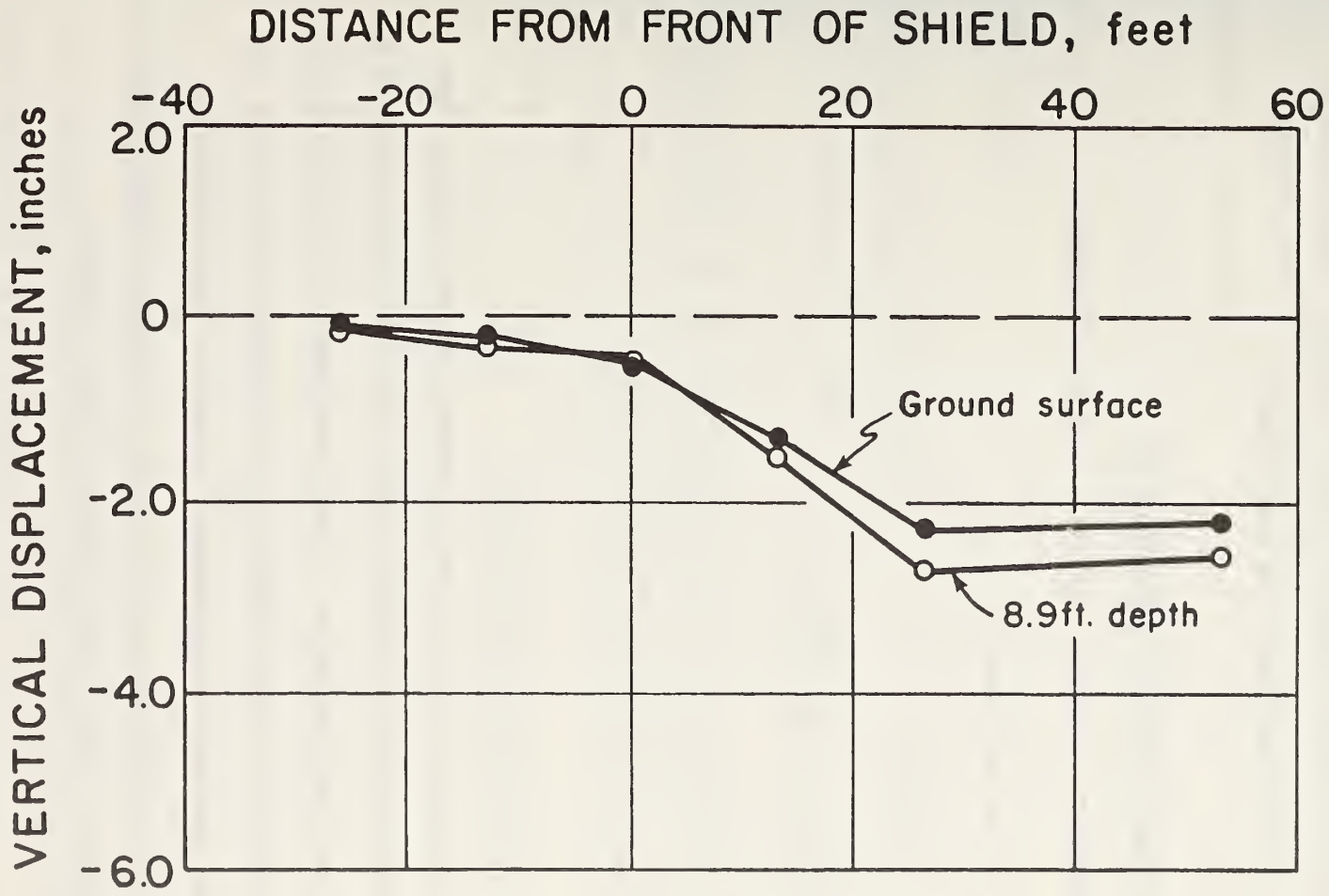

Figure 6.17: Settlement at Depth - EPB Shield

This suggests that the ground surface settlement does not give an accurate indication of the amount of ground loss into the tunnel. The ground surface settlement underestimates the actual ground loss at depth, as is well known from field measurement.

6.9 EVALUATION OF MOVEMENT CONTRIBUTIONS

Contributions to volume loss are from three sources:

1. The face of the tunnel
2. Over the shield
3. At the tail of the shield

Some of these contributions can be determined from the finite element results and used for comparison with field data.

6.9.1 Over the Shield And At The Tail

There are two sources of loss of ground over the shield. One source is caused by the overcutter, a bar usually installed around a portion of the shield perimeter. These appendages to the shield cut openings of slightly larger diameter than the body of the shield. Of course, these analyses do not account for either the presence of overcutters or the occurrence of pitching and yawing. Thus, there is zero contribution to the volume loss from these sources.

6.9.2 At The Face

Volume loss at the face can develop in flowing, squeezing or ravelling ground, but these situations were not considered in this study. However, the volume loss at the face can be estimated using geometrical approximations.

Using the results from the selected runs, the estimated volume loss at the face are 0.13% for the conventional shield and 0.06% for the slurry shield.

6.10 VOLUME OF SETTLEMENT TROUGH

For undrained soil conditions, the volume of the settlement trough provides a measure of the total volume loss due to tunneling. This includes that due to the face and tail void. The procedure used to get the settlement trough volume is described in Chapter 2. The volume of the settlement trough is used to estimate volume loss after passage of the conventional and slurry shields.

The maximum settlement at a section 2.6 feet (8 meters) behind the face of the tunnel are 1.7 in. (43 mm) for the conventional shield and 0.9 inches 23 mm) for the slurry shield. Using equations 2.8 and 2.9 the volume of the settlement trough and hence the volume loss are 1.3% and 0.94% for the slurry shields, respectively. The value of 1.3% for the conventional shield is less than maximum value of 10% reported by Clough and Schmidt (1977), but in the range of values of volume loss documented by Cording and Hansmire (1975).

Contribution from the face to this total volume loss is approximately 10% for the conventional shield and 7% for the slurry shield. Thus, in the absence of face collapse, contribution to the volume loss from the face is small compared to that from the tail or over the shield. Also, as expected, the face contribution to the volume loss is greater for the conventional shield than is the case for the slurry shield.

6.11 EFFECT OF OPENING TUNNEL FACE ON STRESS CONDITIONS

The tunneling activity leads to a stress redistribution around the tunnel opening. To examine the stress effects, the non-dimensional vertical stress at the center of each element was considered. The plots for the conventional shield on a cross-section at the tunnel face and on a longitudinal section were given in Chapter 5 (Figures 5.15 and 5.16). The corresponding plots for the slurry shield are given by Figures 6.18 and 6.19, respectively. As can be seen from Figures 6.18 and 6.19, in general, the vertical stress in the zones above and below the tunnel are reduced from their initial values by the tunnel opening. At the springline, the vertical stresses are generally increased. This is similar to the patterns observed for the conventional shield. However, it is important to note that the change in stresses produced by tunneling around the opening is less for the slurry shield than for the conventional. This is logical since the slurry pressure prevents the decompression effect which occurs with the conventional shield.

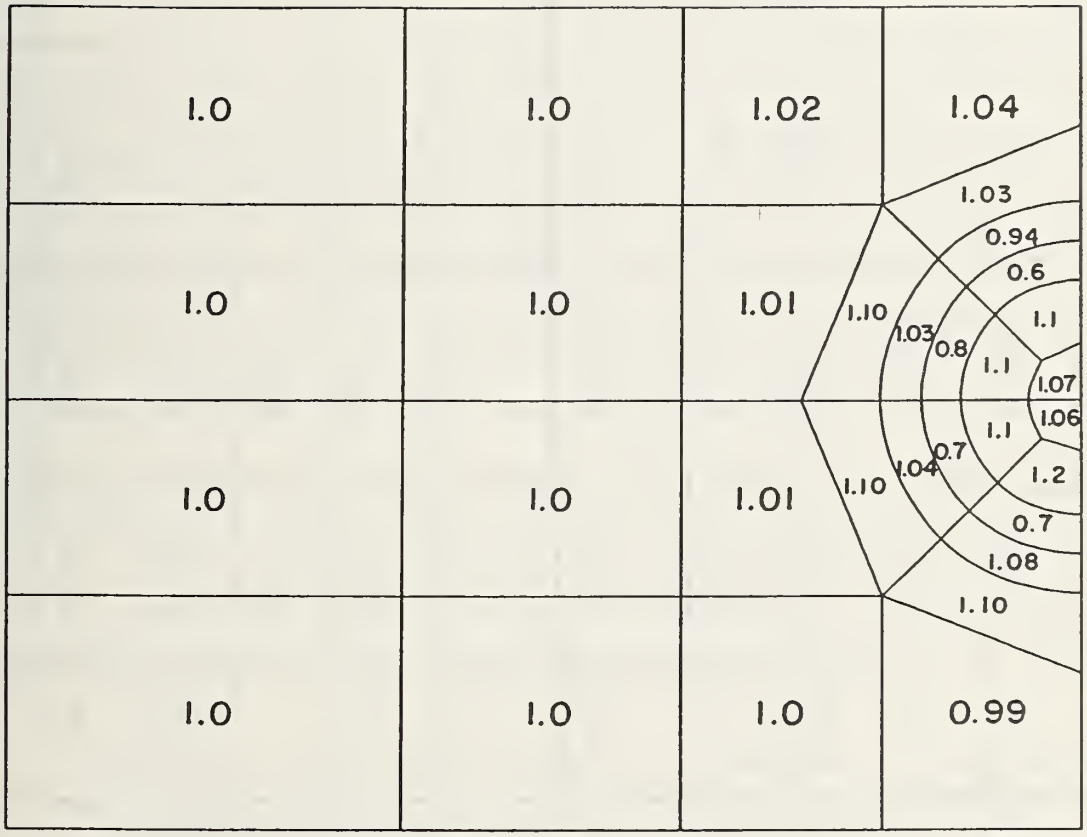

Cross Section at the Face

Figure 6.18: Non-Dimensionalized Vertical Stresses on Cross-Section at Tunnel Face-Slurry-Shield

FACE
↓

1.02	0.95	1.20	0.92	1.04	1.0	1.0	1.0
1.40	1.43	1.02	1.38	1.02	0.99	1.02	1.0
1.10	0.88	1.10	1.10	0.94	1.01	1.0	1.0
1.20	0.99	1.08	1.01	0.60	0.84	0.96	0.90
				1.10	1.12	1.09	1.07
1.0	1.10	1.05	1.30	1.07	1.01	1.0	1.0
1.0	1.31	0.95	1.21	1.06	1.03	0.99	1.0
1.10	0.63	0.94	0.99	1.20	1.10	1.06	1.06
				0.7	0.81	0.94	0.9
1.3	1.0	0.6	1.08	1.08	1.06	1.05	1.06
1.20	1.26	0.80	0.94	1.10	1.02	1.0	0.99
1.01	0.95	0.96	0.98	0.99	1.01	0.99	1.0

Figure 6.19: Non-Dimensionalized Vertical Stresses on Plane Along Longitudinal Axis - Slurry Shield

6.12 SURFACE SETTLEMENT PRODUCED BY ALL SHIELD TYPES

As a means of comparing the effects of the shield types, the surface settlement profiles produced by each are shown together on one diagram (Figure 6.20). Both slurry shield cases are included in order to demonstrate the influence of tail void support.

The predicted settlements after shield passage are from the largest to the smallest produced by the conventional shield, the EPB shield, the slurry shield with only slurry pressure at the face, and the slurry shield with slurry pressure at the face and in the tail void area. Interestingly however, in spite of the support of the face of the tunnel provided by the EPB and slurry shield with face pressure only, the maximum settlements in these cases are not greatly reduced from that of the conventional shield. Only when slurry pressure support is added in the tail void area is there a dramatic improvement in the predicted settlement values. These results suggest the following:

1. Since tail void closure occurs for all shields it serves as an "equalizer" and significantly negates any positive effects achieved by face support.

2. Application of pressures at the face does ultimately lead to a small reduction in settlements. The pressures ideally should be large enough to cause a slight heave of the ground surface ahead of the shield.

3. Control of closure into the tail void is the surest means of reducing ground settlements.

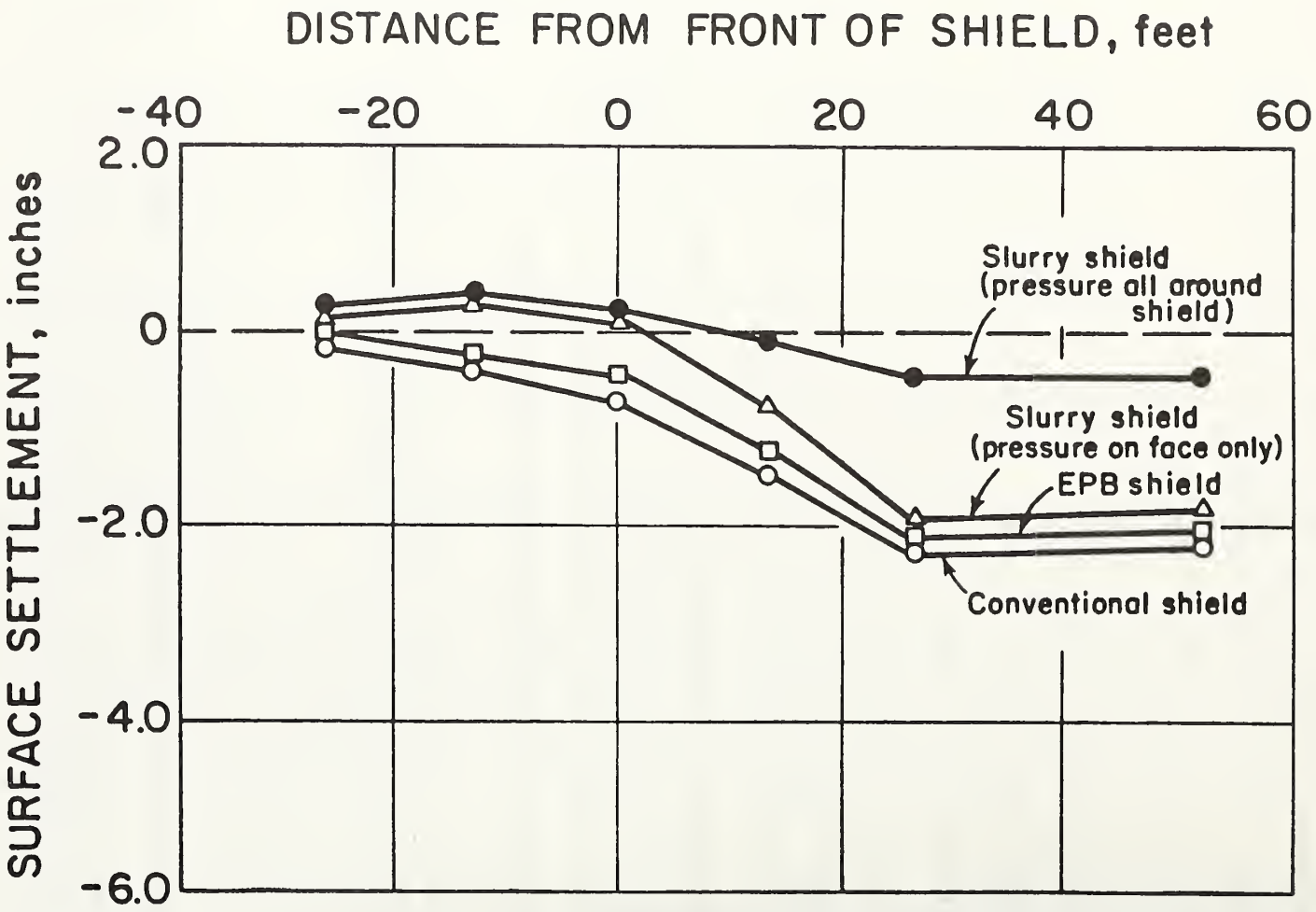

Figure 6.20: Comparison of Shield Types

The foregoing conclusions may be accepted at face value since they are supported by the theoretical data. However, it must be noted that there is an important facet of potential soil behavior not considered which could show an additional significant benefit of the advanced shield support mechanisms. In the analysis considered herein, the soil behavior is assumed to be linear elastic, and no ground water flow problems could be included. Should ground water flow occur in a permeable soil in actuality, a ground run could ensue leading to a surface collapse. It is evident that the advanced shields could prevent such a failure, whereas it is a possibility in the case of the conventional shield.

Considering all the factors then, the following conclusions may be drawn relative to the ground support provided by advanced shields:

1. The possibility of catastrophic ground failures is greatly reduced.

2. Ground movements at the face are reduced, or possibly even reversed, relative to a conventional shield.

3. Where face control is adequately maintained by all types of shields, surface settlements are likely to be only slightly smaller for the case of the advanced shields assuming no more than conventional methods are used to prevent tail void closure.

4. If in the case of a slurry shield, slurry under pressure should migrate into the tail void area, unusual control over settlements can be obtained.

Because of the significance of the last finding, it is important that future research be directed at the question of whether the slurry does or does not help support the soil in the tail void area.

Chapter VII

SUMMARY AND CONCLUSIONS

In order to tunnel in soil, it is generally necessary to use a shield which allows soil excavation at the front end and liner erection at its rear. The shield advances by pushing off of the in-place liner segments. By simultaneously excavating and installing a liner, the shield can move forward while continuous protection is provided to the tunnel workers. In the past, the shield has been open at front and excavation has been by hand or semi-automated. Because of lack of support at the face of a conventional shield, problems can occur in sandy soils, particularly under the water table, or in weak silts and clays. To overcome these problems, compressed air was used in the tunnel; this serves to enhance face stability and ground control, but it also affects the working environment in the tunnel. In recent years, costs associated with compressed air tunneling have skyrocketed.

Because of the problems associated with conventional shield tunneling new procedures have been proposed. European and Japanese contractors especially have developed shields which provide continuous face support. These include the slurry shield, the earth pressure balance shield, the water pressure balance shield of the earth pressure type, and the mud shield. Use of these machines in difficult ground conditions and urban areas has increased rapidly overseas. The first application of advanced shield technology in the United States took place in 1981 for a tunnel in San Francisco.

In spite of the heightened interest in this new construction technology, however, the actual mechanism of ground support generated by these machines is not fully understood. Perhaps most importantly for designers and potential future users, it is not clear how much, if any, improvement can be expected in terms of ground movement reduction relative to the conventional shields. It is the general objective of this work to develop analytical procedures which can help provide answers to the questions surrounding the performance of advanced shields.

Basic to the research described herein is the analytical approach to allow realistic simulation of shield tunneling effects. It is felt that such a tool is needed for the following reasons:

1. Available field data for advanced shield performance is meager at best.

2. Direct comparison of one project to another is difficult since many variables are involved.

3. Effects of individual parameters are often masked in model or field tests due to other overriding variables.

4. Neither field nor model tests can provide information on stress conditions in the soil around the shield.

The analytical technique chosen for use in this research is the finite element method. It offers considerable flexibility in modeling

sequential construction procedures and can predict displacement as well as stress patterns. For this work, it was necessary to develop the first, full three dimensional code, which could model various types of shield tunneling in soil. Basic objectives in creating the program were to allow for a realistic simulation of shield tunneling processes, non-homogenous soil profiles, and gravity stress conditions. Also, every opportunity was exercised to maximize the efficiency of the code as well as to build in a flexibility so it can be modified and improved in the future.

In Chapters 3 and 4, the development of the basic code is described along with the general procedures to simulate shield tunneling. The soil model used is limited to a linear elastic response. Although this model is restricted and is not able to allow for changes in soil stiffness with increasing shear stress levels, it offers a number of advantages, especially considering this effort is the first of its kind:

1. The analyses are economical since no iteration is required to insure model convergence.

2. Superposition of results is possible.

3. The results can be interpreted without concern for the effects of some complex model behavior facet.

In addition to these advantages it should be noted that soil nonlinearity and yielding effects are approximately included in the linear elastic analyses by using values of modulus representing secants

to nonlinear stress-strain curves. Also effects of changes of soil stiffness with depth are included by allowing modulus values to change with depth as they are known to do in the field.

Verification problems are also presented in Chapter 3 where results are predicted by the new code are compared to closed-form theoretical results. In all cases, very good agreement is obtained.

Methods for modeling the advancing soft ground tunneling shield and the associated erection of a liner are presented and discussed in Chapter 4. A number of aspects of this process posed serious challenges. In particular, there was the question of how to allow for the presence of the void created between the soil and the liner with the advance of the shield. A reasonable, approximate technique is proposed which as shown by subsequent analyses, generates inward soil movements towards the tunnel which are consistent with observed field behavior. Procedures to simulate the effects of tunneling with a slurry or earth pressure balance shield are also set forth. This involves the use of pressure loadings at the face of the tunnel and, where appropriate, at other interfaces between the tunnel and the soil. As finally developed, the code provides for a modeling of the shield which comes reasonably close to the sequential soil excavation, shield advance and liner erection process used in the field.

After completing the basic code development for shield tunneling, Chapter 5 is devoted to a series of parametric studies designed to tune the options so as to get predictions of behavior as accurate as possible. Questions related to shield stiffness, shield and liner

weights, and nature of support provided by advanced shields are examined.

Finally, using what are believed to be the best predicted tunneling responses, comparisons are made in Chapter 6 between the conventional, earth pressure balance and slurry shield performances and related ground movements. In making comparisons it is well to remember that there is no single predicted response for either the slurry shield or the earth pressure balance shield. In the case of these machines, the pressure exerted on the soil at the face can vary by design depending upon the operator. There is little available information as to the actual pressures that are used, although some evidence suggests that it is high enough to initially force the soil outwards from the face. For the present analyses the advanced shield representations caused some degree of initial outward movement of soil away from the face of the tunnel. The pressure levels simulated were based on a set of reasonable assumptions. After passage of the shield past any given reference point, the movement of the soil was predominately inwards towards the tunnel, reflecting the effect of the tail void.

The predicted levels of displacements for the slurry shield were found to depend strongly on what assumptions were made as to whether the slurry pressure aided in supporting the soil in the tail void area. In order for the support to be present in the tail void, the slurry would have to migrate from the face of the shield where it is applied, around the shield, and into the tail void. No published data could be found to confirm or deny that the slurry migration occurs; some discussion with

slurry shield manufacturers yielded conflicting opinions. The importance of this issue illustrated by the fact that ground surface settlements predicted by the program were four times larger without the tail void slurry than with it. Obviously, this is a subject which needs further investigation, in future field projects.

Even without slurry support provided in the tail void, the calculated ground movements for the slurry shield were smaller than those of the other shields. Movements with the conventional shield were the largest with the earth pressure balance shield case falling between the slurry and conventional shields. Interestingly, however, the differences between the final settlements after shield passage were not that great. This reflects the fact that regardless of the degree of face control exercised, the major factor in the ground movements is the tail void and soil displacement into it. Since the size of the tail void for all shields is about the same it serves as an "equalizer" of the final behavior. It is important to note that this conclusion is made assuming that the face of the tunnel is basically stable for all types of shields. Of course, ground movements due to face instability are far more likely with the conventional shield than with the others.

Examination of stress changes produced in the soil surrounding the tunnel lead to conclusions which are tied into the behavior described for the displacements. The smaller the displacements predicted, the smaller the stress changes in the soil. Thus, the stress changes were smallest for the slurry shield, followed by those for the earth pressure balance shield and the conventional shield.

Based on all of the results presented herein, the following primary conclusions are drawn:

1. The three dimensional finite element program developed in this research provides a useful tool to study and compare shield tunneling techniques.

2. Despite using a linear elastic model for soil behavior, the program has been shown to predict behavior patterns which are consistent with those observed in the field.

3. The amount of ground settlement induced by the slurry shield is a function of the amount of pressure assumed to act at the tunnel face and whether or not support is provided by the slurry in the tail void.

4. As with the slurry shield, the ground movements for the earth pressure balance shield are also affected by assumed face support pressures.

5. Using reasonable values of face support pressures for the advanced shield, the ground movements predicted for the different shield tunneling procedures are from largest to smallest - conventional, earth pressure balance, and slurry shield. However, if the face of the tunnel is basically stable, the differences between the movements for the shields are relatively small.

6. In most cases, the tail void influence is of paramount importance to the final ground movements, and, since this is the same for all shields, it serves to "equalize" the behavior for the different shields.

7. Future research should be directed at the important questions of the degree of support pressure applied at the face of the advanced shields, and the likelihood that slurry pressure supports the tail void in the case of the slurry shield.

8. Additional research should be devoted to improvement of the modeling procedures for shield tunneling in the three-dimensional program. Items where work is needed includes:

   a) Provision of a slip element between the shield and the soil.

   b) Incorporation of a thin shell element to better model the shield and liner.

   c) Inclusion of a nonlinear soil model to allow for soil yielding effects.

REFERENCES

Abe, T., Sugimoto, Y. and Ishihara, K. (1979), "Development and Application of Environmentally Acceptable New Soft Ground Tunneling Method," Tunneling Under Difficult Conditions, Editor, I. Kitamura, Pergamon Press, pp 315-320.

Abel, J.F. and Lee, F.T. (1973), "Stress Changes Ahead of an Advancing Tunnel," International Journal of Rock Mechanics and Min. Sci. and Geom. Abs., Vol. 10, Number 6, November, pp. 673-698.

Adachi, T., Mochida, Y. and Tumura, T., (1979), "Tunneling in Fully Saturated Soft Sedimentary Rocks," Proceedings 3rd Conference on Numerical Methods in Geomechanics, Aachen 2,, pp. 599-610.

Atkinson, J.H., Brown, E.T. and Potts, D.M., (1978), "Ground Movements Near Shallow Model Tunnels in Sand," Large Ground Movements and Structures, Editor, J.D. Geddes, Pentech, London, pp. 372-386.

Atkinson, J.H. and Potts, D.M., (1977a) "Stability of a Shallow Circular Tunneling Cohesionless Soil," Geotechnique, 27, pp. 203-215.

Atkinson, J.H. and Potts, D.M., (1977b), "Subsidence Above Shallow Tunnels in Soft Ground," Proceedings ASCE Journal Geotechnical Engineering Division, 103, GT4, pp. 307-325.

Attewell, P.B. and Farmer, I.W., (1974), "Clay Deformations Resulting From Shield Tunneling in London Clay," Canadian Geotechnical Journal, Vol. 11, Number 3, August, pp. 380-395.

Azzouz, A.S., Schwartz, C.W. and Einstein, H.H. (1979), "Finite Element Analysis of the Peachtree Center Station in Atlanta," Reports on Improved Design of Tunnel Supports Civil Engineering Department, M.I.T., Cambridge, Massachussetts.

Bartlett, J.V., Biggard, A.R. and Triggs, R.D. (1973), "The Bentonite Tunneling Machine," Proceedings, Institution of Civil Engineers, Vol. 54, November, pp. 605-624.

Bathe, Klaus-Jurgen, Wilson, E.L. and Peterson, F.E., (1974), "SAP IV A Structural Analysis Program for Static and Dynamic Response of Linear Systems," Earthquake Engineering Research Center Report No. EERC 73-11, University of California, Berkeley, California.

Boresi, A.P., Sidebottom, O.M., Seely, F.B. and Smith, J.O., (1978), Advanced Mechanics of Materials, John Wiley and Sons, New York. pp. 1-20.

Brebbia, C.A. and Connor, J.J., (1974), Fundamentals of Finite Element Techniques for Structural Engineers, John Wiley and Sons, pp. 146-174.

Breth, H. and Chambosse, G., (1972), "Das Verformungsverhalten des Frankfurter Tons beim Tunnelvortrieb," Heft 10, TH Darmstadt.

Chambosse, G., (1972), "The Deformation Behaviour of Frankfurt Clay During Tunnel Driving," Mitt. Vers.-Anst. Bodenmech. u. Grundg., TH Darmstadt, No. 10, 103 pp.

Chandrasekaran, V.S. and King, G.J.W., (1974), "Simulation of Excavation Using Finite Elements," Journal of the Geotechnical Engineering Division, ASCE, Vol. 100, No. GT9, September, pp. 1086-1089.

Chang, C.Y., (1969), "Finite Element Analyses of Soil Movements Caused by Deep Excavation and Dewatering," Ph.D. Thesis, Department of Civil Engineering, University of California, Berkeley, California.

Christian, J.T. and Wong, I.H., (1973), "Errors in Simulating Excavation in Elastic Media by Finite Elements," Soils and Foundations, Japanese Society of Soil Mechanics and Foundation Engineering, Vol. 13, No. 1, March, pp. 1-10.

Clough, G.W. (1969), "Finite Element Analyses of Soil-Structure Interaction in U-Frame Locks," Ph.D. Thesis, Department of Civil Engineering, University of California, Berkeley, California.

Clough, G.W. (1980), "Advanced Soil and Soft Rock Tunneling Technology in Japan" Technical Report No. CE 252, Department of Civil Engineering, Stanford University, Stanford, California.

Clough, G.W. (1981), "Innovation in Tunnel Construction and Support Techniques,"' Bulletin of the Association of Engineering Geologists, Vol. 18, No. 2, May, pp. 151-167.

Clough, G.W. and Duncan, J.M., (1969), "Finite Element Analysis of Port Allen and Old River Locks," Contract Report S-69-6, U.S. Army Engineer Waterways Experiment Station, Corps of Engineers, Vicksburg, Mississippi, September.

Clough, G.W. and Schmidt, B., (1977), "Design and Performance of Excavations and Tunnels in Soft Clay," A State-of-the-Art Report, International Symposium on Soft Clay, Bangkok, Thailand, July.

Clough, G.W., Sweeney, B.P., Finno, R. and Kavazanjian Jr., E., (1982) "Prediction of Behavior of Shallow Tunnels in Soils, Vol. 3: Observed Behavior of EPB Shield in San Francisco Bay Mud," To Be Published.

Cording, E.J. and Hansmire, W.H., (1975), "Displacements Around Soft Ground Tunnels," General Report Session IV, Tunnels in Soil, 5th Pan American Conf. Soil Mech., Buenos Aires, Argentina.

Costa, F.M., DeMariano, M. Monteiro, Jr., J.T., Taglaivinii, R., Yassao, K., (1974) "Passagem dos Shields Sob o Viaduto Boa Vista-Oberservacoes de Movimento," Anais Do V Congresso Brasileiro De Mechanica Dos Solos Sao Paulo, Vol. 1, pp. 323-338

Deere, D.U., Peck, R.B., Monsees, J.E. and Schmidt, B.,(1969), "Design of Tunnel Liners and Support Systems," Report for U.S. Department of Transportation, OHSGT, Contract 3-0152, February.

Desai, C.S. and Abel, J.F., (1972), Introduction to the Finite Element Method, Van Nostrand Company, New York.

Desai, C.S. and Christian, J.T., (1977), Numerical Methods in Geotechnical Engineering, McGraw-Hill, New York.

Duncan, J.M. and Chang, Ching-Yung, (1970), "Nonlinear Analysis of Stress and Strain in Soils," Journal of the Soil of Mechanics and Foundation Division, ASCE, Vol. 96, Number SM5, Proc. Paper 7513, September, pp. 1629-1653.

Dunlop, P., Duncan, J.M and Seed, H.B., (1968), "Finite Element Analysis of Slopes in Soil," Report to Waterways Experiment Station, U.S. Army Corps of Engineers.

Felippa, C.A., (1975), Solution of Linear Equations with Skyline Stored Symmetric Matrix, Computer and Structures 5., pp. 13-30.

Galle, E.M. and Wilhoit Jr., J.C., (1969), "Stress Around a Well Bore Due to Internal Pressures and Unequal Principal Geostatic Stresses," Society of Petroleum Engr. Jour., Vol. 2, No. 2, pp. 835-848.

Gartung, E., Bauernfeind, P., Bianchini, Jean-Claude, (1981), "Three Dimensional Finite Element Method Study of a Subway Tunnel at Nuremberg," The Atlanta Research Chamber, U.S. Dept. of Transportation Report No. UMTA-GA-0007-81-1, Authors, Don Rose et al.

Ghaboussi, J. and Gioda, G., (1977), "On the Time-Dependent Effects in Advancing Tunnels," International Journal for Numerical and Analytical Methods in Geomechanics, Vol. I, pp. 249-269.

Hansmire, W.H., (1975), "Field Measurement of Ground Displacements About a Tunnel in Soil," Ph.D. Thesis, University of Illinois at Urbana, Champaign.

Hansmire, W.H. and Cording, E.J., (1972), "Performance of a Soft Ground Tunnel on the Washington Metro," Proc., 1st Rapid Excavation and Tunneling Conf., Chicago, Vol. 1, pp. 371-389.

Hansmire, W.H., Ghaboussi, H.W., Casey, E.F. and Lentell, R.L., (1981), "Effect of Shield Tunneling over Subways," Proceedings RETC, San Francisco, California, pp. 254-275.

Johnson, W. and Mellor, P.B., (1962), Plasticity for Engineers, Van Nostrand Company Ltd., London, pp. 26-32.

Johnston, P. and Clough, G.N., (1982), "Prediction of Behavior of Shallow Tunnels in Soils, Vol. 1: Time Dependent Response Due to Consolidation in Clays," To be Published.

Kasali, G. and Clough, G.W., (1982), "Prediction of Behavior of Shallow Tunnels in Soils, Vol. 2: Analysis of The Behavior of Advanced Shields by Three Dimensional Finite Element Techniques," Report to be Published by U.S. Department of Transportation.

Kawamoto, T. and Okuzono, K., (1977), "Analysis of Ground Surface Settlement Due to Shallow Shield Tunnels," International Journal for Numerical and Analytical Methods in Geomechanics, Vol. I, pp. 271-281.

Kitamura, Masao, Sumikichi, Ito, Fugiwara, Tashio, (1981), "Shield Tunneling Performance and Behavior of Soft Ground," RETC Proceedings, Vol. 1, San Francisco, pp. 201-220.

Kuesel, T.R., (1972), "Soft Ground Tunnels for BART Project," Proceedings, First Rapid Excavation Tunneling Conference, AIME, Vol. I, No. 2, pp. 287-313.

Kurosawa, S., (1979), "Explanation of Soil Pressurized Shield Method," Internal Report, Ohbayashi-Gumi, Ltd., Tokyo, Japan, 40 pp.

Ladd, C.C. and Foott, R., (1974), "New Design Procedure for Stability of Soft Clays," Proceedings, Journal of the Geotechnical Engineering Division, Vol. 100, No. GT7, July, pp. 763-786.

Leeney, J.G., "Japanese Slurry Shield Tunneling," Tunnels and Tunneling, Vol. 10, No. 1, January, pp. 35-39.

MacPherson, H.H., (1975), University of Illinois Internal Report.

Mana, A.I., (1978), "Finite Element Analyses of Deep Excavation Behavior in Soft Clay," Ph.D. Thesis, Department of Civil Engineering, Stanford University, Stanford, California.

Mana, A.I. and Clough, G.W., (1976), "Lessons Learned in Finite Element Analysis of Temporary Excavations in Soft Clay," Proceedings of Numerical Methods in Geomechanics, Vol. 1, pp. 496-510.

Mayo, R.S., Adair, T. and Jenny, R.J., (1968), "Tunneling, the Stateof-the-Art," U.S. Department of Housing and Urban Development, January, pp. 52-72.

Miki, G., Saito, T. and Yamazaki, H., (1977), "The Principle and Field Experiences of a Slurry Mole Method for Tunneling in the Soft Ground," Proc. Specialty Session I, Tunneling in Soft Ground, 9th International Conference on Soil Mechanics and Foundation Engineering, Tokyo, Japan.

Mondkar, D.P. and Powell, G.H., (1974a), "Towards Optimal In-Core Equation Solving," Computer and Structures, Vol. 4, No. 3, May, pp. 531-548.

Mondkar, D.P. and Powell, G.H., (1974b), "Large Capacity Equation Solver for Structural Analysis," Computer and Structures, Vol. 4, No. 4, August, pp. 699-728.

Muir Wood, A.M. and Gibb, F.R., (1971), "Design and Construction of the Cargo Tunnel at Heathrow Airport, London," Institute of Civil Engineers, Vol. 48, January, pp. 11-34.

Murayama, S. and Matsuoka, H., (1969), "On the Settlement of Granular Media Caused by the Local Yielding in the Media," Proc. Japan Society of Civil Engineers, 172, pp. 31-42.

Obert, L. and Duval, W.I., (1967), Rock Mechanics and the Design of Structures in Rock, John Wiley and Sons, Inc., New York, pp. 89-94.

Orr, T.L., Atkinson, J.H. and Wroth, C.P., (1978), "Finite Element Calculations for Deformation Around Model Tunnels," Computer Methods in Tunnel Design, Institution of Civil Engineers, pp. 121-144.

Parker, H.W., Semple, R.M., Rokhsar, A., Febres-Cordero, E., Deere, D.U. and Peck, R.B., "Innovations in Tunnel Support Systems," Report No. FRA-RT-72-17, Office of High Speed Ground Transportation, Federal Railroad Administration, May.

Peck, R.B. (1969), "Deep Excavations and Tunneling in Soft Ground," Proc. 7th International Conference on Soil Mechanics and Foundation Engineering, State-of-the-Art Volume, pp. 225-290.

Ranken, R.E. and Ghaboussi, J., (1975), "Tunnel Design Considerations: Analysis of Stresses and Deformations Around Advancing Tunnels," Federal Railroad Administration, Department of Transportation, Washington, D.C., Report No. FRA OR & D 75-84, August.

Rebull, P.M., (1972), Earth Responses in Soft Ground Tunneling Proceedings, ASCE Specialty Conference, Purdue University, Lafayette, Indiana, Vo. 2, pp. 1517-1535.

Saenz, J.T. and Utesa, L.V., (1971), "Settlement Around Shield Driven Tunnels," Proc. of the 4th Pan American Conference on Soil Mechanics and Foundation Engineering, San Juan, Vol. 2, pp. 225-241.

Sakurai, S., (1978), "Approximate Time-Dependent Analysis of Tunnel Support Structure Considering Progress of Tunnel Face," International Journal for Numerical and Analytical Methods in Geomechanics, Vol. 2, pp. 159-175.

Sauer, G. and Lama, R.D., (1973), "An Application of New Austrian Tunneling Method in Difficult Builtover Areas in Frankfurt/Main Metro," Symposium on Rock Mechanics and Tunneling Problems, Indian Geotechnical Society, December, pp. 70-92.

Schmidt, B., (1969), "Settlements and Ground Movements Associated with Tunneling in Soil," Ph.D. Thesis, University of Illinois, Urbana-Champaign.

Schmidt, B., (1974), "Predictions of Settlements Due to Tunneling in Soil: Three Case Histories," Proc. 2nd RETC, San Francisco, Vol. 2, pp. 1170-1199.

Schmidt, B., (1976), Monitoring Soft Ground Tunnel Construction, U.S. Department of Transportation, Report No. UMTA-MA-06-0025-76-6.

Smyth-Osborne, K., (1971), Discussion to "Design and Construction of the Cargo Tunnel at Heathrow Airport, London," by A. Muir Wood and F. R. Gibb, Proceedings, Institute of Civil Engineers, Vol. 48.

Takahasi, H. and Yamazaki, H., (1976), "Slurry Shield Method in Method in Japan," Proceedings, Third Conference on Rapid Excavation and Tunneling, 1976, pp. 261-277.

Tan, D.Y. and Clough, G.W., (1979), Development of Design Procedures for Stabilized Soil System for Soft Ground Tunneling: Analysis of Performance and Design Methods, Vol. III, U.S. Dept. of Transportation, Report Number DOT/RSPA/DPB - 50/70/26.

Taylor, R.L., (1977), "Computer Procedures for Finite Element Analysis," The Finite Element Method 3rd Edition, Editor O.C. Zienkiewicz, McGraw-Hill Book Company, London, pp. 677-757.

Terzaghi, K., (1943), "Liner-Plate Tunnels on the Chicago Subway," Transactions, ASCE (and Discussion by K. Terzaghi), Vol. 108, pp. 970-1007.

Vinnel, C. and Herman, A., (1969), "Shield Tunneling in Brussels, Sand," Proceedings 7th International Congress Soil Mechanics and Foundation Engineering, Mexico City, Vol. 2, pp. 487-494; Discussion, Vol. 3, pp. 369-370.

Ward, W.H., (1969), Discussion of: Peck, R.B., "Deep Excavations and Tunneling in Soft Ground," Proceedings, 7th International Conf. Soil Mech. Found. Eng., Mexico City, Vol. 3. pp. 320-325.

Ward, W.H. and M.J. (1981), "Tunneling in Soft Ground - General Report (Preliminary)," Tenth International Conference of the International Society for Society Soil Mechanics and Foundation Engineering, Stockholm.

Wilson, E.L., (1965), "Structural Analysis of Axisymmetric Solids," AIAA Journal, Vol. 3, pp. 2269-2274.

Wilson, E.L., Bathe, K.J. and Doherty, W.P., (1974), "Direct Solution of Large Systems of Linear Equations," Computers and Structure, 4, p. 363.

Zienkiewicz, O.C. (1977), Finite Element Method, McGraw-Hill, London, 1977.

Appendix A

THE GONIOMETRIC METHOD

As shown in Chapter 3, for a general state of stress at any point, the principal stresses are given by equation 3.2

$$\sigma^3 + I_1\sigma^2 + I_2\sigma - I_3 \qquad \text{A1}$$

where σ, I_1, I_2, I_3 are as defined in Chapter 3.
Equation A1 can be solved for σ using the goniometric method. This method is better illustrated using an example.

Consider the stress system shown in Figure A.1
Using the equations 3.4, 3.5, and 3.6, the values of I_1, I_2, I_3 are

$$I_1 = 15, \quad I_2 = -60, \quad \text{and} \quad I_3 = 54$$

Thus, equation A1 becomes

$$\sigma^3 - 15\sigma^2 + 60\sigma - 54 = 0 \qquad \text{A2}$$

The σ^2 term can be removed by substituting $(\sigma' + 5)$ for σ in equation A2. The resulting equation is

$$\sigma'^3 - 15\sigma' - 4 = 0 \qquad \text{A3}$$

From trigonometry, we obtain the identity

$$\cos 3\theta = 4\cos^3\theta - 3\cos\theta$$

or

$$\cos^3\theta - 3/4\cos\theta - 1/4\cos 3\theta = 0 \qquad \text{A4}$$

Substituting $\sigma' = r\cos\theta$ in equation A3 we obtain

$$\cos^3\theta - 15/r^2\cos\theta - 4/r^3 = 0 \qquad \text{A5}$$

Equations A4 and A5 are identical if

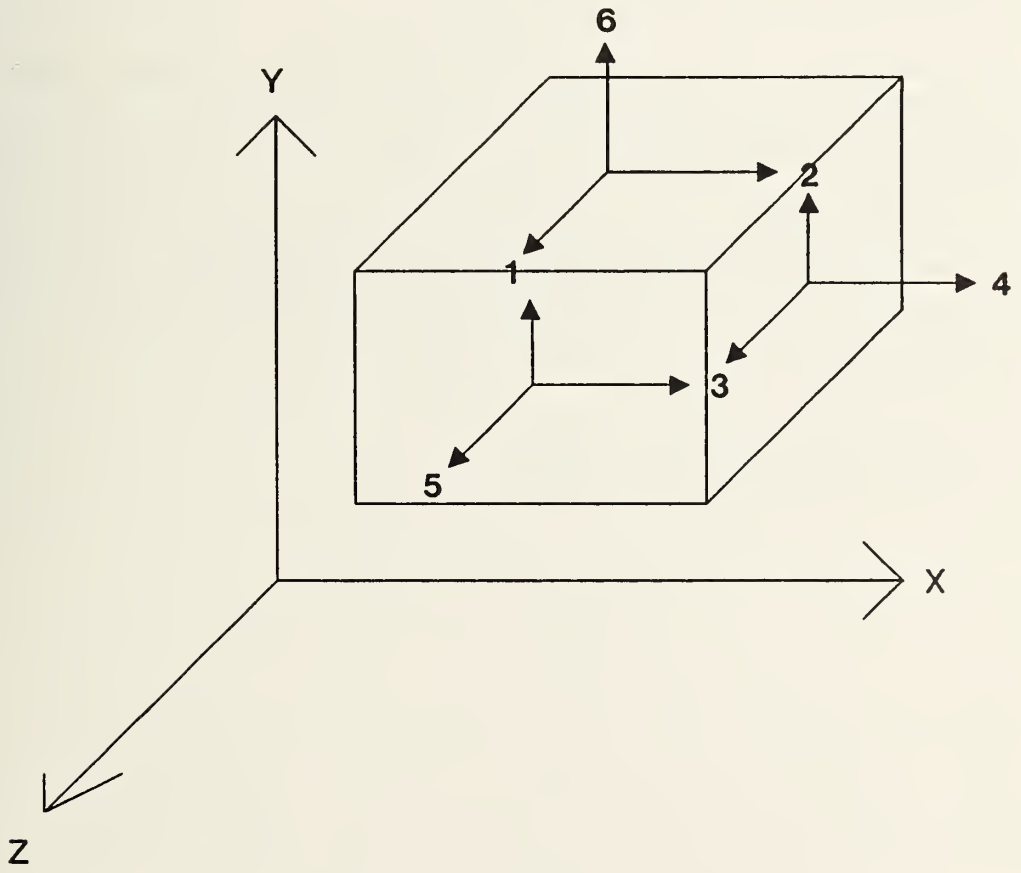

Figure A.1: Particular Stress System

$$15/r^2 = 3/4 \qquad \text{A6}$$

and

$$4/r^3 = \cos 3\theta/4 \qquad \text{A7}$$

The value of r is obtained from equation A6 and the three principal values of θ are given by equation A7. Knowing r and θ, σ' and hence σ, the principal stresses, can be computed.

From the above example, it can be deduced that, in general, the principal stresses from equation A1 are σ and

$$\sigma = r\cos\theta + I_1/3$$

θ and hence $\cos\theta$ has the three principal values given by

$$\cos 3\theta = (2I_1^3 + 9I_1I_2 + 27I_3)/2*\text{Square Root}\{(I_1^2 + 3I_2)^3\}$$

Also,

$$r = 2/3*\text{Square Root}(I_1^2 + 3I_2)$$

Appendix B

USERS MANUAL FOR 3D TUNNELS

B.1 INTRODUCTION

This three dimensional finite element code was developed at Stanford University as a tool for a study of conventional and Advanced Shield tunneling procedures. Some of the subroutines in 3D Tunnels were adopted from the general purpose program SAPIV. The program is coded in Fortran IV and operates without modification on the IBM 370 system. It has been used on an IBM 3033 computer at Stanford University and on a "Triplex" system (Two IBM System/370 Model 168 computers and one IBM System/360 Model 91 computer operating as a single system) at the Stanford Linear Accelerator Center (SLAC).

The code uses double precision for all real variables in order to improve the accuracy of the results obtained. In its current form, it can only handle linear elastic material behavior, but plans are afoot to incorporate a nonlinear constitutive model into it.

B.2 ELEMENTS AVAILABLE

The code as developed has only one element type--the three dimensional element which may have a maximum of 21 nodes and a minimum of 8 nodes. When 8 nodes are used, the formulation becomes that of an 8

node brick element. This variable number of nodes element is shown in Figure B.1. The element nodes are numbered as shown in the same figure. The element can be described as "versatile" because it can be used as a three dimensional element or as a thick shell element. Thus, in tunnel analysis, it can be used for the representation of the soil medium as well as for the modeling of the liner and the shield.

B.3 STIFFNESS MATRIX STORAGE AND EQUATION SOLVING SCHEME

The stiffness matrix is stored in core using a scheme severally called the "skyline" or "profile" or "active column" storage method. An equation solver consistent with this storage scheme is the Modified-Crout reduction procedure and this solver was used in the code.

B.4 CAPACITY OF CODE

The capacity of the code is dependent on the amount of storage available to the user on the computer installation where it is to be used. This is because all the arrays are stored in core memory. At each of the two computer installations mentioned above, an analysis with a region requirement of 3.9 megabytes was run successfully.

To increase the capacity of the code, the size of array A is increased and only the MAIN program will need to be recompiled and then link-edited, if a compiled form of the code has been stored on disk.

B.5 MACRO PROGRAMMING

The code utilizes the macro programming concept. This concept eliminates the problems associated with fixed algorithm codes: they are too restrictive and often a user has to modify such codes to solve a particular problem at the expense of another user. In the macro programming technique, the code is divided into modules with variable algorithm capabilities. The variability is attained by using a macro instruction language to construct specific modules as needed. This language is composed of mnemonics or commands instructing the code on the order in which subroutines should be called. This flexibility makes it possible to add new subroutines to the code without the loss of its previous capabilities.

B.6 DYNAMIC STORAGE SCHEME

Because of the variable sizes of the arrays required in different problems, the dynamic storage scheme is used instead of the fixed dimension method. In this scheme, the array storage capacity is determined by the dimension of vector A in the Main or Master program. In 3D Tunnels, the locations and lengths of arrays stored in vector A are as follows:

STORAGE IN VECTOR A

First Array Address	Array
N1 = 1	X(NUMNP)
N2 = N1 + NUMNP	Y(NUMNP)
N3 = N2 + NUMNP	Z(NUMNP)
N4 = N3 + NUMNP	MAT(NUMEL)
N5 = N4 + NUMEL	NRL(NUMDOF)
N6 = N5 + NUMDOF	IR(NUMDOF)

```
N7  = N6  + NUMDOF                NA(NUMDOF)
N8  = N7  + NUMDOF                IE(NUMEL*MAXNOD)
N9  = N8  + NUMEL*MAXNOD          NELPAR(NUMEL*4)
N10 = N9  + NUMEL*4               NOD9M(NUMEL*(MAXNOD-8))
N11 = N10 + NUMEL*(MAXNOD-8)      D(NUMDOF)
N12 = N11 + NUMDOF                F(NUMDOF)
N13 = N12 + NUMDOF                TOTF(NUMDOF)
N14 = N13 + NUMDOF                TOTD(NUMDOF)
N15 = N14 + NUMDOF                SIG(NUMEL*NGAUSS*6)
N16 = N15 + NUMEL*NGAUSS*6        SIGC(NUMEL*6)
N17 = N16 + NUMEL*6               TLOD(NUMDOF)
N18 = N17 + NUMDOF                NSTORE(NUMNP*3)
N19 = N18 + NUMNP*3               S(NAMAX)
MST = N19 + NAMAX                 Total required storage; this should
                                  be less than MAX for execution.
```

where

```
X(N)                    = X coordinate of node number N
Y(N)                    = Y coordinate of node number N
Z(N)                    = Z coordinate of node number N
MAT(M)                  = Material number of element M
NRL(N)                  = Boundary condition of degree of freedom N
IR(NUMDOF)              = Rearranging Vector
NA(NUMDOF)              = Vector defining the location of the diagonal
                          terms in the stiffness matrix
IE(M,N)                 = Global nodal number of node N of element M
NELPAR(M,1)             = First of four parameters of element M
NOD9M(NUMEL(MAXNOD-8)) = Global nodal numbers corresponding to nodes
                          9 to 21 of each element
D(NUMDOF                = Working vector
F(NUMDOF)               = Working vector
TOTF(NUMDOF)            = Total global load vector
TOTD(NUMDOF)            = Total global displacement vector
STG(M,2,1)              = Stress in the direction at integration
                          point 2 of element M
STGC(M,2)               = Stress in the Y direction at the center of
                          element M
TLOD(NUMDOF             = Working vector for incremental load application
NSTOR (NUMNP*3)         = Array for the storage of boundary conditions
                          defined by NRL
MAX                     = Storage allocated to vector A
S(NAMAX)                = Stiffness matrix vector
NUMNP                   = Total number of nodal points
NUMEL                   = Total number of elements
NUMDOF                  = Total number of possible degrees of freedom
                          (i.e., NUMNP*3).
MAXNOD                  = Maximum number of nodes in a single element
                          in the finite element mesh.
NAMAX                   = Number of locations in the stiffness matrix
                          vector
```

B.7 OVERVIEW OF CODE

The code is divided into two modules:

1. Control and Data input module, and

2. Solution and Output module.

The control and data input module is made up of subroutines PCONTR, MEMCHK, MESHG, PMESH and NRESTR; and the Solution and Output module is made up of subroutine PMACRO and the other 21 subroutines.

Initially. the Main or Master program sets the capacity of the code and then calls the Control and Data input module which in turn calls the Solution and Output Module. The subroutines within each module are called according to the commands or mnemonics specified by the user.

The Main or Master program, the 27 subroutines and their functions are given below:

Name	Functions
Main or Master Program	Sets the capacity of the code by defining the size of vector A
PCONTR	Reads the control data and calls appropriate subroutines to read element data.
MEMCHK	Monitors available memory in vector A and triggers an error flag if the allocated storage in vector A is less than the required storage.
MESHG	Reads and prints mesh data stored on disk by a three dimensional mesh generator.

PMESH	Reads or generates data related to the nodal coordinates, boundary conditions and element connectivity.
NRESTR	Computes the number of degrees of freedom and also determines the locations of the diagonal terms in the stiffness matrix.
PMACRO	Controls the solution and output algorithms.
INITAL	Calculates initial stresses in soil deposit
SHAPE	Determines the interpolation functions and its derivatives for the 8 to 21 variable number of nodes element. It also evaluates the Jacobian matrix and computes its determinant.
BMATRX	Evaluates the strain-displacement matrix
SURFPR	Computes the forces at the nodes of an element due to the application of surface pressure loading or hydrostatic pressure to a face of the element.
LOADIN	Controls the reading and printing of applied nodal forces or displacements and surface pressure loading.
EXCAV	Simulates the excavation process.
CHANGE	Changes the material numbers of specified elements and the nodal restraints of specified nodes. It also reactivates nodes deactivated during excavation.
GROUT	Calculates the equivalent nodal forces due to grout pressure (Routine has not been tried).
SUBSTP	Prepares the load vector for the application of loads in increments.
PZERO	Zeroes the working vector D.
SHELL	Reactivates nodes deactivated during excavation in order to simulate the installation of a liner or the presence of a shield.
ASEMBL	Initializes and assembles the overall stiffness and load vector.
EQUNDF	Calculates the equivalent nodal forces

	due to known stresses at the integration points within the element.
REDUCE	Triangularizes or reduces the stiffness matrix.
SOLVE	Reduces the load vector and back substitutes to solve for the unknown displacements. It is an entry in the subroutine REDUCE.
RESULT	Computes stresses for all elements.
CONST	Generates the stress-strain matrix for an element.
HEXAST	Generates the element stiffness matrix.
STRESS	Computes stresses either at the integration points or the center of an element.
PRINST	Calculates the principal stresses and their direction cosines due to known stresses.
OUTPUT	Prints displacements and reactions at the element nodes as well as the stresses at either the integration points or the center of an element.

INPUT

B.8 CONTROL AND DATA INPUT MODULE

B.8.1 CONTROL DATA (Subroutine PCONTR)

B.8.1.1 CARD 1 --- Format (20A4)

Columns	Variable	Description
1 - 5	NUMNP	Total number of nodal points.
6 - 10	NUMEL	Initial number of elements in finite element mesh.
11 - 15	NUMAT	Total number of material types.
16 - 20	MAXNOD	Maximum number of non-zero nodes in a single element in the finite element mesh.

21 - 25	INTRS	Standard integration order for the natural R-S coordinate.
26 - 30	INTT	Standard integration order for the natural T - coordinate.
31 - 35	NDISC	Code for determining whether mesh data will be read off disk unit 8 where it was stored by the pre-processor program or input by the user. = 0 Data not on disk = 1 Data is on disk
36 - 40	LIST	Code for determining whether generated data read from disk should be printed = 0 Don't print data = 1 Print data

B.8.2 GENERATED MESH DATA (Subroutine MESHG)

- Required ONLY if NDISC = 1 (See Section B.5.1.2)

CARD 1 --- Format (16I5)

Columns	Variable	Description
1 - 5	N	Element Number
6 - 10	NELPAR(N,1)	No. of nodes to describe element displacement field. = 0 Default set to MAXNOD
11 - 15	NELPAR(N,2)	No. of nodes to be used in describing element geometry = 0 Default set to NELPAR (N,1) (= NELPAR(N.1) --> Isoparametric) (< NELPAR(N,1) --> Subparametric)
16 - 20	NELPAR(N,3)	Integration Order for R-S Coordinate = 0 Default set to INTRS
21 - 25	NELPAR(N,4)	Integration Order for T Coordinate = 0 Default Set to INTT

B.8.3 INPUT MESH DATA (Subroutine PMESH)

Required ONLY if NDISC = 0 (See Section B.5.1.2)

There are seven Control Statements or Mnemonics:
COOR, ELEM, MATE, BOUN, ENDI, PRIN, NOPR

B.8.3.1 Control Cards --- Format (A4)

* The Input of Each Data Segment is controlled by the value assigned to CST. Each CST or control card must be immediately followed by the appropriate data.

CST (Mnemonic)	Description
COOR	Coordinate Data
ELEM	Element Data
MATE	Material Data
BOUN	Boundary Restraint Data
PRIN	Implies print subsequent mesh data. This is the default.
NOPR	Implies do not print subsequent mesh data.
ENDI	Must be the last card in mesh data. It terminates mesh input.

NB Except for the ENDI card, the data segments can be in any order. If the CST value of a mnemonic requiring data input is ZERO, no data input is necessary for that CST.

B.8.3.1.1 COOR - Coordinate Data --- Format (I5,3F10.4,I5)

The following data must immediately follow a COOR card

Columns	Variable	Description
1 - 5	N	Node Number
6 - 15	X(N)	X - Coordinate of Node N
16 - 25	Y(N)	Y - Coordinate of Node N
26 - 35	Z(N)	Z - Coordinate of Node N

36 - 40	KN	Increment for generating nodes

* Repeat for NUMNP Nodes

B.8.3.1.2 ELEM --- Element Data

The following data must immediately follow an ELEM card.

B.8.3.1.2.1 CARD 1 --- Format (16I5)

Columns	Variable	Description
1 - 5	M	Element Number
6 - 10	MAT(M)	Material Number of Element
11 - 15	IE(M,1)	Global Node Number of Element Node 1
16 - 20	IE(M,2)	" " " " " " 2
21 - 25	IE(M,3)	" " " " " " 3
26 - 30	IE(M,4)	" " " " " " 4
31 - 35	IE(M,5)	" " " " " " 5
36 - 40	IE(M,6)	" " " " " " 6
41 - 45	IE(M,7)	" " " " " " 7
46 - 50	IE(M,8)	" " " " " " 8
51 - 55	IE(M,9)	" " " " " " 9
56 - 60	IE(M,10)	" " " " " " 10
61 - 65	IE(M,11)	" " " " " " 11
66 - 70	IE(M,12)	" " " " " " 12
71 - 75	IE(M,13)	" " " " " " 13
76 - 80	IE(M,14)	" " " " " " 14

B.8.3.1.2.2 CARD 2 --- Format (16I5)

This card is required only if MAXNOD is greater than 8. Also, if there is a mixture of elemens in the mesh (e.g., 20 node and 8 node elements) then even for 8 node elements, CARD 2 is required, but with ZERO entries.

Columns	Variable	Description
1 - 5	IE(M,15)	Global Node Number of Element Node 15
6 - 10	IE(M,16)	" " " " " " 16
11 - 15	IE(M,17)	" " " " " " 17
16 - 20	IE(M,18)	" " " " " " 18
21 - 25	IE(M,19)	" " " " " " 19
26 - 30	IE(M,20)	" " " " " " 20
31 - 35	IE(M,21)	" " " " " " 21

* (See Figure B1)

B.8.3.1.2.3 CARD 3 --- Format (16I5)

This card defines four parameters relating to the element M.

Columns	Variable	Description
1 - 5	M	Element Number
6 - 10	NELPAR(M,1)	No. of nodes to be used to describe element displacement field = 0 Default set to MAXNOD

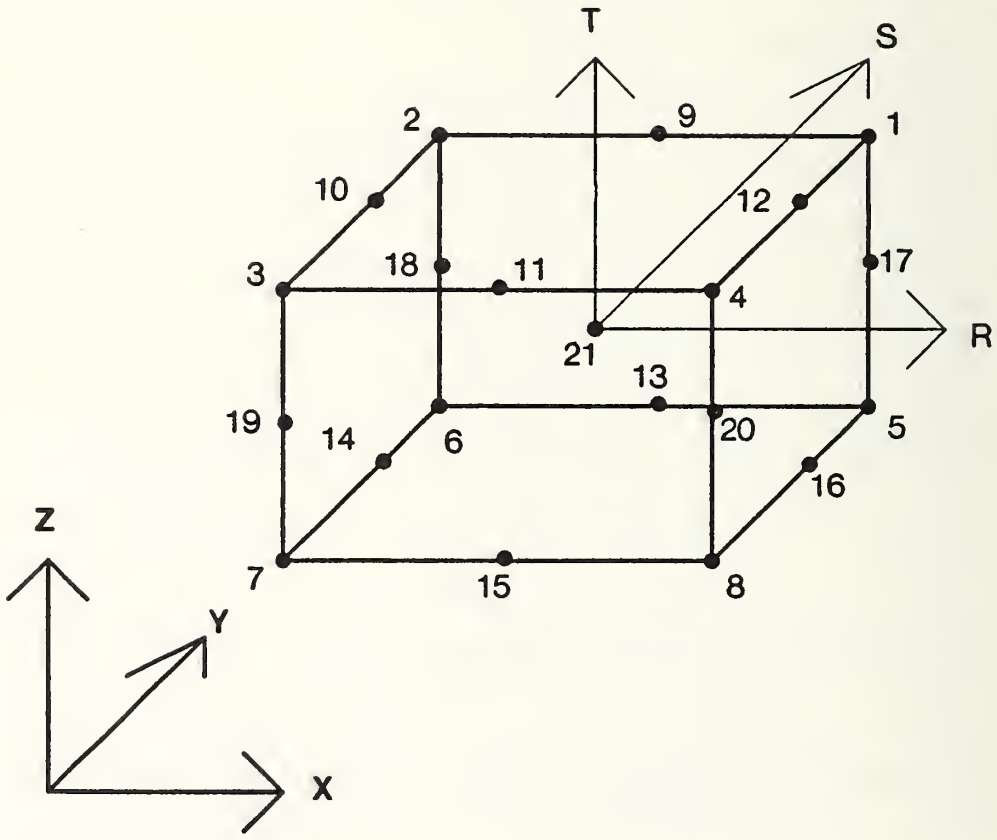

Figure B.1: Element Numbering System and Global Axes

11 - 15	NELPAR(M,2)	No. of nodes to be used to describe element geometry = 0 Default set to NELPAR(M,1) (= NELPAR(N,1) --> Isoparametric) (< NELPAR(N,1) --> Subparametric)
16 - 20	NELPAR(M,3)	Integration order for RS coordinate = 0 Default set to INTRS
21 - 25	NELPAR(M,4)	Integration Order for T coordinate = 0 Default set to INTT
26 - 30	INC	Node number increment for element data generation = 0 Default set to 1.

* Repeat Cards 1, 2, 3 for NUMEL elements

B.8.3.1.3 Material Properties Data

Must immediately follow a MATE card

B.8.3.1.3.1 CARD 1 --- Format (I5,3F10.3,F20.5)

Columns	Variable	Description
1 - 5	MTNUM	Material Type Number
6 - 15	RO(MTNUM)	Unit Weight Of Material Type
16 - 25	PR(MTNUM)	Poisson Ratio Of Material Type
26 - 35	CAYNOT(MTNUM)	At Rest Coeff. Of Material Type
36 - 55	E(MTNUM)	Young's Modulus Of Material Type

* Repeat for NUMAT material types

B.8.3.1.4 Boundary Restraint Data

Must immediately follow a BOUN card

For each node a boundary condition card must be input.

The convention used for boundary restraint is as follows:

= 0 No restraint

= 1 Restrained

B.8.3.1.4.1 CARD 1 --- Format (16I5)

Columns	Variable	Description
1 - 5	N	Node Number
6 - 10	NRL(3*N-2)	Boundary Restraint Code for DOF in X-dirn.
11- 15	NRL(3*N-1)	Boundary Restraint Code for DOF in Y-dirn.
16 - 20	NRL(3*N)	Boundary Restraint Code for DOF in Z-dirn.
21 - 25	KN	Increment for Boundary restraint code generation

* Repeat for NUMNP nodes

NB AXES SYSTEM (Right Hand Rule: Point Right Fingers in the positive direction of X - axis, turn them towards positive direction of Y - axis and thumb will point towards positive direction of Z axis) (See Figure B1).

B.9 Solution and Output Module

B.9.1 Control Information (Subroutine PMACRO)

B.9.1.1 CARD 1 --- Format (10I5)

Columns	Variable	Description
1 - 5	NSHOVE	Number of shoves of shield = 0 if calculating initial stresses ONLY
6 - 10	INTL	Code indicating how initial stresses are to be obtained. = 0 Calculate the initial stresses using gravity turn on = 1 Input the initial stresses = 2 Calculate the initial stresses using the simplified computation method.
11 - 15	NINC	Number of increments for load appliation.
16 - 20	IOUTIN	Output code for initial stress calculated by gravity turn on. = 0 Don't print initial stresses = 1 Print initial stresses
21 - 25	IRUN	Code for indicating whether initial stresses

will be written on or read from disk

= 0 Initial stresses will not be written

= 1 Initial stresses will be written on disk

= 2 Initial stresses will be read from disk

If IRUN = 2, INTL should be 1

B.9.1.2 CARD 2 --- Format (10I5)

Columns	Variable	Description
1 - 5	IOUTP	Output code for results other than those from Initial stress analysis. = 0 Don't print results = 1 Print results
6 - 10	ISTRES	Code indicating the location of stress computation = 0 Calculate stresses at element center. = 1 Calculate stresses at the integration points of the element.

* This card is required for each shove.

B.9.1.3 MACRO COMMANDS

There are 13 macro commands and provision for an additional one (EXTN). These commands are: INIT, LOAD, EXCA, CHAN, PEF, STIF, REDU, SOLV, RESU, LOOP, SHEL, EXTN, NEXT, ENDS.

These macro commands or mnemonics are defined below.

Mnemonic --- Format (A4)

The data input required is controlled by the value of the mnemonic CST. Each CST card must be followed immediately by the appropriate data.

CST (Mnemonic)	Description
INIT	Initial Stress Calculation
LOAD	Obtain Data for Load Application
EXCA	Excavation process
CHAN	Change Material type or boundary conditions of nodes
PERF	Perform Analysis
STIF	Assemble overall structural stiffness matrix

REDU	Reduce the coefficient matrix of symmetric set of equations AX = B
SOLV	Solve for unknowns in symmetric set of equations
RESU	Obtain results of analysis performed
LOOP	Prepare load vector for application of load increment
SHEL	Obtain data for shell elements
EXTN	Provision for future extension. Not yet developed
NEXT	Preparation for next shove
ENDS	Terminates current analysis. Must be the last card in the chain of macro commands.

B.9.1.3.1 INIT - Initial stress analysis (Subroutine INITAL)

This is initiated by specifying the value of CST as INIT. The initial stresses are calculated or read depending on the value of INTL (See Section B.6.1.1).

B.9.1.3.1.1 INTL = 0

Initial stresses are calculated using gravity turn on.

No data input is required.

B.9.1.3.1.2 INTL = 1 Input uniform initial. Stress within element

INITIAL STRESSES AT INTEGRATION POINTS --- FORMAT (8F10.4)

Columns	Variable	Description
1 - 10	SIG(I,1,K)	Initial Stress in K-dirn at Intg. Pt. 1 of Element I
11 - 20	SIG(I,2,K)	" " " " " " " 2 " " "
21 - 30	SIG(I,3,K)	" " " " " " " 3 " " "
31 - 40	SIG(I,4,K)	" " " " " " " 4 " " "
41 - 50	SIG(I,5,K)	" " " " " " " 5 " " "
51 - 60	SIG(I,6,K)	" " " " " " " 6 " " "

61 - 70 SIG(I,7,K) " " " " " " " 7 " " "

71 - 80 SIG(I,8,K) " " " " " " " 8 " " "

* Continue on other cards if NGAUSS is > 8 * Repeat for all six stress directions and for all elements

B.9.1.3.1.3 INTL = 2

Calculate initial Stresses using the Simplied Method.

CONTROL CARD --- FORMAT (16I5)

Columns	Variable	Description
1 - 5	ISIMPL	Code for printing sgresses from Simplified Computation. = 0 Print stresses at element center = 1 Print stresses at integration points of element
6 - 10	IUNIF	Code indicating whether stresses of integration point should be equal to those at the center (i.e., uniform stresses within element) = 0 Stresses calculated at each integration

point

= 1 Stresses are uniform within the element

B.9.1.3.2 LOAD - Loading data (Subroutine LOADIN)

The following must immediately follow a LOAD card

B.9.1.3.2.1 Control information

CARD 1 --- Format (10I5)

Columns	Variable	Description
1 - 5	NLN	Number of Nodes with Applied Nodal Load
6 - 10	NADD	Number of nodes with Applied Nodal Displacement
11 - 15	NSL	Number of elements with Applied Surface Pressure

B.9.1.3.2.2 Applied Nodal Load

CARD 1 --- Format (I5, 3F10.3)

Required only if NLN is NOT equal to 0

Columns	Variable	Description
1 - 5	J	Global Node Number
6 - 10	FXX	Nodal Load in X-direction
11 - 15	FYY	Nodal Load in Y-direction
16 - 20	FZZ	Nodal Load in Z-direction

* The sign of the loads is determined by the direction of the loads with respect to the global axes. If the loads are in the positive direction of the axes the sign is positive.

* Repeat Card 1 for NLN nodes

B.9.1.3.2.3 Applied Nodal Displacement

CARD 1 --- Format (I5, 3F10.3)

Required ONLY if NADD is NOT equal to 0

Columns	Variable	Description
1 - 5	J	Global Node Number
6 - 10	FXX	Applied Nodal Displ. in X-dirn.
11 - 15	FYY	Applied Nodal Displ. in Y-dirn.
16 - 20	FZZ	Applied Nodal Displ. in Z-dirn.

* Repeat Card 1 for NADD nodes

B.9.1.3.2.4 Surface Pressure Load

B.9.1.3.2.4.1 CARD 1 -- Format (10I5)

Columns	Variable	Description
1 - 5	N	Number of the element with Surface Pressure
6 - 10	LFACE	Face Number of Element on Which Pressure is Acting (See Table B1)
11 - 15	LT	Surface load type = 1 Distributed Face Pressure

= 2 Hydrostatic Pressure

B.9.1.3.2.4.2 (i) LT = 1: Distributed Pressure Intensities at Corner Nodes

CARD 2 --- Format (7F10.3)

*Required only if LT = 1

*Should immediately follow Card 1

Columns	Variable	Description
1 - 10	PL(1)	Pressure Intensity at Corner Node 1 of Loaded Face
11 - 20	PL(2)	Pressure Intensity at Corner Node 2 of Loaded Face EQ.0 Default set to PL(1)
21 - 30	PL(3)	Pressure Intensity at Corner Node 3 of Loaded Face EQ.0 Default set to PL(1)
31 - 40	PL(4)	Pressure Intensity at Corner Node 4 of Loaded Face EQ.0 Default set to PL(1)

* Input Compressive Pressure as Positive

(ii) LT = 2: Hydrostatic Pressure

CARD 2 --- Format (7F10.3)

* Required ONLY if LT = 2

Columns	Variable	Description
1 - 10	PL(1)	Weight density of the fluid γ (Units = Force/Unit of Fluid Vol.)
11 - 20	PL(2)	X - ordinate of point S in the free surface of the fluid
21 - 30	PL(3)	Y - ordinate of point S in the free surface of the fluid
31 - 40	PL(4)	Z - ordinate of point S in the free surface of the fluid.
41 - 50	PL(5)	X - ordinate of a point n on the normal to the fluid surface
51 - 60	PL(6)	Y - ordinate of a point n on the normal to the fluid surface
61 - 70	PL(7)	Z - ordinate of a point n on the normal to the fluid surface

* Repeat Card 1 and the appropriate card 2 for each of NSL elements.
* Point S is any point in the free surface of the fluid, and point n is located such that the direction from S to n is normal to the free surface and is positive with increasing depth.

Hydrostatic Pressure in Contact with an element face causes element compression, i.e., pressure resultant acts toward the element centroid. Nodes located above the fluid surface are automatically assigned zero pressure intensities if an element face is not (or only partially) submerged in the fluid.

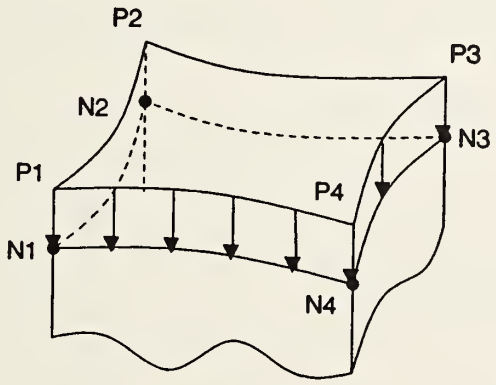

Face Corner nodes are N1, N2, N3, N4
Pressure Intensities at Corner nodes are P1, P2, P3, P4

Surface Pressure

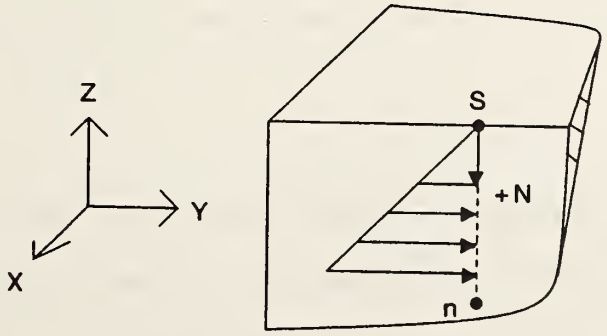

Hydrostatic Pressure

TABLE B.1

Element Face Numbers

	FACE NUMBERS					
	1	2	3	4	5	6
Node 1 of Face No or Corner Node 1	1	2	1	4	1	5
Node 2 of Face No of Corner Node 2	4	3	5	8	2	6
Node 3 of Face No or Corner Node 3	8	7	6	7	3	7
Node 4 of Face No or Corner Node 4	5	6	2	3	4	8
Node 5 Of Face No	12	10	17	20	9	13
Node 6 Of Face No	20	19	13	15	10	14
Node 7 Of Face No	16	14	18	19	11	15
Node 8 Of Face No	17	18	9	11	12	16

B.9.1.3.2.5 EXCA - Excavation Analysis (Subroutine EXCAV)

The following must immediately follow an EXCA card.

B.9.1.3.2.5.1 Parameters of Excavated Layer

Card 1 - Format (16I5)

Columns	Variable	Description
1 - 5	NELEX	Number of elements excavated
6 - 10	NNPLD	No. of nodes exposed by excavation

B.9.1.3.2.5.2 Elements Excavated

Card 2 - Format (16I5)

Columns	Variable	Description
1 - 5	IEXC(I)	Element number of excavated element
6 - 10	IEXC(I+1)	" " " "
11 - 15	IEXC(I+2)	" " " "
.	.	" " " "
.	.	" " " "
.	.	" " " "
	IEXC(NELEX)	Element number of excavated element

* Continue on other cards until NELEX elements being excavated are covered.

B.9.1.3.2.5.3 Nodes on Exposed Surface

Card 3 - Format (16I5)

Columns	Variable	Description
1 - 5	NPLD(I)	Global Nodal Number on Exposed Surface
6 - 10	NPLD(I+1)	" " " " " "
.	.	" " " " " "
.	.	" " " " " "
.	NPLD(NNPLD)	Global Nodal Number on Exposed Surface

* Continue on other cards until NNPLD nodes on exposed surface are covered.

B.9.1.3.2.6 CHAN - Change of Material Type or Nodal Restraint (Subroutine CHANGE)

The following must immediately follow a CHAN card.

B.9.1.3.2.6.1 Parameters to Effect Change

Card 2 - Format (16I5)

Columns	Variable	Description
1 - 5	NELCH	Number of elements whose material types are changed
6 - 10	NPOCH	Number of nodes whose restraints are changed
11 - 15	NPRESS	Code for Grout Pressure Application = 0 Yes = 1 No

B.9.1.3.2.6.2 Application of Grout Pressure

Required only if NPRESS = 0

Card 2 - Format (10F6.3)

Columns	Variable	Description
1 - 6	PRESHA	Grout Pressure Applied

B.9.1.3.2.6.3 Elements whose material types are changed

Required only if NELCH = 0

Card 3 - Format (16I5)

Columns	Variable	Description
1 - 5	N	Element Number of element whose material type is to be changed
6 - 10	MAT(N)	New Material type number of element N

* Repeat for NELCH elements

B.9.1.3.2.6.4 Nodes whose restraints are changed

Required only if NPOCH = 0

Card 4 - Format (16I5)

Columns	Variable	Description
1 - 5	J	Global node number of node whose restraint is

to be changed

6 - 10	NRL(3*J-2)	Nodal restraint in X-dirn. for Node J
11 - 15	NRL(3*J-1)	Nodal restraint in Y-dirn. for Node J
16 - 20	NRL(3*J)	Nodal restraint in Z-dirn. for Node J

* Repeat for NPOCH nodes

B.9.1.3.2.7 SHEL - Installation of Liner or Shield (Subroutine SHELL)

The following must immediately follow a SHEL card

B.9.1.3.2.7.1 Control Information

Card 1 - Format (16I5)

Columns	Variable	Description
1 - 5	NSHEL	Number of elements constituting liner
6 - 10	NPARAM	Code for determining whether element parameters passed from Subroutine PCONTR are to be changed

B.9.1.3.2.7.2 Changing element material type to that of liner material

Card 2 - Format (16I5)

Columns	Variable	Description
1 - 5	N	Element Number of element whose material type is to be changed to that of liner
6 - 10	MAT(N)	New material type number of element N

B.9.1.3.2.7.3 Update element parameters if necessary

Required Only if NPARAM = 0

Card 3 - Format (16I5)

Columns	Variable	Description
1 - 5	N	Element Number of element whose parameters need to be updated
6 - 10	NELPAR(N,1)	Number of nodes to describe element displacement field

11 - 15	NELPAR(N,2)	Number of nodes to describe element geometry
16 - 20	NELPAR(N,3)	Integration order for RS-coordinate
21 - 25	NELPAR(N,4)	Integration order for T-coordinate

* Repeat cards 2 and 3 for NSHEL elements

Appendix C

SUBROUTINE INIT

On the IBM computer installations on which the analyses described in this thesis were carried out, it was necessary to suppress underflows to prevent the computer from aborting the job. The suppression was acceptable because the results were not affected by the so-called underflows.

The Center for Information Technology (CIT) at Stanford University has a routine INIT to suppress underflows in cases where they do not affect the results. This routine is initiated by calling it via a CALL statement at the beginning of the code being used. In the code 3D TUNNELS, the routine is called from the Master or Main Program. The routine INIT or an equivalent of one need to be added to 3D TUNNELS if the latter is to be used on an installation where the former is not already available.

```
* SUBROUTINE INIT

* This assembly language routine was
* written by Mark Lawrence of C.I.T.,
* Stanford University.  The routine
* suppresses underflows.
*
```

```
*
INIT        CSECT
            USING * , 15
            N     14, OFF
            SPM   14
            ER    14
            DS    OF
OFF         DC  X'FDFFFFFF'
```

Appendix D
REPORT OF NEW TECHNOLOGY

The work performed under this contract has lead to no new technological inventions. Conclusions and recommendations regarding various types of equipment and procedures, design parameters, and soil/structure interaction are intended to expand and improve the state-of-the-art of tunnel design and construction in soft ground.

352 copies

☆ U. S. GOVERNMENT PRINTING OFFICE: 1983--600-902--366

partment
sportation

rch and
al Programs
nistration

quare
, Massachusetts 02142

Official Business
Penalty for Private Use $300

Postage and Fees Paid
Research and Special
Programs Administration
DOT 513

U.S.MAIL